Urban Heat Islands, Built Form, Thermal Inequity, and Green Vegetation Interactions in Rapidly Urbanizing Dryland Cities

By

JOHN DIALESANDRO

DISSERTATION

Submitted in partial satisfaction of the requirements for the degree of

DOCTOR OF PHILOSOPHY

in

Geography

in the

OFFICE OF GRADUATE STUDIES

of the

UNIVERSITY OF CALIFORNIA

DAVIS

Approved:

_____

Stephen Wheeler, Chair

_____

Noli Brazil

_____

Helen Dahlke

Committee in Charge

2021

Abstract:

Exposure to heat exacerbated by an increase in urbanization as well as increasing global temperatures has become a growing concern for cities and their residents. Excess heat can cause increased heat-related morbidity, mortality, and energy costs. A large goal of climate adaptation is to reduce this urban heat island effect. However, cooling strategies for dryland cities will likely be different from those for wetter, temperate cities. In addition, different socioeconomic and racial groups often face unequal exposure to heat as well as increased heat-related sickness, mortality, and energy costs. Many experts have found that historically red lined neighborhoods often experience the greatest amount of excess urban heat with the least amount of resources to mitigate it.This dissertation consists of three standalone articles that make independent scientific contributions to the same problem of measuring and mitigating urban heat in dryland cities. The articles use thermal infrared remote sensing to measure the thermal footprint of cities, and a variety of sociodemographic and biophysical ancillary data. In the first article we measure how urban heat behaves in 10 large global cities in relation to different types of land cover and built form. The cities included desert cities of Cairo, Egypt and Dubai, UAE, as well as monsoon dryland cities like Delhi, India which goes 9 months of the year with almost no rainfall. The results showed that urban forest and green spaces can be up to 12° C cooler than city wide averages for both day and night. We also found spillover cooling of up to 5 km for the urban green spaces. In the second article we mapped the thermal footprint of 20 southwestern US cities for average summer, and extreme heat event temperatures. We then compared the wealthiest and poorest block groups as well as LatinX and white neighborhoods. We found that low income block groups were subject to temperatures 2-5° C warmer than wealthier block groups as were LatinX neighborhoods. In the final chapter we developed a vulnerability index for the cities of Bakersfield and Fresno California as well as utilizing the InVEST Urban Cooling model from the Stanford Natural Capital Project to model cooling scenarios from planning interventions such as increasing surface albedo of built form and increasing tree canopy. By modeling 10 and 25% increases of tree canopy and albedo we found increasing tree canopy on developed land uses by as little as 10% could lead to a decrease in temperatures of 1.2° C (2° F) or more throughout the cities, and made a greater difference for low income block groups compared to higher income block groups. The cooling impact of urban trees based on the InVEST model extended up to 2 kilometers. Increasing albedo of paved surfaces by 10% resulted in a non substantial decrease in temperatures throughout the cities. Our research using this model showed that increasing tree canopy is more effective at mitigating high temperatures for vulnerable neighborhoods than decreasing albedo, and high vulnerability neighborhoods. This research demonstrates that unequal heat burden exists amongst dryland cities, but there are effective ways to mitigate the excess heat.

Acknowledgements

First and foremost I would like to thank my advisor Dr. Stephen Wheeler for the immense amount of support in every step of the research and graduate school process. I learned so much about writing and research from Dr. Wheeler's help. This dissertation and the publications that stem from it would not be possible without his incredible help. I would also like to thank Dr. Noli Brazil for the help with statistical modeling and R studio troubleshooting in the data analysis stage as well as chairing my qualifying exam committee. I would also like to thank Dr. Helen Dahlke for her support throughout my time at UC Davis, especially giving me the opportunity to TA every spring and learn how to effectively teach GIS. I also would like to thank our program coordinator Carrie Ruport Armstrong who spent countless hours helping me with all of the paperwork, TA positions and program support. Without the help of these people at UC Davis I never would have made it through the program.

I would also like to thank the following professors in no particular order for their support throughout my time at UC Davis. Dr. Clare Cannon, Dr. Mary Cadenasso, Dr. Yaser Abunnasr of the American University of Beirut, and Dr. Michaela Buenemann of New Mexico State University.

I also would like to thank my high school, and college track and field coaches for taking a chance on me and whom without their help I never would have been able to attend college. In addition, I would like to acknowledge the sacrifices that my parents made that enabled me to pursue higher education. Without their support this would never have been possible.

Finally I need to thank my partner Farnaz Feizi who believed in me when I did not believe in myself and took care of me for the last two years as I went through four life changing surgeries. Without you I certainly would not be here today. I could not ask for a better person to leave footprints next to mine as we go through our life together.

Co-Authorship and Publication Statement

Each of the manuscripts contained within the dissertation has been submitted for/will be submitted for publication in peer-reviewed journals. John Dialesandro is the principal author of all chapters and conducted research conceptualization, data collection, and analysis. All three committee members contributed advice on the process, content, and framing of the research. Professor Stephen Wheeler specifically helped in all of the chapters by providing input to restructure the literature review, and analysis along with major text edits. In addition, Professor Stephen Wheeler has provided academic manuscript editing in chapters 1, 2, and 3. Dr. Noli Brazil assisted with the analysis in chapters 2 and 3. Dr. Helen Dahlke provided extensive feedback and edits of chapter 3. Below is a list of journal destinations for each of the manuscripts.

Chapter 1: Is accepted and published by the Journal of Environmental Research Communications (2019)

Chapter 2: Is accepted and published by the International Journal of Environmental Research and Public Health (2021)

Chapter 3: Is prepared to be submitted to the Journal of Urban Climate

TABLE OF CONTENTS

I. INTRODUCTION

Anthropogenically-driven changes in dryland environments impact local climate, energy use, human well being, and ecosystem services. Sustainability of cities can be impacted greatly by the presence of urban heat islands, which then require use of excess electricity for air conditioning or excess water to maintain green spaces to cool urban environments through evaporation and shading. According to the EPA just a 1° Celsius increase in temperatures can drive cooling load up 10-20% while only decreasing the electric need for cool season heating by as little as 3-15% (EPA 2014). With dryland environments already resource stressed, knowledge of what types of built form, and vegetation can mitigate the warmer surface and ambient air temperatures is very valuable.

Growing up in a dryland urban environment has made me particularly interested in the impacts that anthropogenic changes have had on desert cities. I am particularly interested in how urban climate can be altered by the changes in surface complexion by altering reflectivity, surface materials, built form architecture, fabric and dimensions. In addition to the quantitative elements of urban heat islands, a more subjective thermal inequity exists within many cities resulting in disadvantaged groups being more vulnerable to the negative impacts of urban heat islands, oftentimes due to lack of resources, or the locations of their neighborhoods. Local urban climatology knowledge and the influences that it has on energy use, human well being, and ecosystem surfaces I feel are very important for rapidly developing arid regions.

My formal educational and professional training is in geographical information science (GIS) and remote sensing. My bachelor's degree of GIS is from Kent State University includes a minor in climatology. My masters degree is in geography with a focus on remote sensing

pertaining to thermal surface measurement. From my educational and professional background I have been fortunate enough to learn many useful geospatial tools to measure, model, and extract statistics that can tell a valuable story on the driving factors of urban heat islands.

Within California, climate change and energy use are issues facing resource strained communities. This research can help to provide tools and insight into the overall patterns and complexion of how urban heat islands behave. This information and other benefits from this suite of research such as the temperature relationship with different urban landscapes can lead to informing city planners, and stakeholders in arid cities with the knowledge to implement cost effective mitigation techniques.

For the format of my dissertation I have chosen to go with a three publication method as opposed to the traditional dissertation format. The method of publishing three articles is beneficial as it adds the dimension of making additional progress in research and academic sectors by getting three research articles in circulation for peer review while satisfying the other criteria for graduation. This method seems more practical for transitioning into postdoctoral positions. For myself this three paper dissertation will also be beneficial in future research pertaining to urban heat islands through use of statistical modeling and geographical information science. While prior research has been done, examination of specific neighborhood demographics as well as the urban heat island behaviors in dryland climates are very under-studied in the literature. Additionally, the use of microclimate modelling with the InVEST (Integrated Evaluation of Ecosystem Services and Tradeoffs) Urban Cooling Model is novel and not present in the literature.

II. BACKGROUND

Urban areas make up over 40% of the world's population and this number is expected to grow (Ma et al. 2019). With increases in urban population, more modification and thus more impacts on local climates is expected. Land cover (LC) changes such as urbanization drive changes in land surface temperature (LST) and local climate (Myint et al. 2010). The replacement of natural land covers by urban impervious surfaces, often results in urban heat islands (Schatz and Kucharik 2014) where the temperatures of the urban areas exceed the temperatures in areas in the rural areas. This is true for both air and surface temperatures. Increased air temperatures can lead to higher energy costs, heat related mortality, and exacerbate air quality. While there have been studies that have found a relationship between surface and air temperature (Nichol et al. 2009), most studies have not found a worthwhile relationship between the two (Arnfield 2003).

The urban heat island phenomena has been explored for nearly 200 years with the first observations of temperatures being warmer in cities than adjacent rural areas in London by Luke Howard in 1833 (Stewart 2011). In the 20th century research began to focus on city size impacts on urban heat islands (Arakawa 1937, Oke 1973). Within the 1970s and 1980s Dr. TR Oke began studying the influences that urban geometry had on temperature at the boundary and canopy layers of the urban environment (Oke 1976). As satellite imagery became available, urban heat island studies began to have the capacity to study the phenomena at macroscale city levels using surface temperature readings from the thermal portion of the electromagnetic spectrum. As studies around the world began to increase it was found that vegetation had a

sizable mitigation potential. Within arid environments where cities had a higher amount of vegetation than surrounding rural areas an oasis effect or urban cool island was observed (Cao et al. 2010).

Urban Heat Islands (UHI's) have a detrimental impact on human health, ecosystem services, and energy costs. Warming temperatures can exacerbate smog as the chemical reactions occur faster at warmer temperatures (Akbari and Kolokotsa 2016). Cost from increased cooling demand is perhaps the best monetary measure of the impacts of urban heat islands. Cooling demand can drive energy use by to 10 Kwh per degree of increased temperatures (Santamouris et al. 2015). With temperatures expected to increase, and the amount of peak heat wave days expected to as well by the mid 21st century, the need to reduce or mitigate the UHI is pertinent. For example in the San Fernando Valley in southern California, the number of days above 39° Celsius is expected to increase from 4 to 16 which will further strain energy resources (Levinson et al. 2019).

To date much of UHI research has focused on the relationship of surface temperatures with their surface designation such as agriculture, urban, or rangeland. While the link between temperature and land cover is well documented, three dimensionality, arrangement of land covers and other land system architecture involving built form and green space has only recently emerged as a topic of research pertinent to UHI mitigation (Akbari et al 2016). In the studies that do exist it was found that built form high density such as tall buildings reducing the sky view factor can increase temperatures despite providing shading (Tan Lau and Ng 2016). These results have varied across the year, between day and night as well as across climates.

The aspect of vegetation as a mitigation technique to UHI has long been established as a useful yet resource costly method. For water stressed areas, optimization of green space through

configuration, density, and species of vegetation used, are pertinent. Vegetation can provide cooling in two ways, through shading and evapotranspiration, and has the potential to alleviate heat gained from high amounts of impervious surface. Unfortunately in arid environments, water resources available to maintain vegetation are limited. Growing desert cities such as Phoenix, Arizona and Abu Dhabi, UAE face even higher challenges of water resources as water demand is increasing (Fan et al. 2017). Because of this it may be advantageous for desert cities to use a combination of vegetation and built infrastructure (design, configuration, and albedo) to mitigate the UHI.

Urban heat island research typically follows one of two trends; the surface level urban heat island or temperatures of different surfaces (ie impervious, grass) measured by remote sensing processes (Yuan and Bauer 2007), and canopy and boundary level urban heat island also known as the atmospheric urban heat island and measured in situ by weather stations, and the surface urban heat island. Surface temperatures can be measured using satellite, airborne and drone remote sensing instruments, and can be measured on a broader scale compared to air temperatures which rely on weather station readings (Fan et al. 2017).

In addition to monitoring the factors that influence the UHI, it is necessary to determine which populations are at the highest risk of being negatively affected by the heat. Substantial environmental justice or climate justice concerns may arise because of this disproportionate impact. Measuring population impacts is often done through the use of a heat vulnerability index (HVI), taking into account demographic and geographic information. Although there are many different frameworks for determining vulnerability, one common approach is based on three components: exposure, sensitivity, and adaptive capacity (Wilhelmi & Hayden, 2010). Exposure is defined as the presence of humans in an area where a natural hazard may occur. A more severe

hazard creates greater exposure, and a smaller population means less exposure. Sensitivity is determined by socioeconomic and physiological characteristics of the residents themselves, such as age and disability status, and define the degree to which they can handle the stressors of a natural hazard. Young children and the elderly are particularly sensitive to heat-related and respiratory illnesses due to weaker immune systems and their bodies' inability to cool off efficiently. Adaptive capacity refers to the ability of a community to cope with existing and anticipated stress, including the knowledge, attitude, practices, and resources a population has at their disposal during a natural hazard. Oftentimes the communities that have the highest vulnerability to environmental hazards such as excess heat have the least amount of capital for adaptation and mitigation. Low income and minority neighborhoods have been found in the literature to be disproportionately exposed to excess heat.

In most urban heat island studies, an urban heat island has been defined as the difference between the temperatures measured in the urban core and the temperatures measured in rural areas adjacent to the urban core. The rural in this sense is thought to represent the surface complexion of an area absent of human intervention. Unfortunately for cross comparison studies local geography can make the definition of urban and rural very broad and at times very dissimilar between cities (Stewart and Oke 2012; Middel et al. 2018). Comparing an urban heat island intensity thus between cities can be too general. The World urban database and access portal tools (WUDAPT) has been created to generate a more standardized classification system for urban heat island studies and weather research and forecast (WRF) modeling (Stewart and Oke 2012).

A vast majority of the literature on urban heat islands has been focused on determining the drivers and then creating effective mitigation techniques. While the literature earlier in the

21st century focused on the role of vegetation and configuration of land covers and materials impact on temperature more recently literature has begun to focus more and more on built forms role such as using WUDAPT mentioned earlier. Even more recently there has been an emergence in the literature that has focused on embracing the urban heat islands in cold weather climates to take advantage of the decrease in energy costs UHIs could provide (Yang et al 2018).

The human environmental, urban form, temperature and resource nexus will be explored more thoroughly in the following three papers. In particular I have done a 10 city analysis of dryland urban areas throughout the globe. In this paper I mapped the thermal footprint using satellite data for day and night and measured the gradient of temperatures between the urban and rural surfaces. In addition, I chose six examples of typical built form areas and measured the thermal properties of these areas and compared them to the overall urban mean as well as the surrounding 1km of these patches. Building on paper 1, paper 2 uses a more sophisticated statistical approach to examine neighborhood demographics and their exposure to urban heat. For the study region of the southwest this is a knowledge gap in the literature, as is the spatial regression method used for looking at excess urban heat. Finally the third paper explores a pair of two California cities and examines through a Principal Component Analysis the patterns of thermal inequity of the urban heat island through use of American Community Survey data, thermal imagery, and land cover data. We also utilized the InVEST (Integrated Evaluation of Ecosystem Services and Tradeoffs) Urban Cooling Model, an emerging novel microclimate simulation tool.

REFERENCES

Akbari, H., & Kolokotsa, D. (2016). Three decades of urban heat islands and mitigation technologies research. *Energy and buildings*, 133, 834-842.

Akbari, H., Cartalis, C., Kolokotsa, D., Muscio, A., Pisello, A. L., Rossi, F., ... & Zinzi, M. (2016). Local climate change and urban heat island mitigation techniques–the state of the art. *Journal of Civil Engineering and Management*, 22(1), 1-16.

Arakawa, H. (1937). Increasing air temperatures in large developing cities. *Beitr. Geophys*, 50, 3-6.

Arnfield, A. J. (2003). Two decades of urban climate research: A review of turbulence, exchanges of energy and water, and the urban heat island. *International Journal of Climatology*, 23, 1–26.

Cao, X., A. Onishi, J. Chen, and H. Imura. 2010. Quantifying the cool island intensity of urban parks using ASTER and IKONOS data. *Landscape and Urban Planning* 96 (4): 224-231.

Fan, C., Myint, S. W., Kaplan, S., Middel, A., Zheng, B., Rahman, A., & Blumberg, D. G. (2017). Understanding the impact of urbanization on surface urban heat islands—a longitudinal analysis of the oasis effect in subtropical desert cities. *Remote Sensing*, 9(7), 672.

Levinson, R., Ban-Weiss, G., Chen, S., Gilbert, H., Goudy, H., Ko, J., & Tang, T. (2019). Monitoring the Urban Heat Island Effect and the Efficacy of Future Countermeasures.

Ma, Q., Wu, J., He, C., & Hu, G. (2019). Reprint of "Spatial scaling of urban impervious surfaces across evolving landscapes: From cities to urban regions". *Landscape and Urban Planning* In Print.

Middel, A., Lukasczyk, J., Maciejewski, R., Demuzere, M., & Roth, M. (2018). Sky view factor footprints for urban climate modeling. *Urban Climate*, 25, 120-134.

Myint, S. W., Gober, P., Brazel, A., Grossman-Clarke, S., & Weng, Q. 2011. Per-pixel vs. object-based classification of urban land cover extraction using high spatial resolution imagery. *Remote Sensing of Environment*, 115(5), 1145-116.

Oke, T. R. 1973. City size and the urban heat island. *Atmospheric Environment (1967)* 7 (8): 769-779.

Oke, T. R. (1976). Inadvertent modification of the city atmosphere and the prospects for planned urban climates. *In Proc. Symp. on Meteorology Related to Urban and Regional Land-Use Planning* (pp. 151-175).

Nichol, J. E., Fung, W. Y., Lam, K., & Wong, M. S. (2009). Urban heat island diagnosis using ASTER satellite images and 'in situ' air temperature. *Atmospheric Research*, 94(2), 276–284.

Schatz, J., and C. J. Kucharik. 2014. Seasonality of the Urban Heat Island Effect in Madison, Wisconsin. *Journal of Applied Meteorology and Climatology* 53 (10): 2371-2386.

Santamouris, M., Cartalis, C., Synnefa, A., & Kolokotsa, D. (2015). On the impact of urban heat island and global warming on the power demand and electricity consumption of buildings—A review. Energy and Buildings, 98, 119-124.

Stewart, I. D. (2011). A systematic review and scientific critique of methodology in modern urban heat island literature. *International Journal of Climatology*, 31(2), 200-217.
Stewart, I. D., & Oke, T. R. (2012). Local climate zones for urban temperature studies. Bulletin of the American Meteorological Society, 93(12), 1879-1900.

Tan, Z., Lau, K. K. L., & Ng, E. (2016). Urban tree design approaches for mitigating daytime urban heat island effects in a high-density urban environment. *Energy and Buildings*, 114, 265-274.

United States, Environmental Protection Agency (2014.). Reducing Urban Heat Islands: Compendium of Strategies Urban Heat Island Basics.

Wilhelmi, O. V., & Hayden, M. H. (2010). Connecting people and place: a new framework for reducing urban vulnerability to extreme heat. *Environmental Research Letters*, 5(1), 014021.

Yang, J., & Bou-Zeid, E. (2018). Should cities embrace their heat islands as shields from extreme cold?. *Journal of Applied Meteorology and Climatology*, (2018).

Yuan, F., and M. E. Bauer. 2007. Comparison of impervious surface area and normalized difference vegetation index as indicators of surface urban heat island effects in Landsat imagery. *Remote Sensing of Environment* 106 (3): 375-386

III. THREE PAPERS

Chapter 1: Urban Heat Island Behaviors in Dryland Regions

Abstract

Urban heat island (UHI) characteristics and mitigation strategies for dryland cities differ from those for wetter urban regions. Whereas the latter typically see daytime surface UHIs, the rapid heating and cooling of deserts surrounding arid cities often produces daytime 'urban cool islands' and nighttime UHIs. Degrees of aridness, extent of vegetation, elevation, latitude, humidity, topography, and typical building types are likely to influence dryland UHI dynamics. This study analyzes variations in thermal effects at multiple scales for 10 dryland urban regions representing varied geographies worldwide with an aim to establish a broader understanding of the spectrum of UHI patterns in dryland cities.We used GIS to assemble daytime and nighttime satellite imagery, determined land surface temperature and vegetation at a 30-meter scale, and analyzed typical neighborhood-scale examples of six land cover types in each region. The 10 regions showed large variation in thermal effects. We found a strong daytime surface UHI in only one. Nighttime heat islands were more pronounced. However, all regions showed strong small-scale variation in temperature, averaging a 12.3 °C difference between mean top quintile and bottom-quintile surface temperatures. Samples of urban forest landscapes cooled daytime temperatures an average 5.6 °C compared to metro averages. Irrigated lawn and multistory building land cover samples also had a substantial cooling effect. Xeriscaped landscapes amplified daytime heating. Our results indicate that UHIs for dryland cities are unlikely to be reduced by xeriscape strategies, but that shade-maximizing urban forestry and built form hold promise to reduce heat islands.

Introduction and Background

Urban heat islands (UHIs) often form in temperate climates as buildings and paved surfaces absorb and slowly release solar radiation during the daily cycle, making cities warmer than surrounding vegetated rural landscapes (e.g. Schatz and Kucharik). However, an emerging literature indicates that UHI dynamics are more complicated for dryland cities, a category that includes arid, semi-arid, and Mediterranean climates (Connors et al 2013, Nassar et al 2016). While there are a multitude of studies that focus on temperate regions there are less that focus on dryland regions and even fewer that do a global comparison.

This study analyzes how urban heat island effects vary across 10 dryland urban regions representing a range of geographical environments worldwide. We determine differences between day and night mean urban and rural temperatures derived from satellite imagery, consider variation of temperatures at a detailed (30-meter) scale within the urban area, and correlate land surface temperature with vegetation. To assess the impact that certain built landscape types have on surface temperatures, we analyze representative samples of six land covers in each region—urban forest, irrigated turf and tree, xeriscape, hardscape, urban multistory, and undeveloped and compare their temperature with the urban and rural mean. These methods, described further below, allow us to draw conclusions related to ways that urban temperatures, vegetation, and built form vary across a range of dryland urban regions, and potentially how urban heating and UHIs can be mitigated through landscape planning.

Urban heat islands are the net result of several physical processes that include radiative, thermal, aerodynamics and moisture built form, materials, and vegetation. These processes include the absorption of sunlight and re-radiation of heat by dark surfaces such as pavements

and roofs; the reflectance of sunlight by light-colored materials; shading produced by trees and buildings; and evapotranspiration from plants which cools the surrounding air. The configuration of land covers within the urban environment influences these dynamics (Middel et al 2014, Song and Wang 2015).

UHIs can be identified through satellite land surface temperature measurements or by onsite measurements at 2-m pedestrian or tree-canopy level. They can also be modeled with computer software. Starting in the 1970s researchers showed that dark surfaces tend to produce higher air and surface temperatures than the urban mean (Oke 1973), while green spaces tend to produce lower temperatures (Spronken-Smith and Oke 1998, Onishi et al, Chow et al 2011). Temperature differences between natural and anthropogenic land covers can vary by up to 5 °C for adjacent sites and up to 9 °C between urban core and rural areas (Imoff et al 2010).

Although two-meter air temperatures may be most relevant for human comfort, surface temperatures are more frequently studied owing to the easy availability and comprehensiveness of satellite data. Surface temperatures tend to show heating more strongly than air temperatures. They generally correlate with air temperatures but do not directly correspond due to atmospheric mixing and materials properties as well as technical measurement issues (Zhou et al 2019).

Within the past decade several large-scale studies have documented a daytime ‘urban cool island’ effect for many dryland cities as surrounding landscapes with sparse xeric vegetation, grasses, and dry soils warm more rapidly than urban surfaces (Imhoff et al 2010, Peng et al 2014, Chakraborty and Lee 2019). Surrounding deserts then cool more rapidly at night than urban pavement and rooftops, leading to nighttime UHIs. However, the case study literature suggests variability in this effect. Degrees of aridness, extent of vegetation, elevation, latitude,

humidity, and typical building types are likely to influence dryland urban heat island behaviors (Zhou et al 2014, Heinl et al , He et al).

Research shows the importance of vegetated spaces such as lawns, parks, street trees, and green roofs in reducing dryland UHIs through evapotranspiration and shade (Bowler et al 2010, Rchid 2012, Wang et al 2016). However, conventional turf-and-tree landscapes require consistent irrigation. Xeric landscapes using native and/or drought tolerant species use less water, but are likely to have less cooling effect since xeric species tend to have thin foliage and minimize evapotranspiration (Connors et al 2013).

High-density urban parcels with buildings that create shade can reduce local heating (Emmanuel and Fernando 2007, Norton et al 2015, Nassar et al 2016, 2017). Street width, building height, and tree canopy level all affect this dynamic (Coseo and Larsen 2014). Urban heat islands in most climates are prominent at night because street canyons tend to trap heat in addition to urban materials often experiencing a slower nighttime cooling rate than natural surfaces (Connors et al 2013).

Methodology

We investigated UHI behavior for dryland cities at three scales: the metropolitan region, the neighborhood, and the 30-meter pixel scale available from satellite imagery. We chose a global convenience sample of 10 large dryland urban regions selected to reflect a diversity of dryness, seasonality, urban growth, elevation, and built form. These regions include hyper-arid, arid, Mediterranean, monsoonal, and dry high-altitude climates, but all have an overall water deficit throughout the year and long annual periods with no rain. Eight are located in the northern hemisphere, and two in the southern. We defined urban boundaries for each

metropolitan area using city boundaries from Open Street Map (https://www.openstreetmap.org). Surrounding each region we established a 20 kilometer-wide rural buffer for comparison purposes as can be seen in figure 3. To enhance uniformity, we removed water bodies, as well as areas within 5 km of water bodies for all regions as it has been found that marine influences can vary influence in degree of extent inland (Efthymiadis and Jones), Elevations exceeding 500 feet of the regional mean were also masked out.

We acquired Landsat 8 OLI and ASTER data (30-meter resolution) for daytime and nighttime hot-season dates, and derived land surface temperature (LST) from these sources (table 1). Google Earth Engine, and QGIS were utilized to acquire and process the imagery to Land surface temperature We sampled daytime data near 11 AM local time, and nighttime data near 10 PM. Areas that required two scenes to cover metro areas were mosaiced if scenes were captured on same day (i.e. same path for Landsat), but scenes from different Landsat rows were not mosaiced if they were in different rows due to the temporal differences in scene capture time. For regions with monsoonal influences, we chose dates close to the end of the dry season. At the metropolitan scale we extracted the mean temperatures of the entire region, mean temperatures of upper and lower quintiles of 30- meter pixels, and mean temperature of the surrounding rural areas.

City		Night	Day Image	Night Image
Cairo	07/29/2017	08/08/2015	Landsat 8 OLI	Landsat 8 OLI
Delhi	05/15/2017	08/04/2017	Landsat 8 OLI	ASTER
Dubai	07/28/2016	06/30/2017	Landsat 8 OLI	ASTER
La Paz	11/24/2017	07/07/2018	Landsat 8 OLI	ASTER
Lima	05/10/2017	05/07/2018	Landsat 8 OLI	ASTER
Los Angeles	08/09/2016	07/08/2016	Landsat 8 OLI	Landsat 8 OLI
Madrid	07/17/2017	06/25/2016	Landsat 8 OLI	Landsat 8 OLI
Mexico City	05/28/2016	05/17/2017	Landsat 8 OLI	Landsat 8 OLI
Tehran	06/23/2017	06/09/2016	Landsat 8 OLI	ASTER

Phoenix	08/15/2017	08/12/2016	Landsat 8 OLI	Landsat 8 OLI

Table 1.1: Dates and source of thermal imagery

We employed a broadly used method from the Landsat Handbook for LST retrieval. In this method, only TOA (Top of Atmosphere) radiance and NDVI (Normalized Difference Vegetation Index) are required. According to the handbook, the TOA radiance of thermal infrared band is converted to TOA (or at-sensor) brightness temperature based on the formula (equation (1)) (Chander et al 2009, Jimenez- Munoz et al 2014):

$$Tsensor = K1/ \ln (K2/(Ll + 1)) \quad (1)$$

where Tsensor is the at-sensor brightness temperature in Kelvin (K) and L is the TOA radiance in W/m2Srum. For Landsat-8 TIRS, K1 is 774.89 W m−2 Srμm) and K2 is 1321.08 K for band 10 (USGS, n.d.).

The following equation (equation (2)) calculates the LST based on the brightness temperature obtain previously (Artis and Carnahan 1982).

$$LST = Tsensor/((1 + l * Tsensor/a) * \ln (e)) \quad (2)$$

where LST is the land surface temperature in Kelvin (K), λ is the wavelength in meters and = 1.438 × 10−2 mK. represents the surface emissivity which differs from various land cover types (Shen et al 2016). For ε, water (NDVI < 0) was assigned a value of 0.9925, urban impervious areas and bare soil (0 = <NDVI < 0.15) were assigned a value of 0.923, and vegetation (NDVI > 0.727) was assigned a value of 0.986. Otherwise, there was a modeling relationship with the NDVI values through the following equation:

$$e = 1.0094 + 0.047 * \ln (NDVI)) \quad (3)$$

For ASTER imagery we used the same conversion to surface brightness temperature as Landsat. The imagery was then corrected to surface temperature using band 13 (10.6 micrometers) because of the thermal bands available for ASTER, band 13 lined up closest in spectral wavelength designation as that of Landsat 8 OLI Band 10.

$$LST = band13/(1.0094 + 10.6 * band\ 13)/14388 * \ln(emissivity)) \quad (4)$$

To analyze neighborhood-scale effects, we used Google Earth Engine to visually identify representative samples exceeding one square kilometer in size of six different land cover types (see figure 1). We elected to use this domain expert approach to ensure near 100% accuracy, rather than employing a machine learning classification algorithm such as the World Urban Database Access Portal Tools (Verdonck et al 2019) to quickly classify such areas with moderate accuracy (70%–85%). Our approach was similar to that used by the HERCULES model for classifying urban patches (Cadenasso et al 2007). The selected land covers were:

- Urban Multistory: urban neighborhoods with closely spaced buildings of three stories or more, able to cast substantial amounts of shade
- Irrigated Turf and Tree: large areas of turfgrass with scattered trees (less than 25% tree canopy), including parks, golf courses, playing fields, and residential neighborhoods with sizable yards
- Xeriscape: developed areas with sparse, native and/or drought-tolerant vegetation, typically also including substantial amounts of bare dirt
- Hardscape: low-rise urban environments with extensive impermeable surfaces such as streets, parking lots, and rooftops

- Urban forest: areas with dense tree canopies (native and non-native) (>70%), typically found along waterways or in densely vegetated parks
- Unbuilt: undeveloped land areas within or external to the urban area

Urban Multistory (Los Angeles)

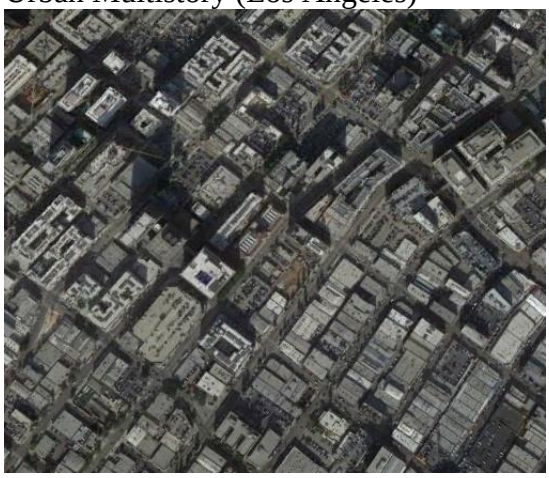

Irrigated Turf and Tree (Dubai)

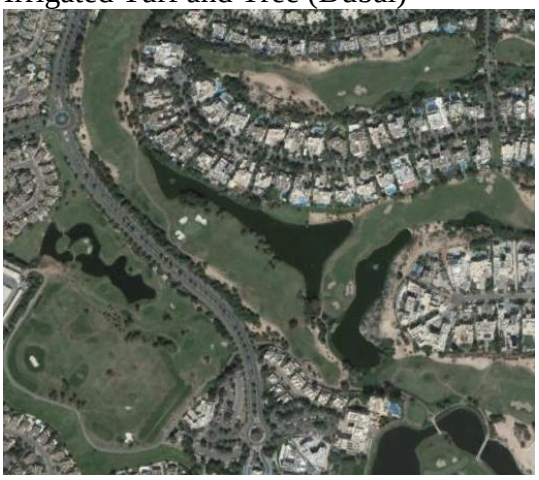

Xeriscape (Phoenix)

Urban Forest (Madrid)

Hardscape (Mexico City)

Undeveloped (Tehran)

Figure 1.1: Examples of Landscape Types in Dryland

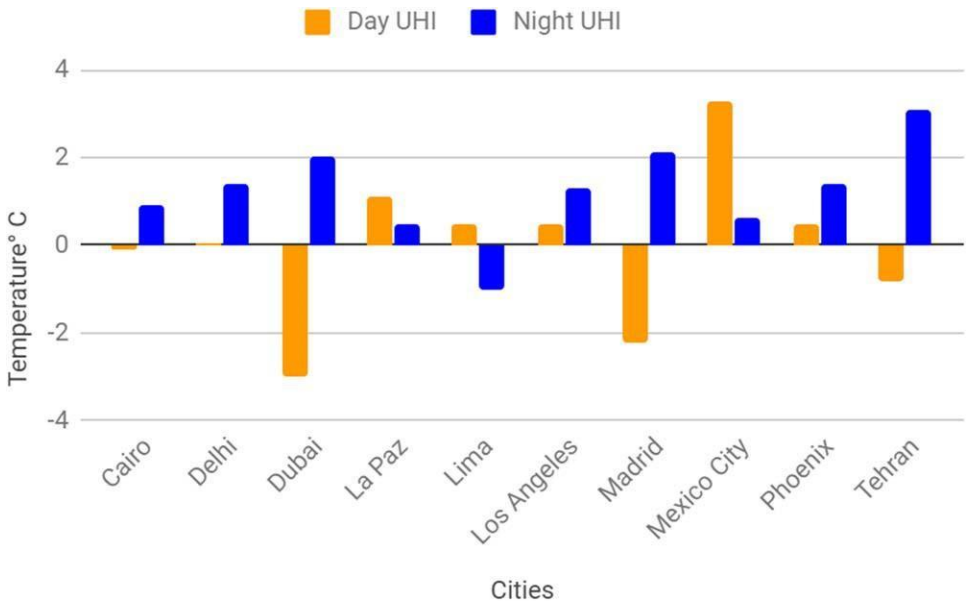

Figure 1.2: Daytime and Nighttime UHI Magnitude for Dryland Cities

To assess spillover temperature effects, we also formed one-kilometer buffers around these built landscape samples and analyzed average temperature differences between the six land cover types, surrounding buffer areas, and the urban mean.

Results

At the metropolitan scale, we found that only one of the ten regions (Mexico City) had an average daytime surface temperature substantially higher (>2 °C) than the surrounding rural. mean, in the traditional urban heat island pattern. Two of the regions (Dubai and Madrid) showed substantial daytime urban cool island effects (temperatures >2 °C below the rural mean). Most of the regions had average temperatures close to the rural mean, showing little overall daytime UHI effect (See figure 2). At night three of the 10 regions had substantial (>2 °C) UHI effects (Dubai, Tehran, and Madrid), while five others had lesser effects of around 1 °C. Delhi exhibited no urban heat island pattern (<0.1 °C). Figure 3 presents a comparison of daytime and nighttime urban heat island intensities. In all cases the standard deviation and range of temperatures were lower at night for both urban and rural areas. We assume that this is a result of rapid daytime heating of certain landscape surfaces, and more gradual diffusion of thermal energy at night (Spronken-Smith and Oke 1998).

Although some regions showed little overall surface UHI, particular locations within them experienced strong heating and cooling during both day and night (Tables 3 and 4). The hottest quintile of 30 meter pixel surface temperatures was on average 5.2 °C warmer during daytimes than the mean for rural lands. Meanwhile, the coolest quintile of daytime surface temperatures was an average of 4 °C cooler than the mean of non-urban land (see tables 1 and 2). The mean difference across these 10 regions between the hottest and coolest quintiles of surface pixel temperature was 12.3 °C. Many regions showed weak 30-meter correlations between vegetation and lower surface temperatures. However, the only statistically significant relationship was for rural areas near Cairo during the daytime. This correlation is likely the product of dense agricultural development of the Nile River Delta.

Neighborhood Scale

At the neighborhood scale, different types of land cover appear to vary strongly in surface temperature compared to the mean for these regions (Figure 1.4). Our sample of urban forest land cover produced the greatest daytime temperature reduction, an average decrease of 5.6 °C. In Phoenix, Arizona, the urban forest sample was 16.5 °C cooler than the metro mean during daytime (Table 1.5). A surrounding one-kilometer buffer area around each urban forest sample also experienced spillover cooling effects, with an average temperature reduction of 1.7 °C. These cooling effects of urban forest land covers relative to the regional mean disappeared at night (Table 6).

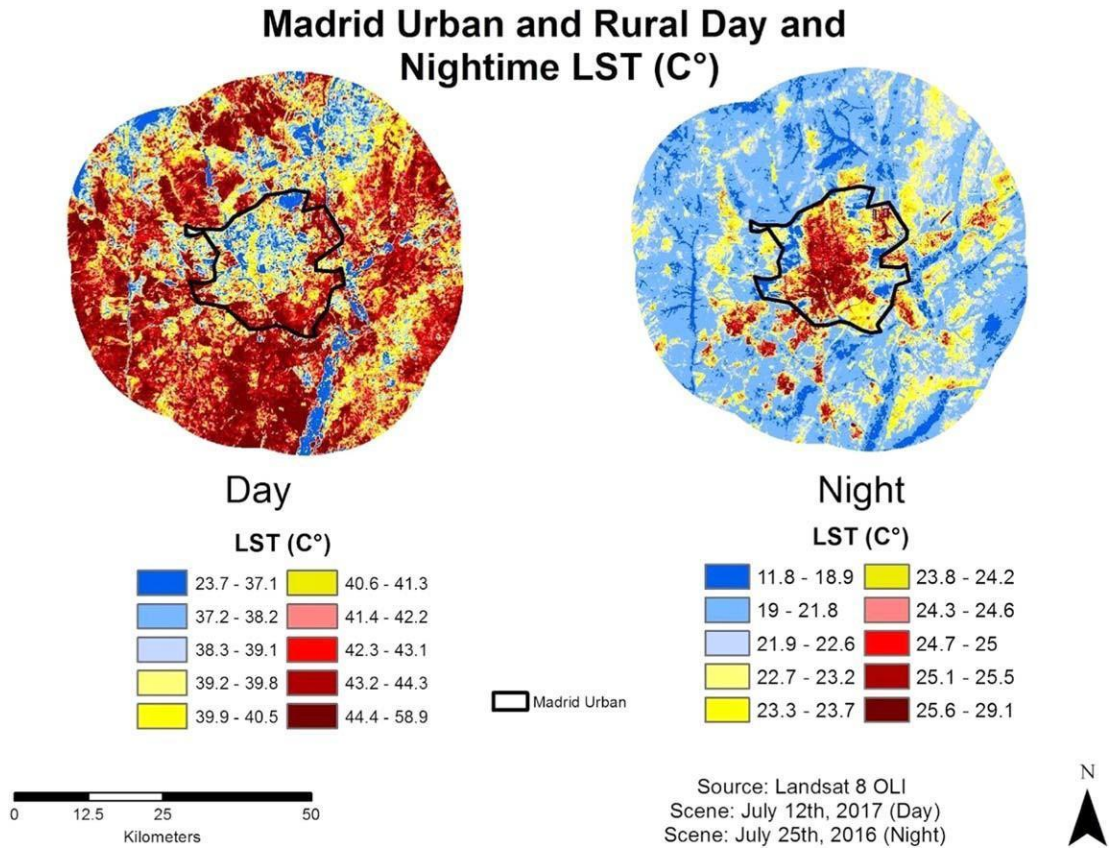

Figure 1.3: Sample day and night time urban heat island maps for Madrid, Spain

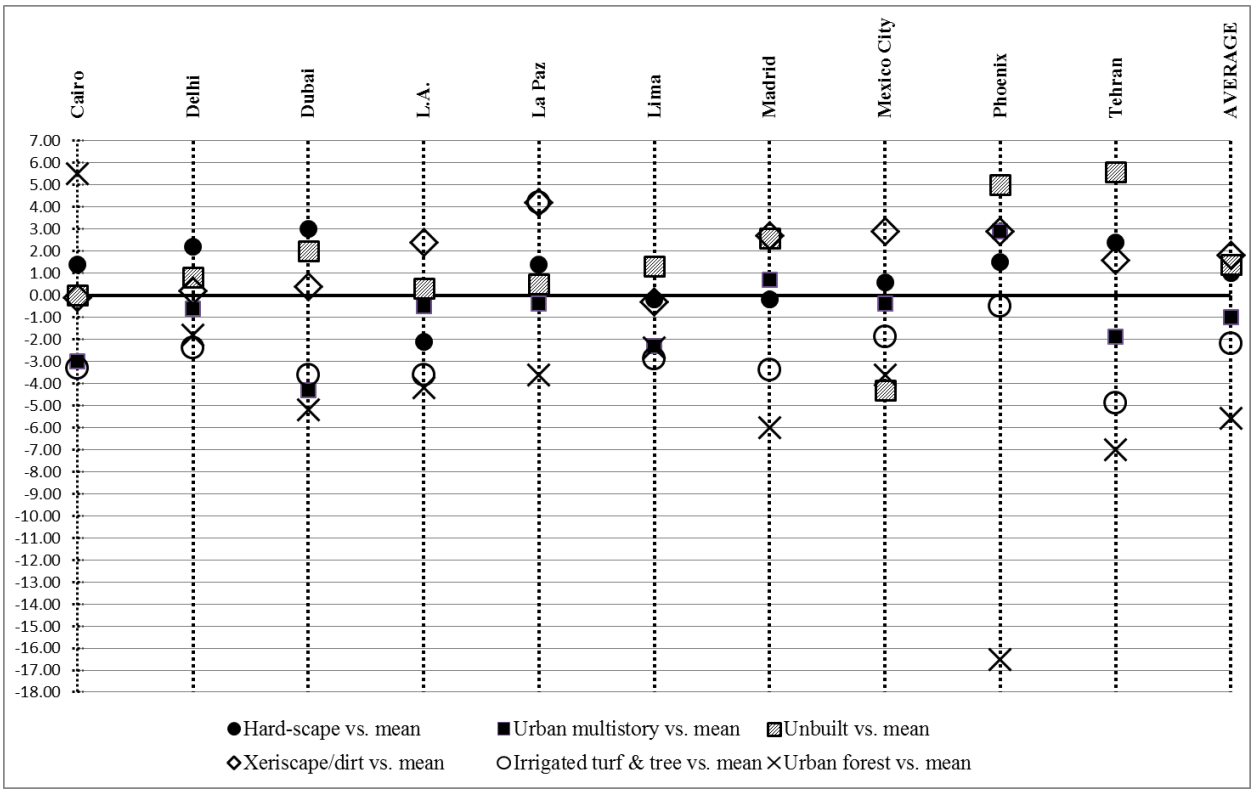

Figure 1.4: Daytime temperature variation by sample neighborhood scale for 10 urban regions

Cities	Rural Mean (°C)	Metro Mean (°C)	Upper 20% of 30 m pixels (°C)	Lower 20% of 30 m pixels (°C)	Difference (°C)
Cairo	38.9	38.8	44.0	32.3	11.7
Delhi	38.4	38.4	43.0	32.6	10.4
Dubai	49.4	46.4	50.1	40.3	9.8
La Paz	30.9	32.0	37.5	28.7	8.8
Lima	26.3	26.8	29.2	20.2	9.0
Los Angeles	36.6	37.1	42.0	26.9	15.1
Madrid	41.7	39.5	46.2	33.3	12.9
Mexico City	28.9	32.3	38.2	18.6	19.6
Tehran	43.8	39.8	45.7	32.8	12.9
Phoenix	40.6	44.3	52.5	38.8	13.7
Average	37.6	37.5	42.8	30.5	12.3

Table 1.2: Average top and bottom quintile daytime temperatures compared with metro and rural means (°C).

Cities	Rural Mean (°C)	Metro Mean (°C)	Upper 20% Lower of 30 m pixels(°C)	20% of pixels 30 m pixels(°C)	Difference (°C)
Cairo	25.6	26.5	28.3	24.8	3.5
Delhi	24.2	25.6	28.4	22.7	5.7
Dubai	24.2	26.2	29.6	23.1	6.5
La Paz	2.5	3.0	4.5	−3.2	7.7
Lima	15.6	14.6	17.2	12.8	4.4
Los Angeles	16.4	17.7	21.5	14.7	6.8
Madrid	21.3	23.4	26.4	17.7	8.7
Mexico City	16.3	16.9	20.1	10.8	9.3
Phoenix	24.4	25.8	29.0	22.7	6.3
Tehran	19.5	22.6	24.8	19.8	5.0
Average	19.0	20.2	23.0	16.6	6.4

Table 1.3: Average top and bottom quintile night temperatures compared with metro and rural means.

Our irrigated turf and tree sample land covers also produced daytime cooling effects in all cities, an average temperature reduction of 2.0 °C from the mean. The spillover cooling impact was weaker than for urban forests, and nighttime temperature differences from the urban mean were negligible.

Urban multistory land cover samples were cooler than the daytime mean in 7 of the 10 metro regions, with an average temperature reduction of 1.0 °C (Table 7). The strongest cooling effects were found in Dubai, Cairo, and Lima. Cooling effects disappeared for multistory samples in most regions at night. For Dubai and La Paz, urban multistory samples had substantially warmer nighttime temperatures than the urban average (Table 1.8). However, these may have risen for contextual reasons: Dubai's downtown is relatively near the Persian Gulf, which likely moderates temperatures, and La Paz is at very high elevation, which leads to very rapid cooling of unbuilt areas and a low mean regional nighttime temperature.

Xeriscape land cover samples were generally warmer than the average daytime metro temperature—an average of 1.8 °C. In five of the 10 regions, the sample of this land cover type was more than 2.4 °C above the metro mean. However, there were few spillover effects to surrounding areas. At night xeriscape samples showed no difference from regional average

temperatures. Samples of unbuilt areas within the metro regions were also typically warmer than the mean for these 10 dryland urban areas—an average of 1.4 °C. At night these samples were cooler than the metro mean—an average of 0.5 °C. These findings are to be expected, as these samples mirror rural arid landscapes with rapid daytime heating and nighttime cooling. We found the unbuilt sample for Mexico City to be much cooler than in the other regions during the daytime, which may be due to more extensive vegetation or topography.

Discussion:

Our analysis confirms that dryland urban regions have substantially different surface UHI characteristics than the literature has shown for wetter, temperate regions. Daytime urban cool islands are likely due to the rapid heating characteristics of surrounding arid terrain. But this phenomenon shows high variability. Modest nighttime UHIs usually occur since rural arid landscapes cool more rapidly than urban ones. The large variation in metro-scale thermal effects between these 10 dryland regions can most likely be explained by factors such as temperatures (light gray) than the mean during daytime for the sampled land covers. Hardscaped, xeriscaped, and unbuilt landscape surface temperatures are often substantially hotter (dark gray) than the mean.

Region	Metro mean temp. (°C)	Urban forest versus Mean of metro area (°C)	<1 km from veg. versus mean of metro area (°C)
Cairo	38.8	−5.5	−0.6
Delhi	38.4	−1.8	−2.0
Dubai	46.4	−5.2	0
La Paz	32.0	−3.6	−1.3
Lima	26.8	−2.4	−1.9
Los Angeles	37.1	−4.2	−0.9
Madrid	39.5	−6.0	−0.2
Mexico City	32.3	−3.6	+0.5
Phoenix	44.3	−16.5	−8.7
Tehran	39.8	−7.0	−2.2
AVERAGE	37.5	−5.6	−1.7

.Table 1.5. Daytime urban forest covers surface temperature compared to the metro mean of the entire area.

Region	Metro mean temp. (°C)	Urban forest versus mean of metro area (°C)	< 1 km from veg. versus mean of metro area (°C)
Cairo	26.5	−0.8	−0.5
Delhi	25.6	−0.6	0.5
Dubai	26.2	−0.7	−1.9
La Paz	3.0	1.0	0.8
Lima	14.6	0.1	0.1
Los Angeles	17.7	−0.7	0.8
Madrid	23.4	1.4	1.5
Mexico City	16.9	1.4	1.8
Phoenix	25.8	−0.1	−0.6
Tehran	22.6	0.2	0.1
AVERAGE	20.2	0.1	0.3

Table1.6: Nighttime urban forest temperature compared to metro mean.

Region	Metro mean temp. (°C)	Urban Forest vs. mean (°C)	Irrigated turf and tree vs. mean (°C)	Urban multis-tory vs. mean (°C)	Hard-scape vs. mean (°C)	Xeriscape/dirt vs. mean (°C)	Unbuilt vs. mean (°C)	Rural (°C)
Cairo	38.8	−5.5	−3.3	−3.0	1.4	−0.1	0	38.9
Delhi	38.4	−1.8	−2.4	−0.6	2.2	0.2	0.8	38.4
Dubai	46.4	−5.2	−3.6	−4.3	3.0	0.4	2.0	49.4
La Paz	32	−3.6	4.2	−0.4	1.4	4.2	0.5	30.9
Lima	26.8	−2.4	−2.9	−2.3	−0.2	−0.3	1.3	26.3
L.A.	37.1	−4.2	−3.6	−0.5	−2.1	2.4	0.3	36.6
Madrid	39.5	−6.0	−3.4	0.7	−0.2	2.7	2.6	41.7
Mexico City	32.3	−3.6	−1.9	−0.4	0.6	2.9	−4.3	28.9
Phoenix	44.3	−16.5	−0.5	2.9	1.5	2.9	5.0	43.8
Tehran	39.8	−7.0	−4.9	−1.9	2.4	1.6	5.6	40.6
AVERAGE	37.5	−5.6	−2.2	−1.0	1.0	1.8	1.4	

Table 1.7. Temperatures by land surface type within dryland urban regions (Daytime).

Region	Metro mean temp. (°C)	Urban Forest versus mean (°C)	Irrigated turf and tree ver-sus mean (°C)	Urban multis-tory versus mean (°C)	Hard-scape ver- sus mean (°C)	Xeriscape/dirt versus mean (°C)	Unbuilt versus Mean (°C)	Rural (°C)
Cairo	26.5	−0.8	0.5	1.2	1.4	0.3	−0.2	25.6
Delhi	25.6	−0.6	0.5	2.1	2.2	2.0	−1.1	24.2
Dubai	26.2	−0.7	−0.2	3.5	3.0	−0.3	−2.2	24.2
La Paz	3.0	1.0	−0.1	4.0	1.4	−0.6	3.8	2.5
Lima	14.6	0.1	−0.2	0	−0.2	−0.3	−0.1	15.6
Los Angeles	17.7	−0.7	−0.4	0.8	−2.1	−0.3	−0.6	16.4
Madrid	23.4	1.4	−1.5	1.5	−0.2	−0.4	−3.4	21.3
Mexico City	16.9	1.4	0.7	1.1	0.6	0.8	0.1	16.3
Phoenix	25.8	−0.1	−0.1	−1.8	1.5	−0.8	1.0	24.4
Tehran	22.6	0.2	1.2	−0.4	2.4	1.4	−2.7	19.5
AVERAGE	20.2	0.1	0.0	1.2	1.0	0.2	−0.5	

Table 1.8: Temperatures by Land Surface Type within Dryland Urban Regions (Nighttime).

The metro areas were all impacted by their degree of aridity, extent of vegetation, elevation, humidity, latitude, topography, and typical building types. However, interactions between these factors are likely complex and a large sample would be required to statistically tease out individual variables responsible for such differences, if that in fact could be done. However, even though surface UHIs may not exist for dryland urban regions or may be mild, our

analysis shows strong local variation in temperature at the 30-meter scale. This variation is likely due to dark surface materials such as asphalt absorbing solar radiation, light colored surfaces reflecting solar energy, the production of shade by structures, or vegetative cooling. These variations will affect human health and comfort, building cooling loads, and social equity considerations. The dryland metro areas studied here do not show strong correlations between vegetation and temperature.

However, overall amounts of vegetation (especially tree canopy) are low in most of these regions, and it is possible that with higher levels of vegetation greater correlations would be found. When we examined sample neighborhood-scale patches of urban forest, we found large cooling effects. One implication is that ambitious regional urban forestry programs might indeed help cool metro areas. However, such programs would need to take water use for irrigation into account. Potentially, low-water tree species could be found that would yield significant cooling when planted citywide. More investigation into low-water, shade-producing vegetation as well as optimal configuration of green spaces for cooling would be desirable.

The sample irrigated turf and tree landscapes we examined had somewhat smaller but still sizable reductions in daytime surface temperature compared to metro means. Use of this landscape strategy would need to be balanced with water consumption. Turfgrass landscapes and water-intensive broadleaf trees are also known to increase local evapotranspiration and humidity, which can cool local landscapes but also traps heat at night.

Xeriscaped landscapes showed little ability to cool urban regions, and the samples we examined were in fact hotter than the daytime metro mean in most regions. Although these landscapes may be desirable for other reasons such as habitat, aesthetic value, and water conservation, they will probably not be able to help reduce urban heat islands.

Shade-producing built form shows potential to reduce daytime urban heating while improving micro-scale human comfort by providing shaded walkways, sidewalks, and courtyards. The samples of this land cover that we examined were 1 °C cooler than metro means, even though their building types and surface materials were usually conventional in nature. Architects, urban designers, and engineers seeking to maximize the shade cast by structures as well as light-colored roof and paving materials might be able to achieve even stronger daytime cooling effects from urban multistorey development.

Our study has limitations that should be mentioned. The spatial resolution of Landsat and ASTER thermal imagery is still relatively coarse, yielding 900 m^2 pixels. Unfortunately, higher spatial resolution thermal imagery is not available. Also, although we attempted to remove noise in the data caused by water bodies, proximity to coasts, and elevation changes, we were not able to do this completely. Even removing a 5 km buffer next to shorelines from analysis in places such as Dubai, Lima, and Los Angeles, urban temperatures were undoubtedly affected to some extent by maritime influences.

Within the neighborhood-scale analysis some challenges arose with consistencies between on-the-ground practices across the ten metro regions. Xeriscape landscape design, for example, is not an active or standardized practice in many of these cities. For those lacking good examples, we chose neighborhoods with a mix of low- water vegetation and bare soil that seemed likely to be closest in performance to xeriscape. The La Paz and Lima regions are lacking in urban forests, and for the urban forest analysis we by necessity chose vegetated riparian canyons on the urban periphery. Shade-producing multistory built form is more common in Mediterranean cities, where narrow streets,

arcades, courtyards, and related urban form elements have been used for millennia to enhance thermal comfort. Multistory buildings in Phoenix, by contrast, tend to stand alone among wider streets and extensive surface parking, and so are unlikely to produce the same cooling effect.

Conclusions

In the era of anthropogenic climate change, keeping cities cool is a growing priority for human health, energy conservation, and greenhouse gas mitigation reasons. Dryland urban regions face different challenges than cities in wetter climates. This study confirms the absence of daytime urban heat islands for many dryland cities, and, conversely, their presence at night. It also highlights the importance of considering building-scale and neighborhood-scale temperature variations—and reducing temperatures at these scales—whether or not regional UHIs exist. Our findings suggest limited correlations between vegetation and cooling for dryland cities at the metropolitan scale, but stronger correlations at the neighborhood scale. The samples of urban multistory landscapes we analyzed also showed the potential of this landscape type to assist in urban cooling. Xeriscape land covers do not appear to have substantial cooling benefit, although they may be desirable for other reasons. A main takeaway is that land covers mixing drought tolerant urban forestry and shade-maximizing built form may help cool dryland cities sustainably, given water limitation.

References

Artis D A and Carnahan W H 1982 Survey of emissivity variability in thermography of urban areas *Remote Sens. Environ.* 12 313–29

Bowler D E, Buyung-Ali L, Knight T M and Pullin A S 2010 Urban greening to cool towns and cities: a systematic review of the empirical evidence *Landscape and Urban*

Planning 97 147–55
Cadenasso M L, Pickett S T A and Schwarz K 2007 Spatial heterogeneity in urban ecosystems: reconceptualizing land cover and a framework for classification *Front Ecol. Environ.* 5 80–8
Chakraborty T and Lee X 2019 A simplified urban-extent algorithm to characterize surface urban heat islands on a global scale and examine vegetation control on their spatiotemporal variability *Int. J. Appl. Earth Obs. Geoinf.* 74 269–80
Chander G, Markham B L and Helder D L 2009 Summary of current radiometric calibration coeffecients for Landsat MSS, TM, ETM+, and EO-1 ALI sensors *Remote Sens. Environ.*113 893–903.
Chow W T, Pope R L, Martin C A and Brazel A J 2011 Observing and modeling the nocturnal park cool island of an arid city: horizontal and vertical impacts *Theoretical and Applied Climatology* 103 197–211
Connors J P, Galletti C S and Chow W T 2013 Landscape configuration and urban heat island effects: assessing the relationship between landscape characteristics and land surface temperature in Phoenix, Arizona *Landscape Ecology* 28 271–83
Coseo P and Larsen L 2014 How factors of land use/land cover, building configuration, and adjacent heat sources and sinks explain Urban Heat Islands in Chicago *Landscape and Urban Planning* 125 117–29
Efthymiadis D A and Jones P D 2010 Assessment of maximum possible urbanization influences on land temperature data by comparison of land and marine data around coasts *Atmosphere* 1 51–61
Emmanuel R and Fernando H 2007 Urban heat islands in humid and arid climates: role of urban form and thermal properties in Colombo, Sri Lanka and Phoenix, USA *Climate Research* 34 241
He B-J *et al* 2019 An approach to examining performances of cool/hot sources in mitigating/enhancing land surface temperature under different temperature backgrounds based on Landsat 8 image *Sustainable Cities and Society* 44 416–27
Heinl M, Hammerle A, Tappeiner U and Leitinger G 2015 Determinants of urban–rural land surface temperature differences–a landscape scale perspective *Landscape and Urban Planning* 134 33–42
Imhoff M L, Zhang P, Wolfe R E and Bounoua L 2010 Remote sensing of the urban heat island effect across biomes in the continental USA *Remote Sens. Environ.* 114 504–13
Jiménez-Muñoz J C, Sobrino J A, Skoković D, Mattar C and Cristóbal J 2014 Land surface temperature retrieval methods from Landsat-8 thermal infrared sensor data *IEEE Geosci. Remote Sens. Lett.* 11 1840–3
Middel A, Häb K, Brazel A J, Martin C A and Guhathakurta S 2014 Impact of urban form and design on mid-afternoon microclimate in Phoenix Local Climate Zones *Landscape and Urban Planning* 122 16–28
Nassar A K, Blackburn G A and Whyatt J D 2016 Dynamics and controls of urban heat sink and island phenomena in a desert city: development of a local climate zone scheme using remotely-sensed inputs *Int. J. Appl. Earth Obs. Geoinf.* 51 76–90
Nassar A K, Blackburn G A and Whyatt J D 2017 What controls the magnitude of the daytime heat sink in a desert city? *Appl. Geogr.* 80 1–14 Norton B A, Coutts A M, Livesley S J, Harris R J, Hunter A M and Williams N S 2015 Planning for cooler cities: a framework to prioritise green infrastructure to mitigate high temperatures in urban landscapes

Landscape and Urban Planning 134 127–38
Oke T R 1973 City size and the urban heat island *Atmospheric Environment* (1967) 7 769–79
Onishi A, Cao X, Ito T, Shi F and Imura H 2010 Evaluating the potential for urban heat island mitigation by greening parking lots Urban Forestry & Urban Greening 9 323–332
Peng S S, Piao S, Zeng Z, Ciais P, Zhou L, Li L Z and Zeng H 2014 Afforestation in China cools local land surface temperature Proceedings of the National Academy of Sciences 111 2915–19
Rchid A 2012 The effects of green spaces (palm trees) on the microclimate in arid zones, case study: Ghardaia, Algeria Energy Procedia 18 10–20
Schatz J and Kucharik C J 2014 Seasonality of the urban heat island effect in Madison, Wisconsin Journal of Applied Meteorology and Climatology 53 2371–86
Shen H, Huang L, Zhang L, Wu P and Zeng C 2016 Long-term and fine-scale satellite monitoring of the urban heat island effect by the fusion of multi-temporal and multi-sensor remote sensed data: A 26-year case study of the city of Wuhan in China Remote Sensing of Environment 172 109–25
Song J and Wang Z H 2015 Impacts of mesic and xeric urban vegetation on outdoor thermal comfort and microclimate in Phoenix, AZ Build Environment. 94 558-568.
Spronken-Smith R A and Oke T R 1998 The thermal regime of urban parks in two cities with different summer climates Int. J. Remote Sens.19 20852104
Verdonck M L, Demuzere M, Bechtel B, Beck C, Brousse O, Droste A and Van Coillie F 2019 The human influence experiment (part 2): guidelines for improved mapping of local climate zones using a supervised classification Urban Science 3 27
Wang Z H, Zhao X, Yang J and Song J 2016 Cooling and energy saving potentials of shade trees and urban lawns in a desert city Appl. Energy 161 437–44
Zhou D, Xiao J, Bonafoni S, Berger C, Deilami K, Zhou Y and Sobrino J 2019 Satellite remote sensing of surface urban heat islands: progress, challenges, and perspectives Remote Sensing 11 48
Zhou D, Zhao S, Liu S, Zhang L and Zhu C 2014 Surface urban heat island in China's 32 major cities: spatial patterns and drivers Remote Sens. Environ. 152 51–61

Chapter 2**:** Dimensions of Thermal Inequity: Neighborhood Social Demographics and Urban Heat in the Southwestern U.S.

Abstract

Exposure to heat is a growing public health concern as climate change accelerates world- wide. Different socioeconomic and racial groups often face unequal exposure to heat as well as increased heat-related sickness, mortality, and energy costs. We provide new insight into thermal inequities by analyzing 20 Southwestern U.S. metropolitan regions at the census block group scale for three temperature scenarios (average summer heat, extreme summer heat, and average summer nighttime heat). We first compared average temperatures for top and bottom decile block groups according to demographic variables. Then we used spatial regression models to investigate the extent to which exposure to heat (measured by land surface temperature) varies according to income and race. Large thermal inequities exist within all the regions studied. On average, the poorest 10% of neighborhoods in an urban region were 2.2 ◦C (4 ◦F) hotter than the wealthiest 10% on both extreme heat days and average summer days. The difference was as high as 3.3–3.7 ◦C (6–7 ◦F) in California metro areas such as Palm Springs and the Inland Empire. A similar pattern held for LatinX neighborhoods. Temperature disparities at night were much smaller (usually ~1 ◦F). Disparities for Black neighborhoods were also lower, perhaps because Black populations are small in most of these cities. California urban regions show stronger thermal disparities than those in other Southwestern states, perhaps because inexpensive water has led to more extensive vegetation in affluent neighborhoods. Our findings provide new details about urban thermal inequities and reinforce the need for programs to reduce the disproportionate heat experienced by disadvantaged communities.

Introduction

Urban heat is a public health hazard that is experienced across the globe independent of jurisdiction, development, and climate. Extreme heat events exacerbate the impact of urban heat and are responsible for a high number of weather-related deaths (Hess et al. 2014). Excess heat has consequences for human health including heat stroke, exhaustion, and amplified respiratory and cardiovascular issues (Wald 2019). Extreme heat is expected to become more common and longer lasting as climate change drives temperatures up.

It has long been known that the paved surfaces of urban areas will absorb and retain solar radiation, increasing urban temperatures (Oke 1976; Oke 1982). For this reason, cities in temperate climates will often have higher temperatures than vegetated surrounding countrysides, a phenomenon known as the urban heat island (UHI) effect (Rizan, Dennis & Chunho 2008; Weng etal. 2008). Dryland cities as well as tropical cities also experience this phenomena (Wong and Yu 2005). Likewise, particular neighborhoods with high levels of paved surfaces may be hotter than others with more vegetation.

Heating patterns in dryland urban regions are often more complex than for wetter temperate regions. Dryland cities often contain more green vegetation than surrounding desert or grassland, and so may be somewhat cooler than surrounding landscapes during daytime (Dialesandro, Wheeler, and Abunassr, 2020). At night this pattern may be reversed, as desert landscapes cool off more quickly than urban ones. However, during both day and night, temperatures in these cities may be high enough to pose serious problems for human communities.

Urban heat can be reduced by lowering the amount of paved surfaces, increasing their albedo, changing built form in ways that produce ground-level shade, and/or increasing the

quantity of vegetation, which cools both through transpiration and by producing shade (Wheeler et al. 2019). Vegetation in particular has been shown to be a strong cooling influence (e.g. Akbari et al. 2016; Abunnasr 2013). Thermal inequities have been less explored in the academic literature than other urban heat dynamics. They can be seen as an environmental justice problem in which poor and non-white communities suffer disproportionately because of prevailing environmental conditions. The term "climate justice" is increasingly used (Scholsberg and Collins 2014; Bullard and Wright 2009). More specifically, the Climate Gap or the unequal impact of the climate crisis on persons and communities of color has received attention as research indicates that communities of color will have a higher degree of suffering during heat waves (Morello-Frosch, Pastor and Shonkoff 2009).

Literature on thermal inequities is beginning to emerge, although studies are often general or limited to specific case studies. Mitchell and Chakraborty (2014, 2018a) used the term to describe the unequal distribution of the urban heat island impacts amongst populations in Florida. Wong et al. (2016) found thermal inequities in age, marital status, occupation, education attainment and income throughout Hong Kong. Also, (Harlan et al. 2007) found older, low-income, and minority populations in Phoenix to be disproportionately impacted by increases in urban temperatures. In a study of New York, Chicago and Los Angeles, Mitchell et al. (2015) found higher temperatures in census tracts to be associated with Black, Hispanic, disabled, non-English-speaking, and low-income populations. Mitchell and Chakraborty (2018b) provided an expanded analysis of 20 cities throughout the US and found census tracts with higher socioeconomic status to be associated with greater heat exposure. However, they found an inconsistent association between minority neighborhoods and greater heat. In a study of Phoenix, Jenerette et al. (2007) found that increases in median income of $10,000 were associated with a

decrease of 0.28° C in neighborhood temperature. In a study of Santiago, Chile , De La Berrera et al. (2019) found low-income neighborhoods to have temperatures 2.5-3.3° C higher than in high-income districts.

Within Europe, the index of multiple levels of deprivation (IMD) (a 37-parameter metric that includes education, income, disability, etc.) has been found to correlate with higher temperatures. Macintyre et al. 2018 found nighttime temperature to range by 3.1° C across deciles of the IMD index within West Midlands, UK. Low-income and elderly populations also typically have lesser ability to mitigate heat effects by accessing green space and cooling centers (Chow et al. 2012; Volkel et al. 2018).

Greenspaces with their cooling benefits appear more frequently in high-income white neighborhoods in dry urban regions than in low-income or non-white neighborhoods (Harlan et al. 2019). Jenerette et al. (2013) found vegetation to be positively correlated with income in seven Southwestern U.S. metropolitan regions. Greenspaces are often absent or fragmented in low-income neighborhoods (Declet-Barreto et al. 2013). While finding white neighborhoods to have more tree canopy, other researchers determined that LatinX and Black neighborhoods have higher potential for tree canopy (Flocks et al. 2011; Locke et al. 2020), indicating that mitigation potential from tree canopy in LatinX and Black neighborhoods exceeds that in white neighborhoods.

In a study of Phoenix, Harlan et al. (2007) found that resident proximity to greenspaces varies widely between wealthy and poor neighborhoods, as well as between white and LatinX neighborhoods. In arid urban regions water is a costly resource, and use of water for aesthetic landscaping is far more apparent in wealthy than poor neighborhoods which also leads to cooler neighborhoods (Zhang, Murray and Turner 2017).

Historic redlining policies (preventing people of color from purchasing homes in certain neighborhoods) heavily influence where tree canopy exists in cities across the U.S. In a recent study Locke et al. (2020) found that neighborhoods previously subject to redlining have 37% less tree canopy, leading to warmer temperatures). Another recent study by Hoffman, Shandas, and Pendleton (2020) of 108 U.S. urban areas found that 94 percent of neighborhoods that had been redlined had elevated temperatures compared to the rest of the city (Hoffman, Shandas, and Pendelton 2020).

Urban greening efforts to reduce heat in neighborhoods with vulnerable populations have been described in the literature (Wolch, Bryne, and Newwell 2014). Other strategies to achieve the same result include investing in cool pavements, high albedo roofing, and reconfiguring built form to add ground-level shade (Thomas and Butters 2018). Within the state of California, the California Global Warming Solutions Act (AB 32) and SB 535 Disadvantaged Communities Actmandate consideration of social equity within climate adaptation programs (Forman et al. 2019).

In this study we seek to provide a detailed understanding of thermal inequities within urban regions both at high risk from heat (due to very hot summers) and containing many low-income and non-white neighborhoods. We chose to develop a comprehensive sample of the 20 largest metropolitan areas in the southwestern U.S. states (Figure 1), and used a more fine-grained geographical scale (the census block group) than previous studies. Phoenix, Arizona is already heavily represented in the literature on UHI studies, but the remaining 19 urban regions are far less studied. To develop a well-rounded understanding of thermal inequities, we analyzed temperature-demographic relationships on average hot days, extreme heat days, and at nighttime.

Methods

Utilizing Google Earth Engine (GEE), we downloaded Landsat 8 Operational Land Imager (OLI) Tier 1 imagery. Tier 1 is in a scaled Digital Number format (often described in the literature as a raw scene). Using the Javascript enabled GEE we processed this data to obtain at-sensor (or Top-of-Atmosphere (TOA)) radiance and surface reflectance. We then used TOA radiance and surface reflectance data to retrieve LST. The geometric fidelity of the Tier 1 Landsat Collections has a Root Mean Square Error (RSME) of less than 12 meters (USGS 2017). We projected all imagery into WGS 1984 UTM format for the specific zone of each city. Dates were selected for cloud free periods (which provide the most accurate readings) in the summer season.

We examined three temperature scenarios for analysis. For the first we chose Landsat scenes coinciding with extreme heat events for each of the 20 metropolitan regions. This was done by selecting the warmest day available between 2013-2019 that coincided with a cloud free day of Landsat 8 OLI imagery capture. For the second scenario we collected scenes for an average summer day based on the average of available landsat scenes during the study period. The dual level analysis allows for comparison of the urban heat island patterns during extreme heat events as well as during conditions close to the median daytime temperature value for the summer season. For the third scenario we used night time thermal imagery for an average summer temperature night close to the median nighttime temperature value for summer imagery available.

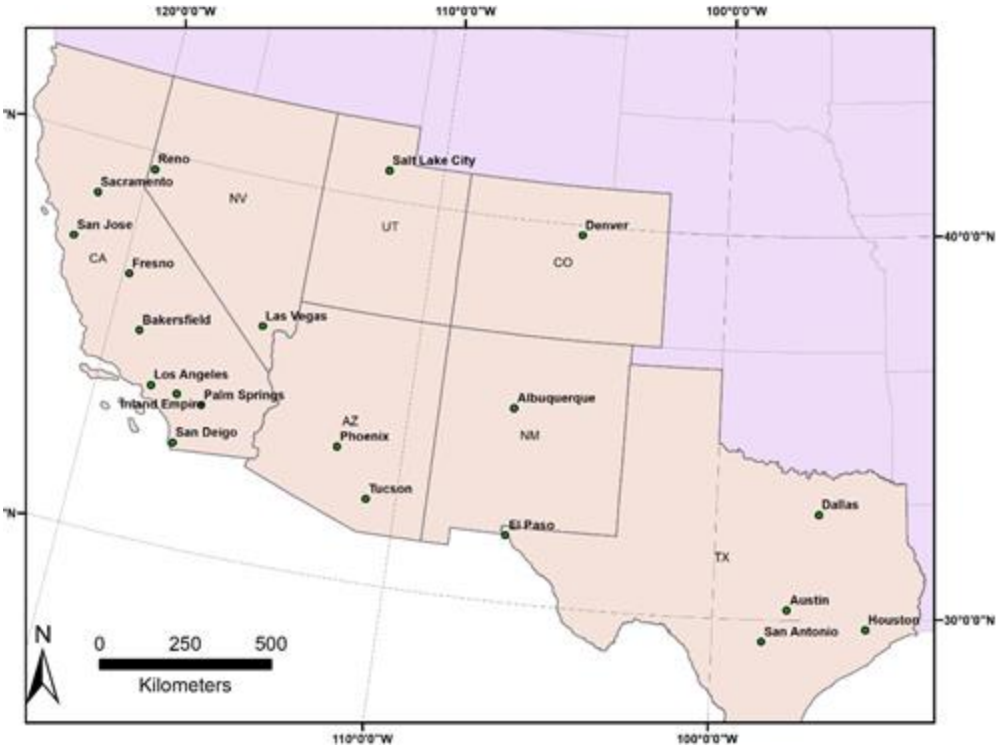

Figure 2.1: 20 Southwestern Cities under investigation.

We collected demographic data from the 5-year 2013-2017 ACS (American Community Survey) at the block-group level. Our primary variables of interest were median household income, percent LatinX, percent black, and percent Asian. We also collected the total population, percent native-born, and percent holding a bachelor degree as control variables. We removed block groups that had missing values on any variables as well as those in areas with airports and detention facilities.

We employed a widely used single-channel method from the Landsat Handbook for LST retrieval. In this method, only TOA (Top of Atmosphere) radiance and NDVI (Normalized Difference Vegetation Index) are required. We converted TOA radiance of thermal infrared band to TOA (or at-sensor) brightness temperature based on the formula (Equation 1) (Chander et al., 2009; Jimenez- Munoz et al. 2014; Wang et al. 2016):

$$Tsensor = K1 / \ln (K2 / (L\lambda + 1)) \quad (1)$$

This single channel algorithm is where Tsensor is the at-sensor brightness temperature in Kelvin (K) and L is the TOA radiance in W/m2srum. For Landsat-8 TIRS, K1 is 774.89 W/(m2 srμm) and K2 is 1321.08 K for band 10 (USGS, n.d.). K1 and K2 are the Band-specific thermal conversion constants. For nighttime imagery we applied a single channel algorithm as well but used the closest available daytime date to extract the emissivity values. The following equation (Equation 2) calculates the LST based on the brightness temperature obtained previously using emissivity and (Artis & Carnahan, 1982). λ is the wavelength in meters and α=1.438 × 10^(-2) mK. εrepresents the surface emissivity which differs from various land cover types (Shen, Huang, Zhang & Wu, 2016). For ε, water (NDVI < 0) was assigned a value of 0.9925, urban impervious areas and bare soil (0 =< NDVI < 0.15) were assigned a value of 0.923, and vegetation (NDVI > 0.727) was assigned a value of 0.986. Otherwise, there was a modeling relationship with the NDVI values through the following equation

$$LST = Tsensor / ((1 + \lambda\ T\_sensor/\ \alpha) * \ln(\varepsilon)) \quad (2)$$

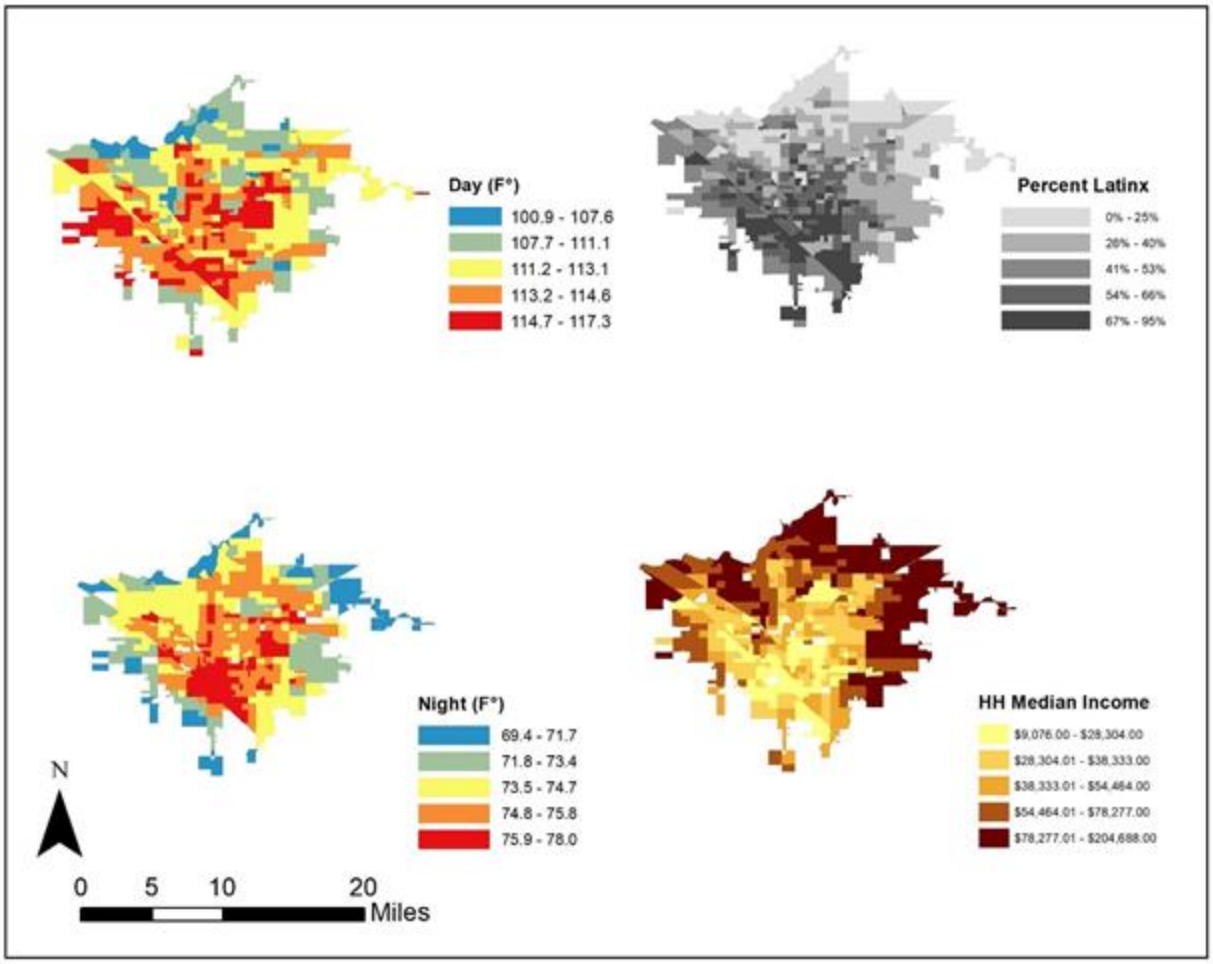

Figure 2.2: Fresno, California located at 36.7° N and 119.8° W: Surface Temperature for an Extreme Heat Day.

In order to establish a baseline of the relationship between surface temperature and neighborhood median household income and racial/ethnic minority composition throughout the 20 southwest metropolitan regions, we ran an Ordinary Least Squares (OLS) regression model using all block groups in the 20 metropolitan areas. We ran three models using the same independent variables of median income, percent LatinX, and percent black for an extreme heat day, an average heat day, and an average warm-season nighttime temperature. In all cases, LST was used as the dependent variable for urban heat. Because classic regression cannot take into

account the variation, we accounted for variation within metropolitan areas by using a fixed effects parameter on the regression (See Table 1: Appendix). In total nine OLS models were run.

Temp(scenario)~Demographic Variable+Population+factor(metro) Example: HotDay~ Income+Population +factor(metro) (3)

We found spatial autocorrelation of LST in 19 out of our 20 metropolitan regions indicated by statistically significant values of Moran's I (Cliff and Ord 1972). The urban environment has a complex matrix of surface materials and surface geometry and the orientation of both (Jun-Hyun et al. 2016),. This plus local convection, conduction, and incident solar radiation can cause spatial autocorrelation in LST readings (Yin et al. 2018). We found spatial autocorrelation of LST in 19 out of our 20 metropolitan regions indicated by statistically significant values of Moran's I (Cliff and Ord 1972). We controlled for this by running spatial error regression models.

In total, we constructed 59 spatial error models to analyze how social indicators of neighborhood demographics influenced the UHI effect: 20 models for extreme heat in each metropolitan area as well as 20 models for average heat. We ran only 19 models for nighttime temperatures due to issues accessing nighttime temperatures for the Dallas metropolitan area. The inferential statistics yielded from our models produce substantial results indicating thermal inequities between demographic groups. However, certain influences from biophysical variables could not be removed. Differences in elevation and proximity to water bodies, for example, may affect neighborhood temperatures. Literature related to socioeconomic inequities often compares population subsets such as the top and bottom deciles (Jones 2015). For our study, using these relatively large subsets of census block groups meant that the effect of such biophysical variables

would be minimized. This method also helps convey the extent of disparities between the poorest and wealthiest in society, and the wide gaps found today among different demographic groups. We thus performed a comparison of means by partitioning our data into deciles for each metropolitan area based on demographic values (income, percent LatinX, etc). We examined the average temperatures for block groups falling within the upper 10% of income throughout a metropolitan region to the mean of the lower 10% of income block groups, as well as upper and lower 10% of block groups by LatinX and black populations.

Results and Discussion

The OLS regression models were run for our three demographic variables (median income, percent LatinX, percent black population against our three temperature scenarios. In each equation population was also used as a control factor. The R2 values were all high indicating strong correlation (Table 1) however there was spatial autocorrelation in the dataset. Large thermal inequities existed for all of the urban regions we investigated. Low-income and LatinX populations were the most impacted. On average we found the poorest 10% of neighborhoods in each region to be about 2.2° C (4° F) hotter than the wealthiest on both extreme heat days and average summer days. The difference was as high as 3.3 to 4° C (6-7° F) in California metro areas such as Palm Springs and the Inland Empire. The neighborhoods that had the smallest differences were seen in Albuquerque and El Paso which also were the cities with the highest LatinX populations at 47.6% for Albuquerque and 83.6% for El Paso.
The top deciles of LatinX neighborhoods in each region were just under 2.2° C(4° F) hotter on average than the lowest decile in LatinX population, with disparities of up to nearly 7° F in some cases. Low-income and high-LatinX population neighborhoods are substantially correlated (-

0.4), with highly LatinX neighborhoods being among the poorest for many cities throughout the Southwestern U.S.

Top decile neighborhoods in black population saw modestly warmer temperatures of 0.5 to 1.1° C (1-2° F) compared to neighborhoods with the lowest black populations. However, black populations throughout southwestern metropolitan areas are relatively small and even the top decile neighborhoods still had low percentages of black population. Salt Lake City (<2.5% even for the top decile), Albuquerque (<3%), and El Paso (<3%) are good examples of this. Temperature disparities were far less at nighttime. On average across these 20 Southwestern U.S. metro areas we found the poorest 10% of neighborhoods in each region to be 2° F hotter than the wealthiest 10% at night, although this difference was as high as 2.5°C (4° F)in Los Angeles, the Inland Empire, and Palm Springs. We found the top decile of LatinX neighborhoods in each region to be 1° C (1.8° F) warmer on average than the lowest decile at night, although up to nearly 4.5° F in some urban regions. At night there did not appear to be a substantial temperature difference between the most heavily black neighborhoods and the least (<0.3° F), again with the caveat that black populations in most of these metro areas are relatively small.

All of our models and statistics support these thermal equity observations. We used regression models to elaborate on the benchmark set by the comparison of means test. These models are able to reveal clues about the direct associations between certain demographics and heat (see Table 1 in the Appendix). Across our sample of Southwestern U.S. metropolitan areas we found that a 10% decrease in income is associated with a 0.22 degree increase in temperature during daytime for both extreme heat and average heat days. At night temperatures were 0.09 degrees warmer for every 10% decrease in neighborhood income. Regression models controlling for spatial dependency yielded similar findings. We found negative associations between

temperature and income across all three temperature scenarios, meaning that higher neighborhood income results in cooler temperatures.

El Paso, Texas on an average heat day, and an extreme heat day had the highest regression coefficients for LatinX neighborhoods indicating a large thermal inequity for LatinX neighborhoods. In both temperature scenarios, Phoenix had the second highest regression coefficients for LatinX populations outside of California. Denver, Colorado had the highest income regression values for both average and extreme heat (Figure 2.6 and Figure 2.8) indicating a high thermal gradient between wealthier and poorer areas. Reno, Salt Lake City, and Albuquerque all also had high regression coefficients as well indicating wealthier neighborhoods were cooler substantially than lower income neighborhoods. All four of these cities configure with wealthier neighborhoods at higher elevations as the metro area encroaches on foothills of their local mountain ranges.

Since low-income and LatinX neighborhoods in many parts of the Southwest have little green space, high amounts of impervious surfaces, and higher urban density (e.g. Harlan et al. 2007; Harlan et al. 2019), it seems likely that these factors explain much about thermal disparities. Satellite imagery could verify this assumption, and further research could develop such an analysis. The implication would be that programs to increase vegetation within disadvantaged neighborhoods and reduce or lighten pavement and rooftops could help reduce thermal disparities between neighborhoods of different socioeconomic characteristics.

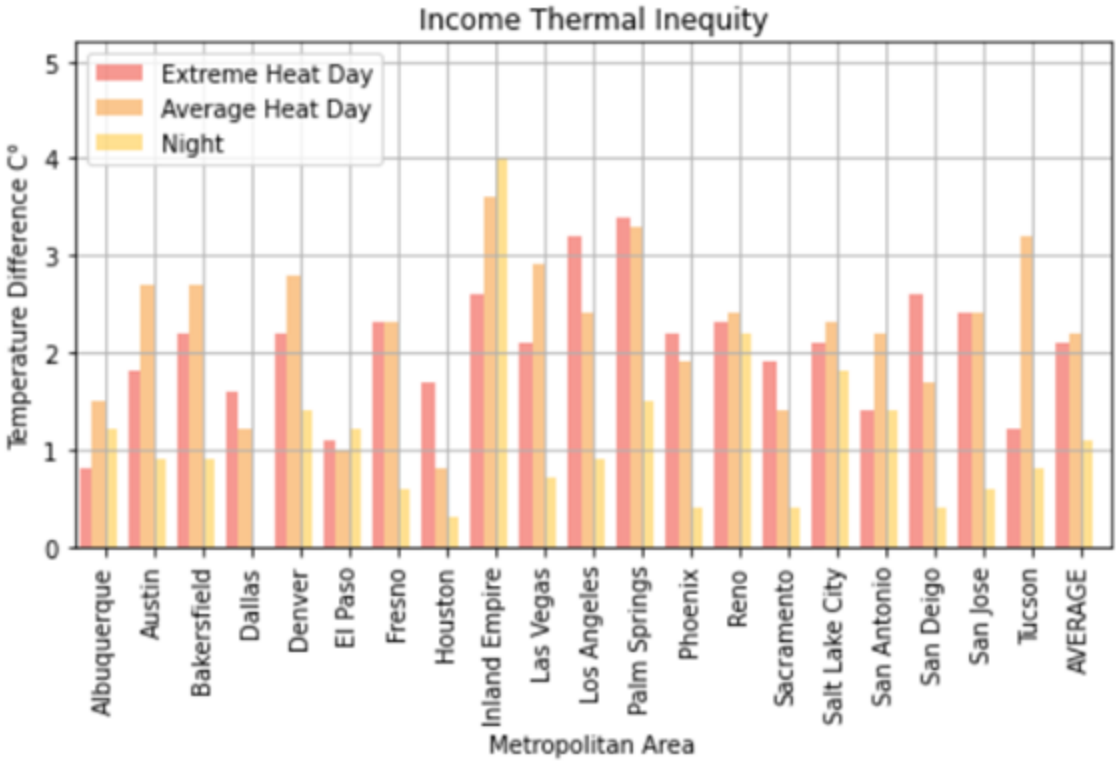

Figure 2.3:Income Thermal Inequity of Income (Right) and LatinX Population (left)a comparison of the temperature difference between the top 10 percentile of block groups and bottom 10 percentiles. of block group income.

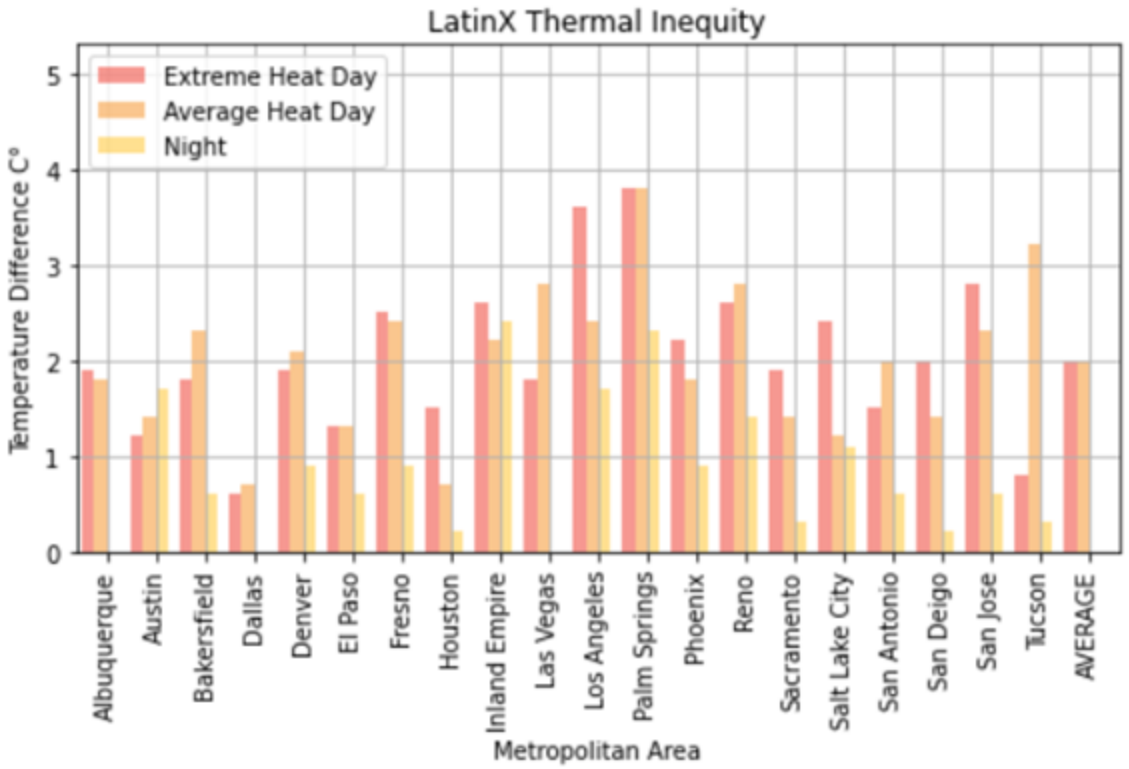

Figure 2.4:LatinX Thermal Inequity: a comparison of the temperature difference between the top 10 percentile of block groups and bottom 10 percentiles of LatinX block group population.

California

Because California represents a large proportion of our sample and is distinct from the rest of the Southwest in terms of its climate and demographics, we examined a subset of the data representing California cities and compared it with data for the rest of the Southwest. We ran additional regression models that separated California neighborhoods from the rest of the sample. We found that California urban regions had much larger temperature differences between wealthiest and poorest neighborhoods than regions in the rest of the Southwest. For extreme heat days the poorest decile of California neighborhoods in each region were 2.6°C (4.7°F) hotter on average than the wealthiest decile neighborhoods, compared to a mean difference of 1.7°C (3.1°F) in other Southwestern urban areas. For average heat days the mean difference was 2.5° C (4.5° F) in California metropolitan areas, compared with 2.1° C (3.8° F) in

other southwestern cities. Nighttime thermal differences in California were 1.3° C (2.2° F) on average, compared to 1° C (1.8° F) for Southwestern urban regions outside the state.

Temperature disparities experienced by LatinX California neighborhoods were similarly larger than those experienced outside the state. The highest decile block groups in terms of LatinX population in the California sample were 2.6° C and 2.3° C (4.7° and 4.1° F) warmer on extreme heat and average heat days respectively, compared with 1.5° C and 1.3° C (2.7° F and 3.1° F) for Southwestern cities outside of California. The largest differences occurred in the Inland Empire (3.6°C (6.5° F for an average heat day)), Palm Springs (3.8°C(6.9° F for an extreme heat day)), and Los Angeles (3.6°C(6.5° F for an extreme heat day)). Nighttime temperature disparities were not as great: 1.1° C (2° F) for California LatinX neighborhoods compared to 0.6° C (1.1° F) for Southwestern LatinX neighborhoods outside the state. Black neighborhoods in California urban regions experienced only slightly greater temperature disparities than in other Southwestern locations. On average heat days California's top-decile black neighborhoods were 0.9° C (1.6° F) warmer than their lowest-decile counterparts, while the average disparity in other Southwestern metro areas was 0.5° C (0.8°F). On extreme heat days in both groups' disparities were just under 1.1°C (2°F).

Regression analysis showed that for LatinX populations the associations for California neighborhoods were more than twice as large (6.41 vs. 2.92) as those for non-California neighborhoods on extreme heat days, and nearly three times as large (3.03 vs. 1.084) for nighttime temperatures. Our model predicts heavily LatinX neighborhoods (75th percentile) in California to be 1.8° C (3.2° F) degrees warmer than less densely populated LatinX neighborhoods (25th percentile) on an extreme heat day. This is nearly 3 times the disparity for LatinX neighborhoods in Southwestern urban areas outside of California. On average heat days

our model predicts that 75th percentile LatinX neighborhoods will be 1.7°C (3.1° F) degrees warmer than less densely LatinX neighborhoods in California, compared with a similar disparity of 0.7° C (1.3° F) degrees within metro regions in the rest of the Southwest. For black populations under extreme heat and average heat days the California coefficients were double those of non-California cities (See Appendix).

For average heat days Palm Springs, Bakersfield, and Fresno had the highest spatial regression coefficients substantially higher than other California cities (Figure 5). These same cities also had substantially higher coefficients in the extreme heat scenario indicating that there were greater thermal inequities in these three metro areas. In both daytime scenarios Sacramento had the lowest regression coefficients. Palm Springs and the Inland Empire had the highest regression coefficients for average and extreme heat days (Figure 6 and Figure 8), indicating that the highest income thermal inequities existed in these metro regions.

Reasons for greater thermal inequities in California likely concern vegetation and geography. While irrigated green space is not uncommon in Las Vegas and Phoenix, high-income California neighborhoods typically have more vegetation than their counterparts in other Southwestern urban regions. A history of state- and federally-funded water projects in California have made cheap water available to many residential developments. Additionally, California's physical environment appears to play a role in that higher-income neighborhoods are often located close to parks, water bodies, natural green space, or irrigated farmland. Urban regions such as Bakersfield and Fresno surround extensive irrigated agriculture. For urban regions such as San Jose and Palm Springs, nearby mountains may ameliorate temperatures within high-income neighborhoods. Wealthy neighborhoods in Sacramento may be disproportionately cooled by the American and Sacramento river greenways. In Los Angeles and San Diego, higher-

income neighborhoods are near the Pacific Ocean. Further research will be necessary to more precisely identify the role of such features in creating greater thermal inequities within California urban areas.

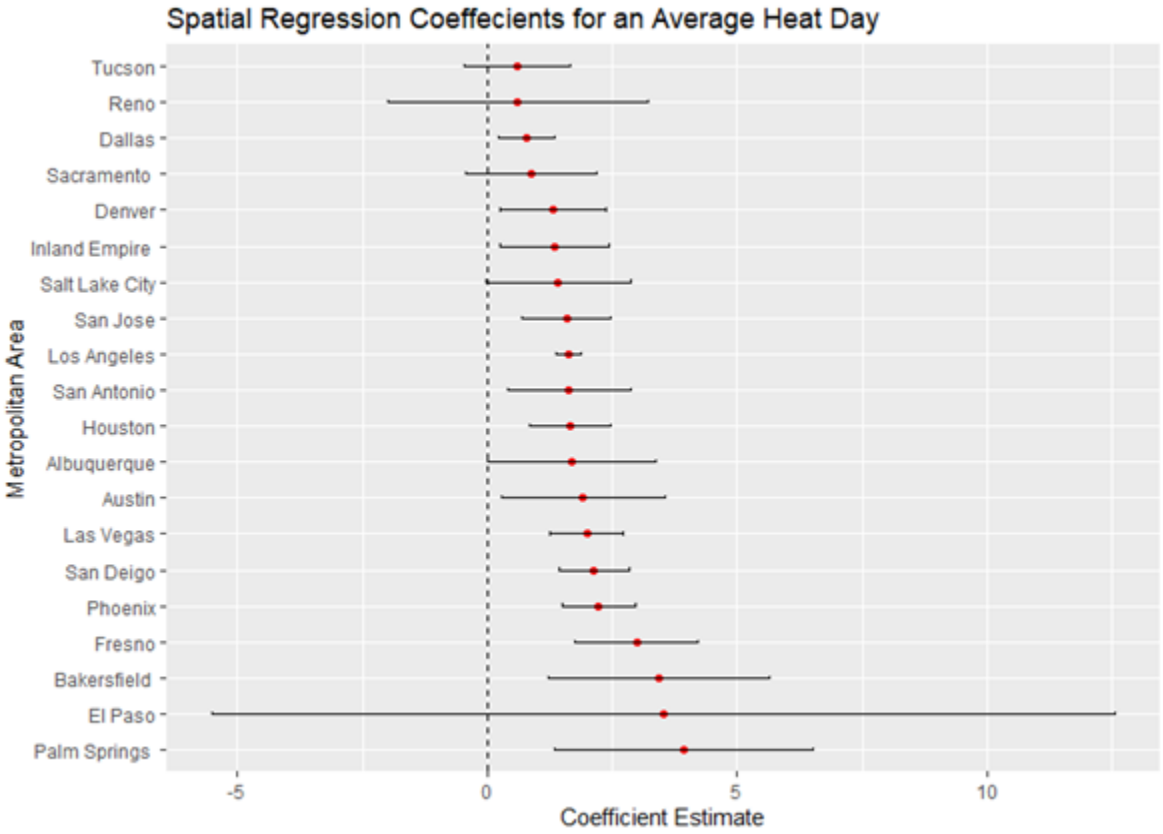

Figure 2.5:Spatial Regression Coefficients for LatinX Populations during an average heat day in 20 Southwest Metropolitan Areas

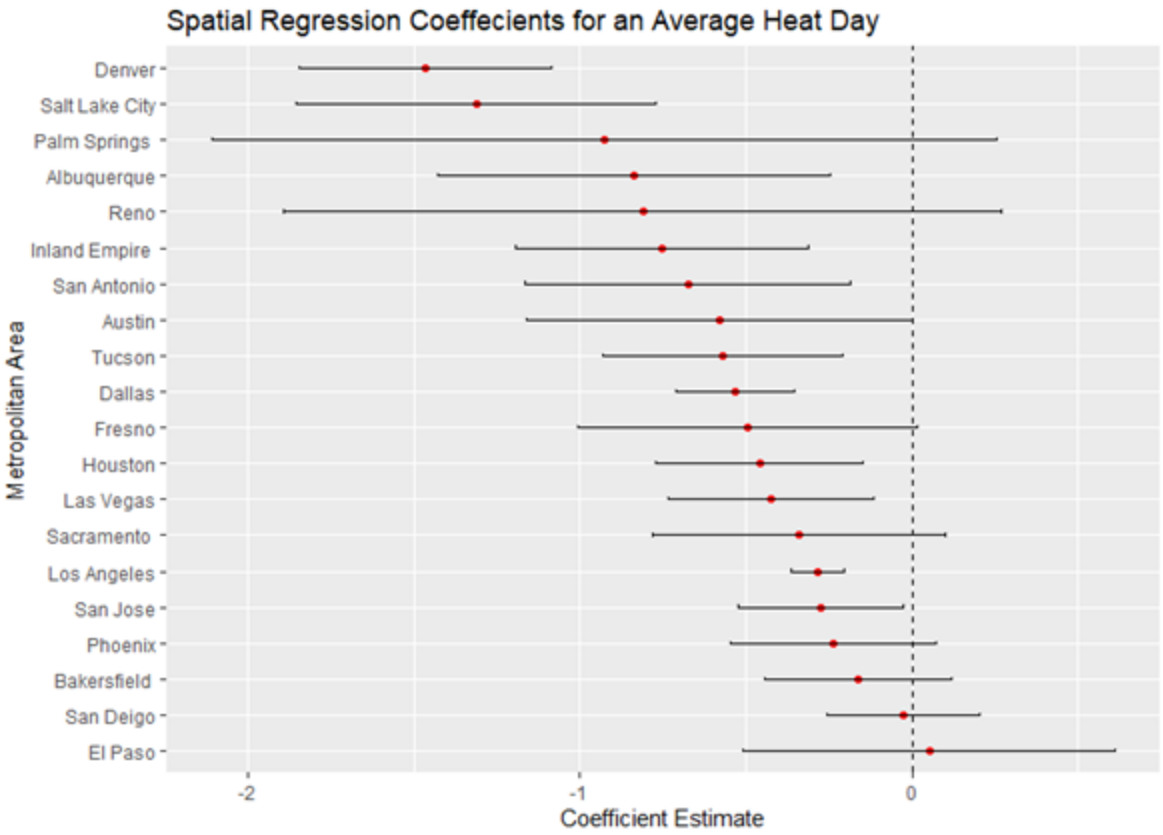

Figure 2.6: Spatial Regression Coefficients for median income during an average heat day in 20 Southwest Metropolitan Areas

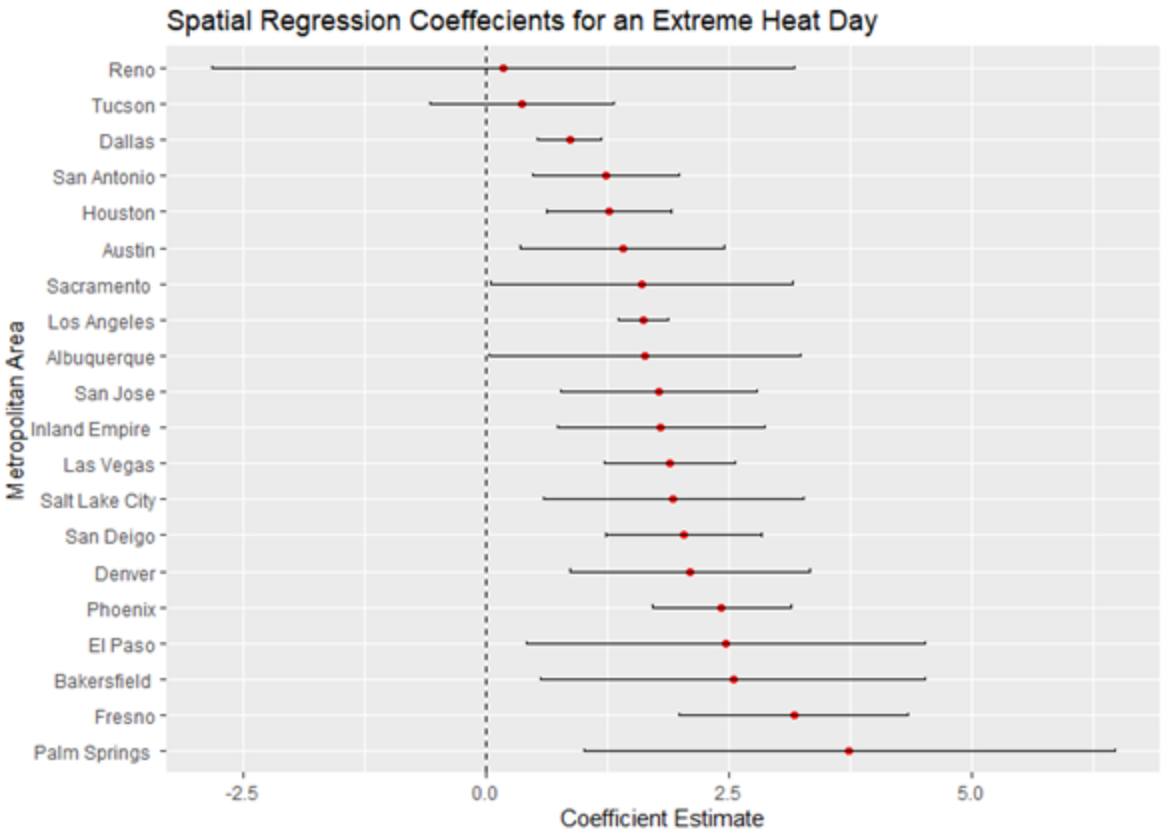

Figure 2.7: Spatial Regression Coefficients for LatinX Populations during an extreme heat day in 20 Southwest Metropolitan Areas

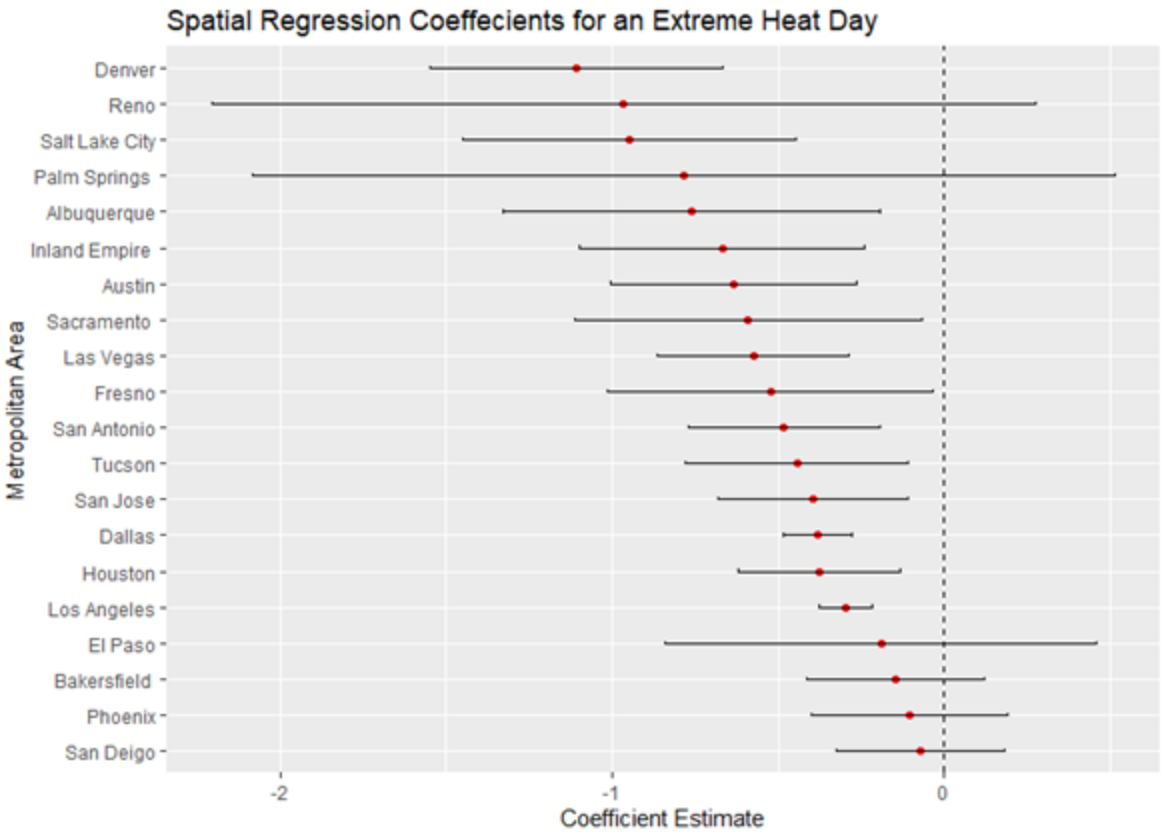

Figure 2.8: Spatial Regression Coefficients for median income during an extreme heat day in 20 Southwest Metropolitan Areas

Conclusion

Our in-depth analysis identifies large and consistent variations often 2.2-3.9°C (4-7° F) between neighborhoods of different class and racial composition within Southwestern U.S. urban regions. Although previous literature has documented thermal inequities elsewhere, we examined the largest number of urban regions at the most detailed scale to date under both day- and nighttime temperature scenarios. On both average and extreme heat days low-income neighborhoods of southwestern U.S. urban regions experience temperatures that are 3.9° C (7° F) higher in some cases and nearly 2.2°C (4° F) higher on average than those experienced by wealthy neighborhoods. The pattern is similar for neighborhoods with different levels of LatinX population. Income has a statistically significant relationship with average daytime heat, extreme

heat, and average nighttime heat. This trend is present in 56 of the 59 spatial error models that we ran. The same significance holds in regards to LatinX population. We found thermal inequalities to be most stark in California, perhaps because of greater amounts of irrigated landscape and agriculture as well as geographical factors mentioned earlier.

Although previous literature has shown heat inequities differences between wealthy and poor neighborhoods in other parts of the world (Wong et al. 2016; Mitchell. & Chakraborty 2018), our in-depth analysis highlights the extent of these disparities under summer daytime, nighttime, and extreme heat scenarios within 20 dryland urban regions at particular risk of high heat. We also looked specifically at percent LatinX a marginalized group throughout the southwestern United States. We also utilized a spatial error model to account for spatial autocorrelation which was prevalent in our biophysical and sociodemographic variables. Finally, although we presented results in majority dryland cities, we also included the humid cities of Houston, and Dallas.

The inequalities are most stark in California, perhaps because of greater amounts of irrigated landscape and agriculture as well as geographical factors, as mentioned earlier. California cities also show huge differences between the top decile and bottom decile of LatinX population neighborhoods compared to the rest of the southwest. These two variables appear highly correlated, as the highest LatinX neighborhoods are also the poorest for many cities throughout the southwest.

In this study we have shown substantial evidence regarding the thermal inequities that exist between income brackets as well as racial demographics to the overall body of literature on climate justice. On both average and extreme heat days residents of low-income neighborhoods of southwestern U.S. urban regions experience temperatures that are 3.9° C (7° F) higher in some

cases and nearly 2.5° C (4° F) higher overall than those experienced by residents of wealthy neighborhoods. The pattern is similar for LatinX populations. Income has a statistically significant relationship with average daytime heat, extreme heat, and average nighttime heat. This trend is present in 56 of the 59 spatial error models that we ran. The same pattern holds in regard to LatinX population.

Our study contributes strong new evidence to the body of literature on climate justice. Certain neighborhoods are shouldering a disproportionate burden of urban heat risk (Harlan et al. 2019). This disproportionate risk exists regardless of urban heat islands, i.e. whether the city is hotter than surrounding rural landscapes. Policy makers and stakeholders may utilize these findings for targeted mitigation protocols, for example involving increased vegetation, shading of paved surfaces, use of light-colored urban surface materials, and built form that creates ground-level shade. Cooling centers and other public health interventions may also be needed. Policies set forth to allocate resources and funds to neighborhoods that meet the criteria of certain income thresholds or demographics could be effective in smoothing the thermal inequity that is present in many cities.

While our study covers a robust set of metropolitan areas over a large geographic region, other cities within the US or elsewhere may show somewhat different patterns. More research is needed to fully develop understanding of neighborhood-scale thermal disparities within urban regions globally. Additionally, the satellite imagery used here, as in the large majority of urban heat studies, measures surface temperatures rather than ambient air temperatures. The latter is most relevant to human comfort and health, but must typically be measured in situ or estimated through modeling. Such techniques are difficult over large metropolitan areas. Finally, the demographics explored here are only a small subsection of the demographics that are potentially

at risk for unequal exposure to heat. Other variables of potential interest to future investigators include education, age, disability, citizenship, median housing value, and percentage of single parent households.

Appendix:

Model	All 20 Metro(R^2)	California (R^2)	Non-California (R^2)
Hot Day and Income	**-2.34(0.87)**	**-2.96 (0.72)**	**-1.51 (0.07)**
Average Day and Income	**-2.27 (0.91)**	**-3.28 (0.11)**	**-1.89 (0.09)**
Night and Income	**-0.90 (0.67)**	**-0.91 (0.24)**	**-0.79 (0.90)**
Hot Day and LatinX	**3.80 (0.87)**	**6.41(0.04)**	**2.92 (0.06)**
Average Day and LatinX	**5.38 (0.88)**	**6.05 (0.08)**	**3.22 (0.23)**
Night and LatinX	**2.37 (0.69)**	**3.03 (0.06)**	**1.08 (0.05)**
Hot Day and Black	**2.91 (0.84)**	**3.52 (0.67)**	**1.81 (0.93)**
Average Day and Black	**3.06 (0.86)**	**3.55 (0.03)**	**1.89 (0.02)**
Night and Black	**-0.16(0.69)**	**-0.76 (0.05)**	**-1.12 (0.00)**

Table A2.1 Regression Coefficients for the entire southwest as well as just California. These values indicate the strength of influence demographics have on surface temperature.

Metro	Extreme Heat	Average Heat	Nighttime
Albuquerque	26.9° -38.2° C 80.7-100.4° F	23.3°-33.2° C 73.4°-92° F	17.8°-23.2° 64-74.1°
Austin	30.2-36.9° C 86.4-98.4° F	22.4-33.3° C 72.4-92° F	11.8°-19.8° C 53.3-67.7° F
Bakersfield	41.6-50.1° C 106.9-122.2°F	32.7-43.9° C 90.8-111°F	22.2-26.1° C 71.2-79° F
Dallas	23.3-37.2°C 73.8-98.9° F	25.2-33.9° C 77.4-93° F	Not Available
Denver	30.2-41.9° C 86.4-107.4° F	21.5-39.4° C 70.7-102.9° F	8.7-14.9° C 47.7-58.9° F
El Paso	37.3-48.9° C 99.1-120° F	35-46.2° C 95-115.1° F	22.4-30.4° C 72.4-86.7° F
Fresno	38.3-47°C 100.9-116.6° F	33.4-42.2° C 92.2-108°F	20.8-25.6° C 69.4-78° F
Houston	25.9-38.4° C 78.6-101.2° F	21.8-35.7° C 71.3-96.3° F	22.8-26.6° C 73-79.8° F
Inland Empire	36-47.8° C 97.5-118°F	28.2-42.8° C 82.7-109° F	18.6-24.7° C 65.4-76.5° F
Las Vegas	37.4-48.2°C 99.3-118.7°F	37.3-45.6°F 98.5-114.4°F	20.7-27.9° C 69.2-82.3°F

Los Angeles	27.2-42.2° C 81-107.9° F	25.6-40.7° C 78.2-105.3° F	13.7-21.2° C 56.6-70.1°F
Palm Springs	40.7-49.5° C 105.2-121°F	37.9-46.7° C 100.3-116° F	23.3-28.5°C 73.7-83.3° F
Phoenix	37.8-49.5°C 1001.1- 121.1°F	36.4-47.1°C 97.5- 116.7°F	23.6-32.1°C 74.5-89.8°F
Reno	33.1-48.4° C 91.5-119.1°F	26.1-39.1°C 79-102.3°F	13-20.7°C 55.4-69.2°F
Sacramento	34.3-47.2°C 93.7-117.1°F	27.7-38.4°C 81.9- 101.2°F	14.2-17.2°C 57.6-62.9°F
Salt Lake City	30.1-43.7°C 86.2-110.6°F	25.2-38.7°C 77.3- 101.6°F	8.7-21.8°C 47.6-71.2°F
San Antonio	30.2-36.5°C 86.3-97.7°F	24.1-32.6°C 75.4-90.6°F	18.3-21.4°C 65-70.5° F
San Diego	27.3-43.5° C 81.1-110.3°F	24.3-37.7°C 75.8-99.8°F	16.3-21.8°C 61.4-71.2°F
San Jose	35-46.6° C 95-115.8°F	24.8-36.2°C 76.7-97.2°F	15-19.6°C 59-67.3°F
Tucson	36.7-43.8°C 98-110.8° F	30.8-40.2°C 87.4- 104.4°F	22.7-27.1°C 72.8-80.8°F

Table A2.2: Land Surface Temperature ranges of each metro area for the three temperature scenarios investigated

References

Abunnasr, Y. (2013). Climate change adaptation: A green infrastructure planning framework for resilient urban regions. University of Massachusetts Amherst.

Akbari, H. et al. (2016) Local climate change and urban heat island mitigation techniques – the state of the art. Journal of Civil Engineering and Management. 22(1) 1-16.

Araujo, R.V., Albertini, M.R., Costa-da-Silva, A.L., Suesdek, L., Franceschi, N.C.S., Bastos, N.M., Katz, G., Cardoso, V.A., Castro, B.C., Capurro, M.L. and Allegro, V.L.A.C.(2015). São Paulo urban heat islands have a higher incidence of dengue than other urban areas. The Brazilian Journal of Infectious Diseases, 19(2), 146-155.

Bullard RD,Wright B. Race, Place, and Environmental Justice After Hurricane Katrina: Struggles to Reclaim, Rebuild, and Revitalize New Orleans and the Gulf Coast. Boulder, CO: Westview Press; 2009.

Chander, G., Markham, B. L., & Helder, D. L. (2009). Summary of current radiometric calibration 108coeffecients for Landsat MSS, TM, ETM+, and EO-1 ALI sensors. Remote Sensing of Environment 113(5), 893-903.

Chow, W.T.L., Chuang, W.-C., Gober, P., 2012. Vulnerability to extreme heat in metropolitan phoenix: spatial, temporal, and demographic dimensions. Professional Geographer, 64(2), 286–302.

Cliff, A., & Ord, K. (1972). Testing for spatial autocorrelation among regression residuals. Geographical analysis, 4(3), 267-284.

Darmofal, D. (2015). Spatial Lag and Spatial Error Models. In Spatial Analysis for the Social Sciences (Analytical Methods for Social Research, pp. 96-118). Cambridge: Cambridge University Press. doi:10.1017/CBO9781139051293.00

De la Barrera, F., Henriquez, C., Ruiz, V., & Inostroza, L. (2019, February). Urban Parks and Social Inequalities in the Access to Ecosystem Services in Santiago, Chile. In IOP Conference Series: Materials Science and Engineering (Vol. 471, No. 10, p. 102042). IOP Publishing.

Declet-Barreto, J., Brazel, A. J., Martin, C. A., Chow, W. T., & Harlan, S. L. (2013). Creating the park cool island in an inner-city neighborhood: heat mitigation strategy for Phoenix, AZ. Urban Ecosystems, 16(3), 617-635.

Dialesandro, J. M., Wheeler, S. M., & Abunnasr, Y. (2019). Urban heat island behaviors in dryland regions. Environmental Research Communications, 1(8), 081005.

Fotheringham, A. S., Brunsdon, C., & Charlton, M. (2003). Geographically weighted regression: the analysis of spatially varying relationships. John Wiley & Sons.

Flocks, J., Escobedo, F., Wade, J., Varela, S., & Wald, C. (2011). Environmental justice implications of urban tree cover in Miami-Dade County, Florida. Environmental Justice, 4(2), 125-134.

Giridharan, R., & Emmanuel, R. (2018). The impact of urban compactness, comfort strategies and energy consumption on tropical urban heat island intensity: a review. Sustainable cities and society, 40, 677-687.

Harlan, S. L., Brazel, A. J., Darrel Jenerette, G., Jones, N. S., Larsen, L., Prashad, L., & Stefanov, W. L. (2007). In the shade of affluence: the inequitable distribution of the

urban heat island. In Equity and the Environment (pp. 173-202). Emerald Group Publishing Limited.

Harlan, S. L., Chakalian, P., Declet-Barreto, J., Hondula, D. M., & Jenerette, G. D. (2019). Pathways to climate justice in a desert metropolis. People and Climate Change: Vulnerability, Adaptation, and Social Justice, 23.

Hess, J.J.; Eidson, M.; Tlumak, J.E.; Raab, K.K.; George, L. An evidence-based public health approach to climate change adaptation. Environ. Health Perspect. 2014, 122, 1177–1186.

Hoffman, J. S., Shandas, V., & Pendleton, N. (2020). The Effects of Historical Housing Policies on Resident Exposure to Intra-Urban Heat: A Study of 108 US Urban Areas. Climate, 8(1), 12.

Hsieh, C.M, Aramaki, T., Hanaki, K. (2007). The feedback of heat rejection to air conditioning load during the nighttime in subtropical climate. Energy and Buildings, 39, 1175–1182.

Hondula, D.M., Barnett, A.G., 2014. Heat-related morbidity in Brisbane, Australia: spatial variation and area-level predictors. Environmental. Health Perspectives 122 (8), 831–836. https://doi.org/10.1289/ehp.1307496.

Kolosna, C., & Spurlock, D. (2019). Uniting geospatial assessment of neighborhood urban tree canopy with plan and ordinance evaluation for environmental justice. Urban Forestry & Urban Greening, 40, 215-223.

Kuo, F. E. (2001). Coping with poverty: Impacts of environment and attention in the inner city. Environment and behavior, 33(1), 5-34.

Leal Filho, W., Icaza, L. E., Neht, A., Klavins, M., & Morgan, E. A. (2018). Coping with the impacts of urban heat islands. A literature based study on understanding urban heat vulnerability and the need for resilience in cities in a global climate change context. Journal of cleaner production, 171, 1140-1149.

Jiménez-Muñoz, J. C., Sobrino, J. A., Skoković, D., Mattar, C., & Cristóbal, J. (2014). Land surface temperature retrieval methods from Landsat-8 thermal infrared sensor data. IEEE Geoscience and remote sensing letters, 11(10), 1840-1843.

Jones, C. I. (2015). Pareto and Piketty: The macroeconomics of top income and wealth inequality. Journal of Economic Perspectives, 29(1), 29-46.

Kim, J. H., Gu, D., Sohn, W., Kil, S. H., Kim, H., & Lee, D. K. (2016). Neighborhood landscape spatial patterns and land surface temperature: An empirical study on single-family residential areas in Austin, Texas. International journal of environmental research and public health, 13(9), 880.

Konisky, D. M. (2016). Environmental justice delayed: Failed promises, hope for the future. Environment: Science and Policy for Sustainable Development, 58(2), 4–15.

Locke, D., Hall, B., Grove, J.M., Pickett, S.T., Ogden, L.A., Aoki, C., Boone, C.G. and O'Neil-Dunne, J.P., (2020). Residential housing segregation and urban tree canopy in 37 US Cities.

Macintyre, H. L., Heaviside, C., Taylor, J., Picetti, R., Symonds, P., Cai, X. M., & Vardoulakis, S. (2018). Assessing urban population vulnerability and environmental risks across an urban area during heatwaves–Implications for health protection. Science of the total environment, 610, 678-690.

Mihalakakou, G., Santamouris, M., Papanikolaou, N., Cartalis, C., & T. Sangrassoulis, A. (2004). Simulation of the urban heat island phenomenon in Mediterranean climates. Pure and Applied Geophysics, 161(2), 429–451.

Miner, M. J., Taylor, R. A., Jones, C., & Phelan, P. E. (2017). Efficiency, economics, and the urban heat island. Environment and Urbanization, 29(1), 183-194.

Mitchell, B. C., & Chakraborty, J. (2014). Urban heat and climate justice: a landscape of thermal inequity in Pinellas County, Florida. Geographical Review, 104(4), 459-480.

Mitchell, B. C. & Chakraborty, J. (2018a). Thermal inequity: the relationship between urban structure and social disparities in an era of climate change. In Jarfy, Tahseen, ed. Routledge Handbook of Climate Justice. London: Routledge.

Mitchell, B. C., & Chakraborty, J. (2018b). Exploring the relationship between residential segregation and thermal inequity in 20 US cities. Local Environment, 23(8), 796-813.

Morello-Frosch, R., Pastor, M., & Shonkoff, S. B. (2009). The climate gap. Los Angeles, CA: USC Center for sustainable cities, University of Southern California.

Oke, T. R. 1976. “The Distinction between Canopy and Boundarylayer Urban Heat Islands.” Atmosphere 14 (4): 268–77.

Oke, T. R. (1982). The energetic basis of the urban heat island. Quarterly Journal of the Royal Meteorological Society, 108(455), 1-24.

Ramírez-Aguilar, E. A., & Souza, L. C. L. (2019). Urban form and population density: Influences on Urban Heat Island intensities in Bogotá, Colombia. Urban Climate, 29, 100497.

Rizwan, A. M., Dennis, L. Y., & Chunho, L. I. U. (2008). A review on the generation, determination and mitigation of Urban Heat Island. Journal of Environmental Sciences, 20(1), 120-128.

Sass, C. K., Lodder, R. A., & Lee, B. D. (2019). Combining biophysical and socioeconomic suitability models for urban forest planning. Urban forestry & urban greening, 38, 371-382.

Schlosberg, D., & Collins, L. B. (2014). From environmental to climate justice: climate change and the discourse of environmental justice. Wiley Interdisciplinary Reviews: Climate Change, 5(3), 359-374.

Sera, F., Armstrong, B., Tobias, A., Vicedo-Cabrera, A. M., Åström, C., Bell, M. L. & Dang, T. N. (2019). How urban characteristics affect vulnerability to heat and cold: A multi-country analysis. Int. J. Epidemiol., 1-12.

Sharma, A., Woodruff, S., Budhathoki, M., Hamlet, A. F., Chen, F., & Fernando, H. J. S. (2018). Role of green roofs in reducing heat stress in vulnerable urban communities—A multidisciplinary approach. Environmental Research Letters, 13(9), 094011.

Tang, Z., Zheng, H., Ren, Z., Zhang, D., Wang, P., Zhai, C., ... & He, X. (2018). Evaluating environmental equities of urban forest in terms of cooling services using ETM+ and Google data. Journal of the Indian Society of Remote Sensing, 46(2), 287-296.

Taylor, J., Wilkinson, P., Davies, M., Armstrong, B., Chalabi, Z., Mavrogianni, A., Symonds, P., Oikonomou, E. and Bohnenstengel, S.I., (2015). Mapping the effects of urban heat island, housing, and age on excess heat-related mortality in London. Urban Climate, (14).517-528.

USGS EROS (2017) Landsat Collection 1 Level 1 Product Definition. Retrieved fromhttps://landsat.usgs.gov/sites/default/files/documents/LSDS-1656_Landsat_Level-1_Product_Co

United Nations. World Urbanization Prospects: The 2018 Revision (st/esa/ser.A/420); United Nations, Department of Economic and Social affairs, Population Division: New York, NY, USA, 2019.

Voelkel, J., Hellman, D., Sakuma, R., & Shandas, V. (2018). Assessing vulnerability to urban heat: A study of disproportionate heat exposure and access to refuge by socio-demographic status in Portland, Oregon. International journal of environmental research and public health, 15(4), 640.

Wald, A. (2019). Emergency Department Visits and Costs for Heat-Related Illness Due to Extreme Heat or Heat Waves in the United States: An Integrated Review. Nursing Economic, 37(1).

Weng, Q., Liu, H., Liang, B., & Lu, D. (2008). The spatial variations of urban land surface temperatures: pertinent factors, zoning effect, and seasonal variability. IEEE Journal of Selected Topics in Applied Earth Observations and Remote Sensing, 1(2), 154-166.

Wheeler, S. M., Abunnasr, Y., Dialesandro, J., Assaf, E., Agopian, S., & Gamberini, V. C. (2019). Mitigating Urban Heating in Dryland Cities: A Literature Review. Journal of Planning Literature, 34(4), 434-446.

Wilson, S. M., Richard, R., Joseph, L., & Williams, E. (2010). Climate change, environmental justice, and vulnerability: an exploratory spatial analysis. Environmental Justice, 3(1), 13-19.

Wong, M. S., Peng, F., Zou, B., Shi, W. Z., & Wilson, G. J. (2016). Spatially analyzing the inequity of the Hong Kong urban heat island by socio-demographic characteristics. International journal of environmental research and public health, 13(3), 317.

Wong, M. S., Ho, H. C., Yang, L., Shi, W., Yang, J., & Chan, T. C. (2017). Spatial variability of excess mortality during prolonged dust events in a high-density city: a time-stratified spatial regression approach. International journal of health geographics, 16(1), 26.

Flocks, J., Escobedo, F., Wade, J., Varela, S., & Wald, C. (2011). Environmental justice implications of urban tree cover in Miami-Dade County, Florida. Environmental Justice, 4(2), 125-134.

Yang, X., & Jin, W. (2010). GIS-based spatial regression and prediction of water quality in river networks: a case study in Iowa. Journal of Environmental Management, 91(10), 1943-1951.

Yang, L., Jin, S., Danielson, P., Homer, C., Gass, L., Bender, S. M., Case, A., Costello, C., DeWitz, J., Fry, J., & Funk, M. (2018). A new generation of the United States National Land Cover Database: Requirements, research priorities, design, and implementation strategies. ISPRS journal of photogrammetry and remote sensing, 146, 108-123.

Yin, C., Yuan, M., Lu, Y., Huang, Y., & Liu, Y. (2018). Effects of urban form on the urban heat island effect based on spatial regression model. Science of the Total Environment, 634, 696-704.

Zhang, Y., Murray, A. T., & Turner Ii, B. L. (2017). Optimizing green space locations to reduce daytime and nighttime urban heat island effects in Phoenix, Arizona. Landscape and Urban Planning, 165, 162-171.

Zhou, W., Wang, J., & Cadenasso, M. L. (2017). Effects of the spatial configuration of trees on urban heat mitigation: A comparative study. Remote Sensing of Environment, 195, 1-12.

Chapter 3: Reducing thermal inequity: Identifying vulnerable neighborhoods and heat mitigation potential for urban cooling in two California cities

Abstract:
Exposure to heat exacerbated by an increase in urbanization as well as increasing global temperatures has become a growing concern for cities and their residents. Excess heat can cause increased heat-related morbidity, mortality, and energy costs. Vulnerability to heat-related illnesses is often correlated to demographics, socioeconomic status, and pre-existing health conditions. Identifying mitigation techniques of urban heat is thus a policy priority and often involves increasing green space and shading as well as reducing low-albedo paved surfaces. In this study we analyze two demographically diverse cities in Southern California--Fresno, and Bakersfield, experiencing increasing urban temperatures. We used Landsat 8 Operational Land Imager (OLI) and Thermal Infrared Sensor (TIRS), and ECOsystem Spaceborne Thermal Radiometer Experiment on Space Station (ECOSTRESS) imagery to identify areas of highest heat based on land surface temperature for both day and night. We also used socioeconomic data from the American Community Survey to derive vulnerability indices and heat priority scores using a Principal Component Analysis (PCA) at the block group level. In addition, we utilized the Integrated Valuation of Ecosystem Services and Tradeoffs (InVEST) urban cooling model that uses inputs of land use/land cover, tree canopy, building material and intensity to model current and future thermal scenarios at a detailed scale for the three California cities. Our results show that the most vulnerable populations to extreme heat are nonwhite populations, those over 65 and living alone, and those with limited English language proficiency. In addition, we found that low income neighborhoods had significantly less tree canopy (>10%) than their wealthier neighborhoods. By modeling 10 and 25% increases of tree canopy and albedo we found increasing tree canopy on developed land uses by as little as 10% could lead to a decrease in

temperatures of 1.2° C (2° F) or more throughout the cities, and made a greater difference for low income block groups compared to higher income block groups. The cooling impact of urban trees based on the InVEST model extended up to 2 kilometers. Increasing albedo of paved surfaces by 10% resulted in a non substantial decrease in temperatures throughout the cities. Our research using this model showed that increasing tree canopy is more effective at mitigating high temperatures for vulnerable neighborhoods than decreasing albedo, and high vulnerability neighborhoods.

Introduction and Background

Urban Heat is a public health hazard that impacts all cities in the western United States. Excess urban heat exacerbated by extreme temperature events has become the leading cause of weather-related deaths, outpacing both floods and wildfires (Weinberger et al., 2017; Livingston 2021). Besides increased mortality, urban heat can cause heat-related illnesses including heatstroke, exhaustion, and amplified respiratory and cardiovascular issues as well as high energy costs (Wald, 2019). Cities in the United States are expected to see increases in temperatures throughout the twenty-first century and thus increased heat strain on their populations (Krayenhoff et al., 2018).

The Southwestern US and especially the State of California have experienced rapid urbanization over the last half century due to significant domestic and international migration. Urbanization has replaced natural desert shrubland, mediterranean scrubland and soils with impervious surfaces and irrigation fed green space oases. While the green spaces in desert cities have been found to form “park cool islands”, impervious surfaces are still ubiquitous to the urban heat island (UHI) effect. The UHI has several negative impacts on a population’s health as well as declines in overall ecosystem services. UHI’s can speed up the formation of smog (Mihalakakou et al. 2004), cause increase in energy use for cooling (Giridharan and Emannual 2018), lead to heat related sickness or mortality (Taylor et al. 2015), and has even been found to exacerbate the spread of vector borne diseases like dengue fever (Araujo et al. 2015).

While it has long been established that larger and denser populations are associated with higher temperatures (Ramirez-Aguilar et al. 2019), the relationship between higher temperatures and neighborhood racial and socioeconomic composition is less explored. Environmental Justice defined by the U.S. Environmental Protection Agency (EPA) as "the fair treatment and meaningful involvement of all people regardless of race, color, national origin, or income with respect to the development, implementation, and enforcement of environmental laws, regulations, and policies' (Konisky 2016) has emerged and taken center stage with urban climate research. In particular, investigation into patterns of exposure, vulnerability, and resilience amongst vulnerable population groups (e.g. underrepresented, impoverished or otherwise disadvantaged minorities) to the UHI effect has risen in the literature. UHI's have been proven to be very costly to cities. Phoenix alone was estimated to lose 436 million dollars a year from costs related to cooling and mitigation efforts due to increased urban temperatures (Miner et al. 2017). Air conditioning use alone has also been proven to contribute to UHIs completing a negative feedback cycle. A study in Taipei found that peak use of air conditioning caused an increase of almost 2° C (Hsieh et al. 2007). Socioeconomic factors are related to the degree to which a population is impacted, subject to, and vulnerable to UHIs (Sharma et al. 2018). Age, educational status, income and housing status have all been found to be correlated with temperature. Older, low income, and minority populations have all been found to be disproportionately impacted by increases in urban temperatures (Harlan et al. 2007; Wilson et al. 2010). Income specifically has been found to be related to increased urban temperatures. Increases in median income of $10,000 were found to cause a decrease 0.28° C in Phoenix, Arizona (Jenerette et al. 2007), while another study in Santiago, Chile found low income neighborhoods to have temperatures of 2.5-3.3° C higher than high income neighborhoods (De

La Berrera et al. 2019). Temperatures throughout the southwest were also found to be 4-7° F warmer in neighborhoods of low income compared to wealthy neighborhoods, and LatinX neighborhoods were found to have the same level of temperature inequity (4-7° F) compared to non LatinX neighborhoods (Dialesandro et al. 2021).

A factor explaining inequalities in heat exposure is the greater prevalence of trees and vegetation in more advantaged neighborhoods. Studies have found greater tree cover in White neighborhoods with LatinX, and Black neighborhoods having higher potential areas for tree canopy (Flocks et al. 2011). These results indicate that heat mitigation potential from tree canopies in LatinX, and Black neighborhoods exceeds that in white neighborhoods due to LatinX and Black neighborhoods having far fewer trees, but far more plantable space (>15% more). In an analysis of 37 US cities, Locke et al. (2021) found that neighborhoods that were historically redlined had 23% less tree canopy than city averages. Benefits of green space go beyond strictly cooling. Green space has been proven to improve cognitive activities of its residents and has even been proven to cause a decrease in crime (Kuo 2001; Flocks et al. 2011). While Urban greening can benefit populations greatly, creation of greenspace can have paradoxical impacts such as driving up property costs and gentrification (Wolch et al. 2014). With mitigation strategies like greenspace proven to provide ecological benefits, and cooling for UHIs, and the pattern of these amenities often absent or complex in low income areas, the thermal and monetary gap appears to be widening (Declet-Barreto 2013). Lack of amenities or resources for mitigation make populations vulnerable to urban heat (Reid et al. 2009).

A number of demographic and biophysical variables have been found to be related to heat vulnerability. Vulnerable populations as well as the urban fabric that is most common in these neighborhoods not only make them more susceptible to heat but also other environmental hazards (Colon et al. 2020). Vulnerability indices generally are developed from sets of sociodemographic data oftentimes at census level scales such as tract or block groups. The set of variables included in an index varies from location to location and are informed via past research derived evidence on what populations have exhibited adverse effects to environmental hazards (Cutter et al. 2003).

Reid et al. (2009) developed a methodology that combined demographic variables, health indicators, and satellite derived vegetation values to obtain vulnerability metrics to heat related morbidity and mortality. This approach has been replicated for cities across the United States in both academic studies, and studies through public health departments (Seroka et al. 2011; Nayak et al. 2018). Harlan et al. (2013) found indices that included elderly and isolated, as well as areas of low vegetation as predictors of heat related deaths. Varying degrees of data resolution or complete lack thereof however can make it challenging to compare vulnerability indices between regions, climates, and even within cities. Additionally, Watkins et al. (2021) found vulnerability indices may not accurately reflect feelings of vulnerability by populations based on the residents' experience of enduring extreme heat in Phoenix, Arizona.

Principal component analysis (PCA) is a technique commonly used to construct heat vulnerability indices (Reid et al. 2009). The appeal of PCA lies in its ability to reduce data by observing the data through different orthogonal planes and refine correlated variables into new independent factors. The number of factors will be equal to the number of variables being subject to the PCA, Thus a suit of 10 demographic and biophysical variables will derive 10 components. The final number of PCA's used can be driven by user defined parameters such as choosing the cumulative explained variance ratio, using a spree plots, or choosing only principal components that had eigenvalues greater than one to be retained (Kaiser, 1960).

More recently studies have emerged in the literature that use habitat modeling to determine areas of cities for implantation of urban forests using low income numbers as a factor candidate to identify highly suitable areas in an effort to prioritize areas previously sharing unequal burden of urban heat island impacts (Sass et al. 2019). The InVEST (Integrated Valuation of Ecosystem Services and Tradeoffs) Urban Cooling Model from Stanford's Natural Capital project can be utilized to highlight opportunities for prioritization of UHI heat mitigation measures throughout cities (Bosch et al. 2020). Milan, Italy and Minneapolis, Minnesota have been studied (Ronchi et al. 2020; Londsdorf et al. 2021). Furthermore, using the InVEST Urban Cooling Model, Kadaverugu et al. 2021 found a 0.5° C cooling potential in neighborhoods near parks in Nagpur City, India. Finally, InVEST urban cooling and heat mitigation model results have been validated through linear regression using land surface temperature data(Zawadzka and Corstanje 2021).

This study seeks to identify the neighborhood demographic and biophysical characteristics associated with higher temperatures. The populations within the hottest areas will be classified as enduring an inequitable amount of the burden from the urban heat. We will compare two major cities, Fresno and Bakersfield, located in the Central Valley, California which both have high LatinX and low income populations (Bohn and Thorman 2020). Additionally, using the InVEST Urban Cooling Model we seek to examine the cooling potential of spatially explicit planning interventions such as increasing tree canopy within both cities. Finally we will model how increases in albedo as well as combined increases in tree canopy and albedo in the built environment could impact temperature in these cities. Specifically we will examine how increases in tree canopy of 10% and 25% and 10% and 25% increases in the surface albedo of built surfaces would impact the thermal environment of Fresno and Bakersfield. Finally, we will model a combination of mitigation measures consisting of a 25% increase in tree canopy and a 10% increase in surface albedo.

Methodology

The two cities of Bakersfield and Fresno, located in the southern San Joaquin Valley were selected based on them being the largest metropolitan areas in the region, and their dryland climate where water resources are strained. For both cities the American Community Survey and the Census Block group level demographic data(United States Census Bureau, 2019) were acquired for the years 2015-2019. In addition, 2016 land cover data from the National Land Cover Dataset from the Multi-Resolution Land Characteristics (MRLC) Consortium as well as the imperviousness product which shows percent of impervious surface in each 30 meter pixel area derived from Landsat data (Yang et al. 2019). We also used tree canopy data from the California Forest Observatory, and local GIS data for building footprints.

City	Population	Mean summer High	Annual Precipitation (mm)	% Impervious Surface	% Tree Canopy
Bakersfield	384,000	35.6° C (96° F)	185	56%	13%
Fresno	542,000	35 ° C (95° F)	320	44%	7%

Table 3.1: Summary statistics of the two cities under investigation

Utilizing Google Earth Engine (GEE), we downloaded the Landsat 8 Operational Land Imager (OLI) Tier 1 product from their online image repository. Using the javascript enabled GEE we extracted at-sensor (or Top-of-Atmosphere (TOA)) reflectance. Here we used reflectance data for the retrieval of land surface temperature (LST) and Normalized Difference Vegetation Index (NDVI). The geometric fidelity of the Landsat Collections has a Root Mean Square Error (RSME) of less than 12 meters (USGS 2017). All the imagery was projected into WGS 1984 UTM Zone 10 N. Dates were selected for cloud free periods in the summer season. Nighttime LST and evapotranspiration (ET) were acquired using data from ISS ECOSTRESS and filtered by a time period of 2018-2020 June to September (ECOSTRESS had June 2018 launch) from the NASA Application for Extracting and Exploring Analysis Ready Samples (AppEEARS). Using ArcPRO we created a median raster to summarize evapotranspiration for the full study period by inputting the rasters in the 'Cell Statistics' tool in the Spatial Analyst toolbox and selecting the 'median' function. The output was a single raster where each pixel is the median evapotranspiration value across the full study period. We next converted the ET values from W m-2 to mm day-1 and normalized the values before using them as an input for InVEST. The unit conversion was done using a conversion factor from the Food and Agriculture Organization of the United Nations (FAO) Irrigation and Drainage Paper No. 56, Table 1 (Allen et al. 1998) where 0.408 mm day-1 = 1 MJ m-2 d-1, shown by Equation 1 below.

$$ET_A[mm\ day^{-1}] = ET_B[W\ m^{-2}] * 0.0864\ \left[\frac{MJ\ day^{-1}}{W}\right] * 0.408\ \left[\frac{mm\ day^{-1}}{MJ\ day^{-1}\ m^{-2}}\right]$$

Equation (1)

where ETA and ETB are the numerical values of the evapotranspiration rate in unit of [mm day-1] and [W m-2] respectively

Demographic data were extracted at the block group level from the 2015-2019 5 year American Community Survey (ACS) for the two study regions. The variables were calculated as a percent population based on the total number of respondents for each block group. Ancillary data such as tree canopy was derived from the California Urban Forest Observatory data as was impervious surface data from the NLCD dataset.

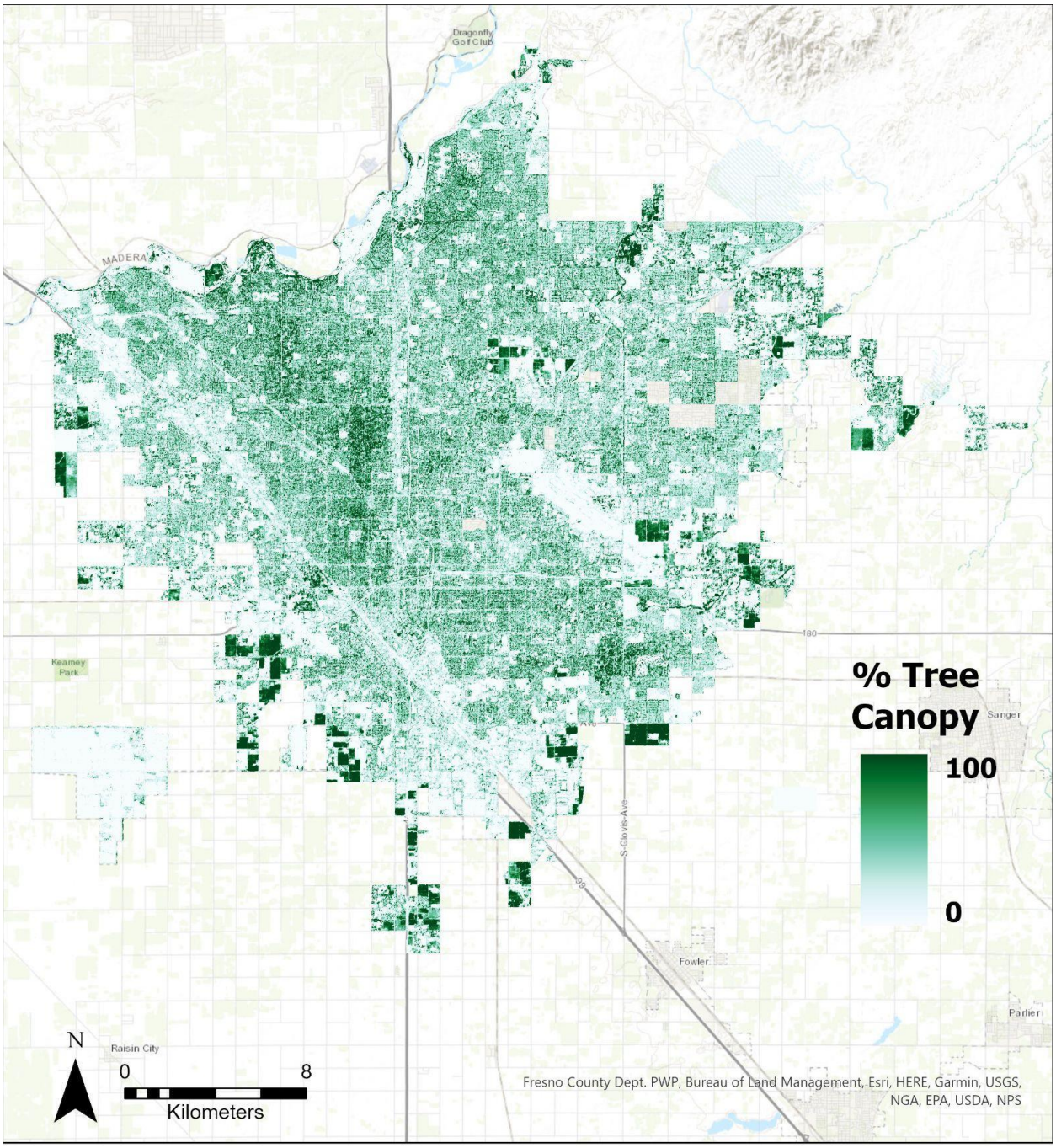

Figure 3.1: Percent tree canopy in Fresno, California. Data Source: California Forest Observatory

We calculated Daytime LST from the Landsat 8 Surface Reflectance Tier 1 Product. Daytime LST was derived by first filtering available cloud-free imagery between June 1st and August 30th for the years of 2016-2020. This resulted in 34 available images. We then calculated for each image the normalized difference vegetation index (NDVI) and emissivity (E) (Shen et

al., 2016), which was then used together with the brightness temperature (BT) to calculate LST (Equation 2). Nighttime LST and evapotranspiration (ET) were acquired using data from the ISS ECOSTRESS (ECOSTRESS June 2018 launch) from the NASA Application for Extracting and Exploring Analysis Ready Samples (AppEEARS) (Table 2).

$$LST = BT/(1 + (0.0000115 * BT/0.01438) * log(E))) \quad (2)$$

The InVEST Urban Cooling Model takes a number of biophysical inputs including; building intensity, tree canopy, evapotranspiration, land cover, and temperature. For our two city analysis, we collectd this data from a variety of sources listed in the data acquisition sections and below (Table 2). Building footprint data were derived from Bakersfield and Fresno GIS repositories in order to extract building intensity values which is the ratio of floor area to land cover area yielding a value between 0 and 1.

The InVEST urban cooling model generates a heat mitigation index (HMI) based on the cooling capacity (CC)of each cell (as defined by the local environmental properties within the cell of shade, evapotranspiration, albedo and building intensity) and its proximity to green areas. For daytime, the CC_{day} is a function of shade, albedo, and evapotranspiration index (ETI) (equation 1). ETI is defined as the ET rate of the cell divided by the maximum ET rate in the study area. Note that all three variables in equation 3 take on values between 0 and 1. For nighttime, the CC_{night} is a function of building intensity (equation 4) since nighttime temperatures are driven by heat release from buildings and impervious surfaces (Ferreira and Duarte, 2019). A third cooling capacity index (CC_{PG}) is generated by InVEST and values cells based on their proximity to green areas. It has been shown that green areas must be bigger than 2 hectares to have a cooling effect on the air around them (MacDonald et al. 2016; Zardo et al. 2017). CC-PG

is the sum of the cooling contributions from all nearby green areas with each contribution depending on the CC of the green area and the distance from the cell. The daytime HMI assumes the larger value between CC-day (CC-night) and CC-PG. With the above definitions, HMI takes on values between 0 and 1.

In order to model planning scenarios, adjusting the biophysical parameters of shade and albedo is necessary. For example, to model a 5% increase in tree canopy (i.e. from 10% to 15%) the shade values in the model parameters would be increased for development land covers (i.e where it would be feasible for the municipalities to add trees) such as road right of way, public spaces, and residential categories. It's important to note that while increasing shade represents an increase in tree canopy, this does not affect the prevalence or influence of "green spaces". In addition, since nighttime HMI is dependent only on building intensity and since model runs did not change the existing land use, only nighttime model runs represent existing conditions.

$$CCday = (0.6 * shade) + (0.2 * albedo) + (0.2 * ETI)$$

(Equation 3) Cooling capacity

$$CC - night = 1 - Building\ Intensity$$

(Equation 4) Cooling capacity for nighttime.

The ability to model scenarios is dependent on the determination of the albedo and shade which depends on the resolution of the Land Use Land Cover (LULC) layer. The LULC data derived from the NLCD dataset had 12 classes in Fresno and 13 classes in Bakersfield (Table 3.3). The classes included four scales of development intensity (low to high), barren land, forest, and agriculture. For our modeling scenarios we applied the aforementioned increases in tree

canopy (10 and 25%) and albedo (10 and 25%) only to the developed land cover classes, which represented urban areas.

Input	Description	Source
Land Use/Land Cover	Code that defines the land use of that area, the municipal data. (Raster)	NLCD https://www.mrlc.gov/data
Biophysical Table	A table containing physical characteristics per land use code (and associated description) present in the LULC raster [csv]	Compiled from various sources
Shade	Derived from tree canopy 2020 (10 meter), represents percent shaded area per land use [0-1]	Forest Observatory 2020 dataset https://forestobservatory.com/download
Albedo	Represents percent of energy reflected from surface per land use [0-1]	Landsat 8 OLI
Building Intensity	Represents the intensity of development, a normalized value of the ratio of floor area to land area per land use [0-1]	Open Street Map https://www.openstreetmap.org/#map=15/36.7827/-119.7562
Evapotranspiration	Normalized evapotranspiration values in mm [raster]	ISS ECOSTRESS ET https://ecostress.jpl.nasa.gov/
AOI	Vector polygon delineating area of interest and aggregation boundaries of census block groups	Derived from metro region shapefile
Green Area Maximum Cooling Distance	Default used of 400m [m]	Model Documentation

Reference Air Temperature	Rural reference temperature, mean LST was used from chosen reference areas [degrees C]	Landsat 8 OLI/TIRS
Magnitude of Urban Heat Island Effect	Magnitude of the UHI Effect: Difference between rural reference temperature and the maximum temperature observed in the city. (average was used since surface temperatures fluctuate more than air) [degrees C]	Landsat 8 OLI/TIRS
Air Temperature Maximum Blending Distance	Air Temperature Maximum Blending Distance: Used default value 500 [m]	Model Documentation

Table 3.2: Summary of Inputs to InVEST Urban Cooling Model.

Fresno		Bakersfield	
LULC	Hectares	LULC	Hectares
Open Water	803.5	Open Water	923
Developed Open Space	5202.3	Developed Open Space	11938.4
Developed Low Intensity	8689.5	Developed Low Intensity	8291
Developed Medium Intensity	15966.8	Developed Medium Intensity	17165
Developed High Intensity	4984.2	Developed High Intensity	3562.5
Barren Land	223.6	Barren Land	1062.1
Shrub/Scrub	3.3	Shrub/Scrub	2464.6
Herbaceous	2141.3	Herbaceous	38864.3
Hay/Pasture	1458.9	Hay/Pasture	665.8
Cultivated Crops	6829.8	Cultivated Crops	79828.1
Woody Wetlands	27.1	Woody Wetlands	1038.8
Emergent Herbaceous Wetlands	16.1	Emergent Herbaceous Wetlands	311.6

Table 3.3: LULC within Fresno and Bakersfield, Developed levels defined as low intensity (impervious surface 20-49%), medium intensity (impervious surface 50-79%), high intensity (impervious surface 80-100%)

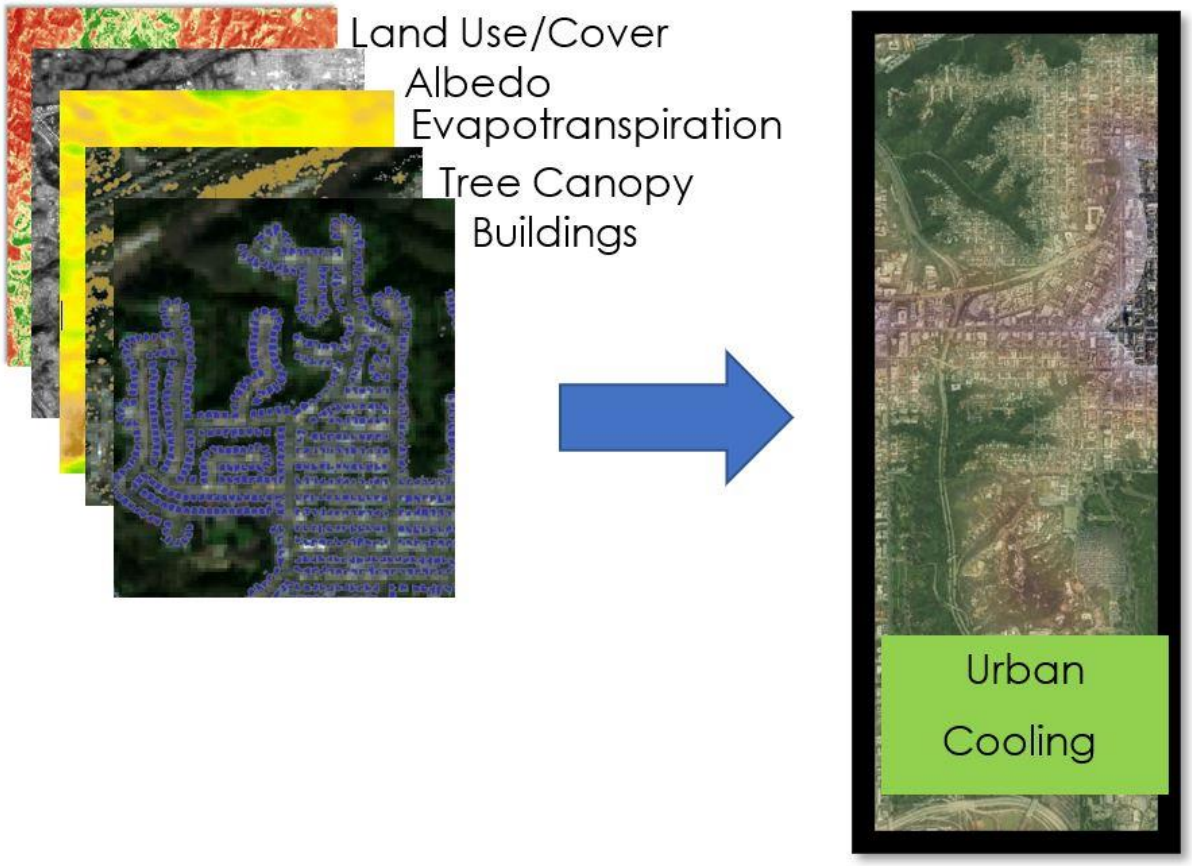

Figure 3.2: InVEST Urban Cooling Model Input Parameters

Heat vulnerability and exposure scores were calculated for each block group within our study regions. Demographic variables including population of over 25 years of age without high school diploma, population of over 65 years in age, populations of over 65 years of age and living alone, english language proficiency, income, and race as well as biophysical variables were included in the calculation. Heat vulnerability seeks to measure the combination of sociodemographics that make a population have an increased susceptibility to hazards such as heat (Leal Filho et al. 2018). The biophysical variables were day and nighttime land surface temperature (Zhang et al. 2012). To calculate exposure, we performed statistical analysis on the corresponding input variables using R (Cutter et al., 2003; Conlon et al., 2020). We used the following equation (Equation 4) to calculate exposure, which was a function of day and

nighttime temperature. Daytime LST values were given a weight half of that of nighttime LST values since research suggests that nighttime temperatures are better predictors of heat-related health outcomes than daytime temperatures (Hajat et al., 2005; Schwartz et al., 2005; Zhang et al., 2012).

$$Exposure = (mDLST*0.5+mNLST)/1.5) \qquad (5)$$

The Heat Vulnerability Index is calculated using Principal Component Analysis (PCA). PCA is a statistical unsupervised method that reduces the dimensionality of a data set by grouping them into linearly uncorrelated principal components that aim to explain most of the data's variance. Because of this, PCA can be used to identify spatial clusters of key factors driving heat vulnerability. We ran a PCA on our Heat Vulnerability Index by first transforming the input variables to z-scores (mean of 0, standard deviation of 1) to be able to compare the variables which originally had different units and ranges. PCA was done using the principal-function in base R with a varimax rotation. Only principal components that had eigenvalues greater than one were retained (Kaiser, 1960). Components also were required to cumulatively explain approximately 70-80% of data variance and where the slope is leveling off in the scree plot (Glorfeld, 1995). Based on these criteria and literature, we used four principal components for the census block groups. Since PCA only detects patterns among input variables, we further evaluated whether the sign, positive or negative, of each component produced by the PCA represented the best current scientific understanding of the real-world relationship between that variable and heat vulnerability. Based on these criteria and literature, we used four principal components for census block groups in Fresno and five for Bakersfield. We then calculated scores for each component and census block group. Factor scores for each component and census

block were calculated by weighing the z-score of each variable by using an 8x4 matrix. To visualize heat vulnerability, the overall vulnerability index scores were then ranked by quintile, and classified as very low, low, medium, high, and very high priority areas. We then mapped the highest and lowest vulnerabilities for both Fresno and Bakersfield (Figures 9 and 12).

Results:

Footprint of urban heat in large San Joaquin Valley cities

Daytime LST varied by nearly 25° C (40° F) across the Fresno area. The warmest temperatures were over 43.5° C (110° F) (>10° F warmer than region mean)and were located at the Yosemite Fresno Airport, Sierra Pavilions/ Sierra Vista Mall and Clovis Commons shopping center. There were also pockets of high daytime heat along the California Highway 99 corridor. The warmer temperatures influenced their adjacent surroundings by up to 1km. The smaller pockets of these warmer temperatures along the highway 99 corridor did not have an extended influence. The coolest areas throughout the region were located at Woodward Park in Northwest Fresno, Fresno State University's campus as well as adjacent agriculture fields, the San Joaquin country club, and the Fig Gardens neighborhood west of California Highway 41 and bisected by West Shaw Avenue. These areas were all low impervious surface and high greenspace or in the case of Fig Gardens neighborhood and Woodward Park high tree canopy. Of note northwest of the Fresno Yosemite Airport, a > 10 hectare area of retention ponds also registered temperatures 6-10° C(10-15° F) below the metro average but did not have a significant cooling impact on adjacent areas based on the LST imagery.

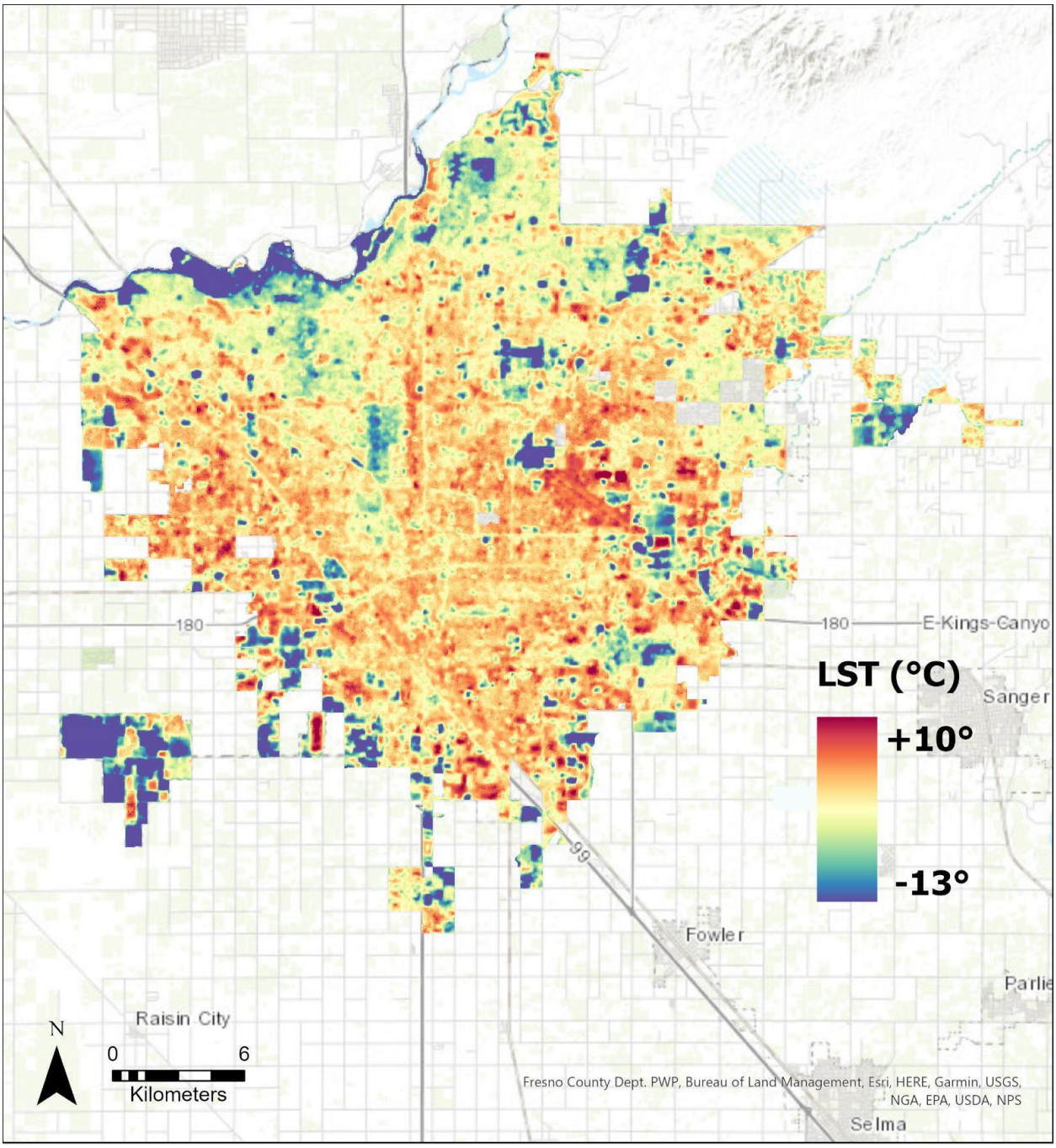

Figure 3.3:Departure from region wide daytime LST (°C) in Fresno Source: Landsat 8 TIRS

Nighttime temperature varied by roughly 17°C (27° F) across the region of Fresno. The warmest nighttime LST temperatures were found to be also around the Yosemite Fresno airport with temperatures 12-15°F (8-10°C) warmer than the region-wide average (mean surface temperature for the entire city. Compared to daytime, the warming influence did not extend

substantially outside of the airport. The Sierra Vista Mall area also had warmer nighttime temperatures than the city region average, although only on the order of 4-5°C (6-8°F). Not surprisingly standing water areas, such as along the San Joaquin River as well as near the Fresno-Clovis Wastewater Treatment Plant were well above the city wide average for nighttime temperature. The coolest areas at night were Woodward Park, and CSU Fresno neighborhoods. Areas south of downtown were also cooler than the region wide average (Figure 3.4).

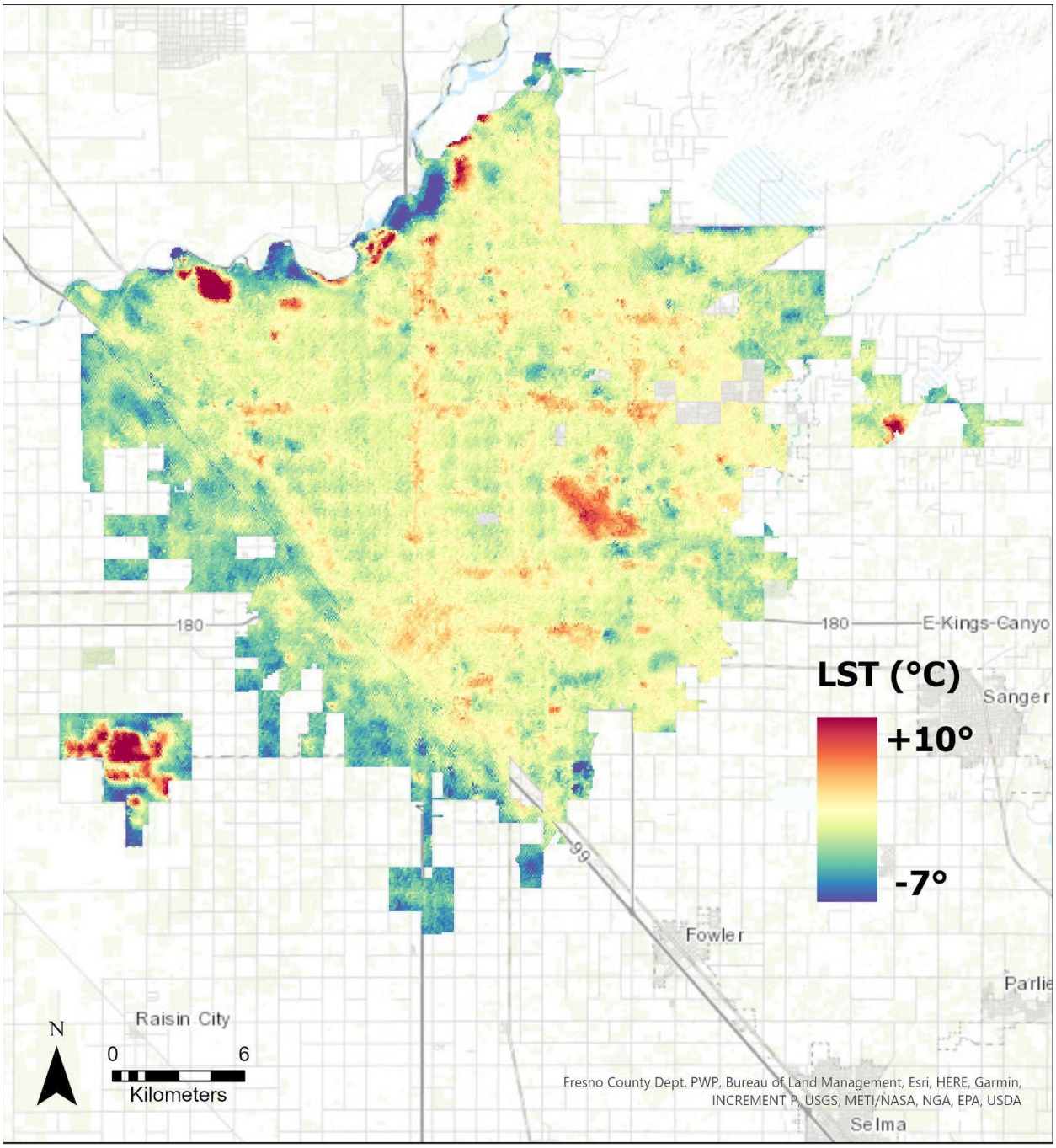

Figure 3.4: Temperature departure from region wide nighttime LST (C°) in Fresno. Source: ECOSTRESS

Daytime LST varied by nearly 30° C (48° F)(Figure 3.5) across the Bakersfield area. The warmest areas throughout the city were located at the Meadows Field Airport in Northern Bakersfield, The Alon USA refinery north of the Kern River, as well as Panama Lane Shopping Center in southern Bakersfield along Highway 99 . Fallow fields of soil also registered very high

daytime temperatures. This may not be an accurate representation of that land cover for other parts of the year outside of summer when crops are irrigated or at different points of the phenological cycle. The coolest areas throughout the City were directly along the Kern River Parkway as well as Bakersfield Country Club located in eastern Bakersfield and at the college campuses of Bakersfield City College, and California State University Bakersfield. These areas were up to 6-7° C (10-12° F) cooler than the city wide mean and all had substantially more green space than the rest of the city.

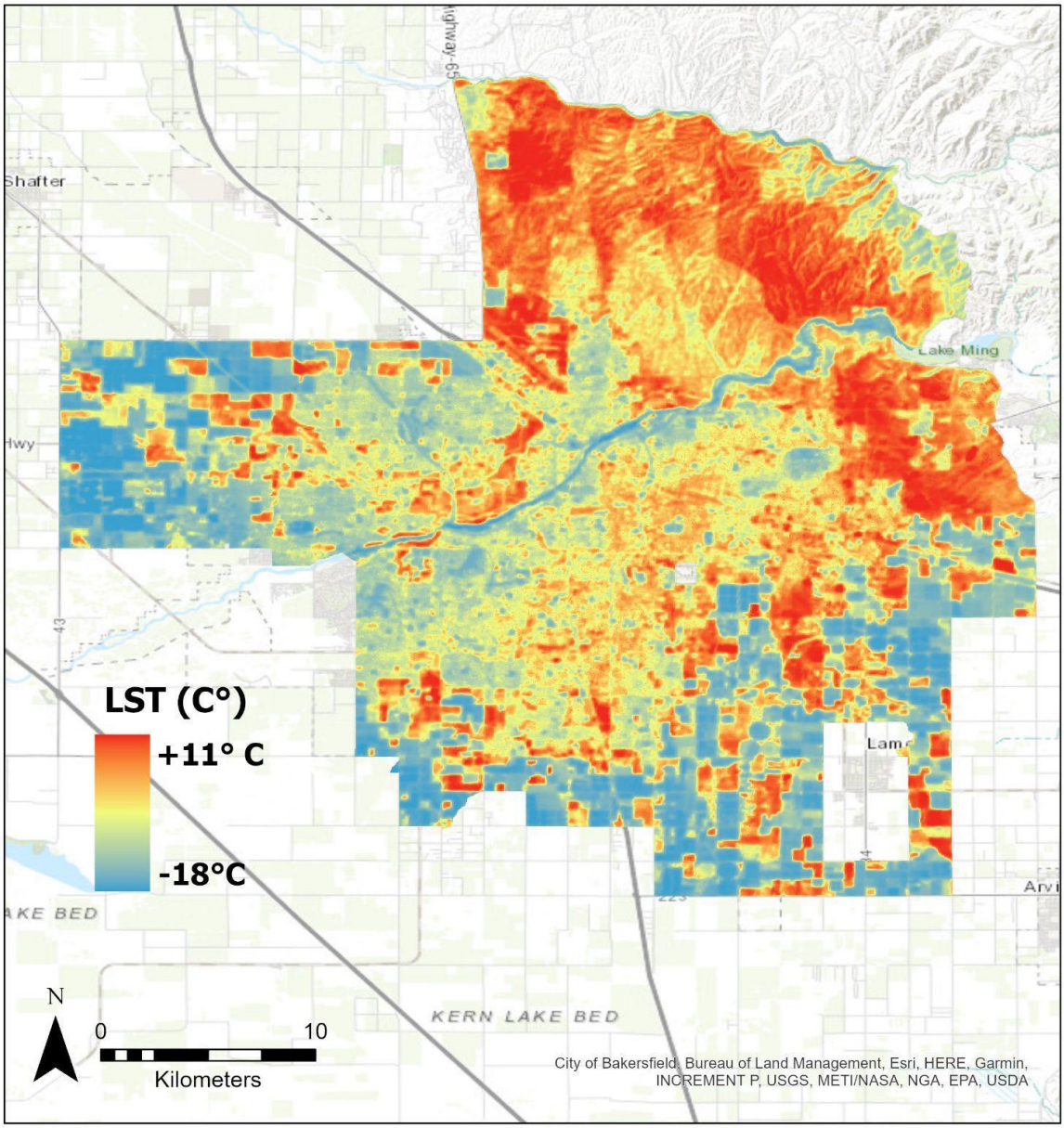

Figure 3.5: Departure from region wide daytime LST (C°) in Bakersfield, Source: Landsat 8 TIRS

Nighttime urban heat varied by 16° C(25°F) across Bakersfield (figure 6). The classic urban heat island pattern was much more pronounced than the daytime LST was, with nearly the entire urban core registering 5-6° C (8-10°F) warmer than the region-wide average. The warmest nighttime temperatures occurred in southern and eastern Bakersfield. The smaller Bakersfield Municipal Airport had the highest nighttime temperatures, followed by Bakersfield Industrial district north of Highway 58. The cooler green areas that had the lowest temperatures

for daytime were not substantially cooler at night. Many of the fallow fields that registered as very warm during the day were also cooler at night indicating low latent heat of that land cover.

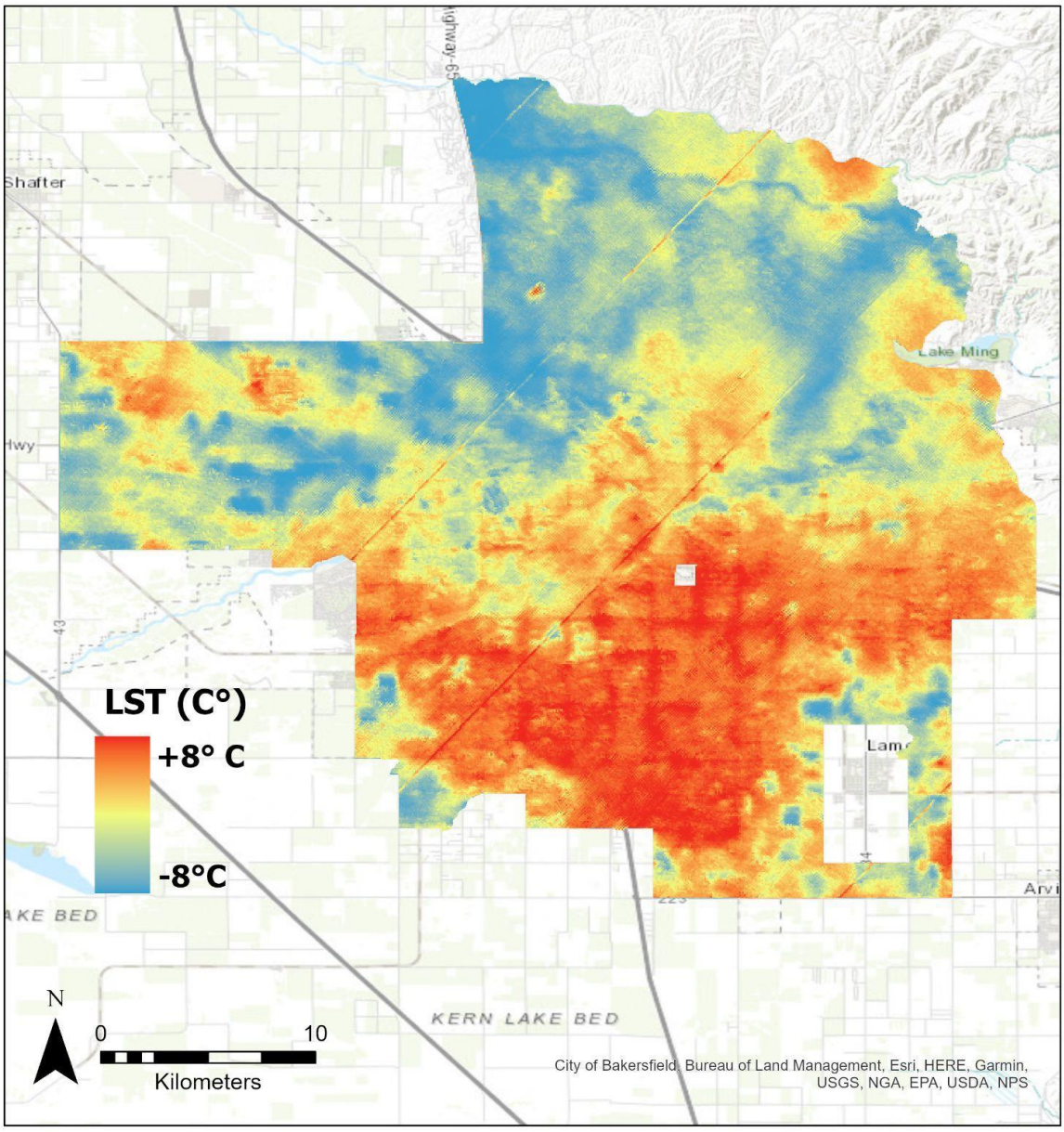

Figure 3.6: Departure from region wide nighttime LST (°C) in Bakersfield. Source: ECOSTRESS

The warmest LST temperatures found in Fresno and Bakersfield were all of high impervious surface and low green/space tree canopy such as the Sierra Vista Mall, and Yosemtite Fresno Airport in Fresno, and the refinery and airport areas in Bakersfield. Areas

throughout Fresno and Bakersfield adjacent to the agriculture fields in the region were much cooler, i.e. between 5-6.1°C (8-10°F) cooler than the City average. Nighttime LST temperatures had a slightly different pattern with a smaller spectrum between the warmest and lowest temperatures. The coolest areas of Fresno, and Bakersfield were all areas with less urbanization although it does appear that green space did not have the same cooling impact at night as it did in the daytime.

Our results indicate that the warmest land surface temperatures in both San Joaquin Valley cities appear to be in heavily developed areas such as commercial and industrial areas. This was observed during both day and nighttime temperatures with the nighttime temperatures having a larger departure from the region wide mean compared to daytime. Additionally, the presence of tree canopy and green space appeared to yield reduced surface temperature consistently throughout our two study regions.

Exposure and Heat Vulnerability Scores by Block Group

For the heat score derivation, we developed two scores: Heat Exposure Score (HES), and a Heat Vulnerability Score (HVS) using the PCA (Cutter et al., 2003; Hammer et al., 2020) across the number of census block groups for each region (i.e. 419 for Fresno).These new variables are called principal components (PC). As such, PCA was used to identify spatial clusters of key factors driving heat vulnerability.

The PCA run on the block group level, including socio demographic indicators listed above, had 80% of the variance explained with four principal components. The first four principal components for census block groups explained 87% of the variance with the first component explaining 49% of the variance. The main sociodemographic variables explaining heat vulnerability included the percent of population over 25 years without a high school

diploma, LatinX and English language proficiency, which had a strong positive loading, and income with a strong negative loading (Figure 3.7). In other words, block groups that had high populations of over 25 year olds without a high school diploma would likely have high LatinX populations (Figure 3.7), as well as higher proportionate populations with limited English language proficiency. Income also had a strong negative loading on principal component one. The second principal component included percent Asian population, and percent of nonwhite population. The last two principal components, PC3 and PC4, respectively explained 17 and 10% of the variance. The vulnerability PCA had a root mean square of the residuals of 0.05 and a fit of 0.98.

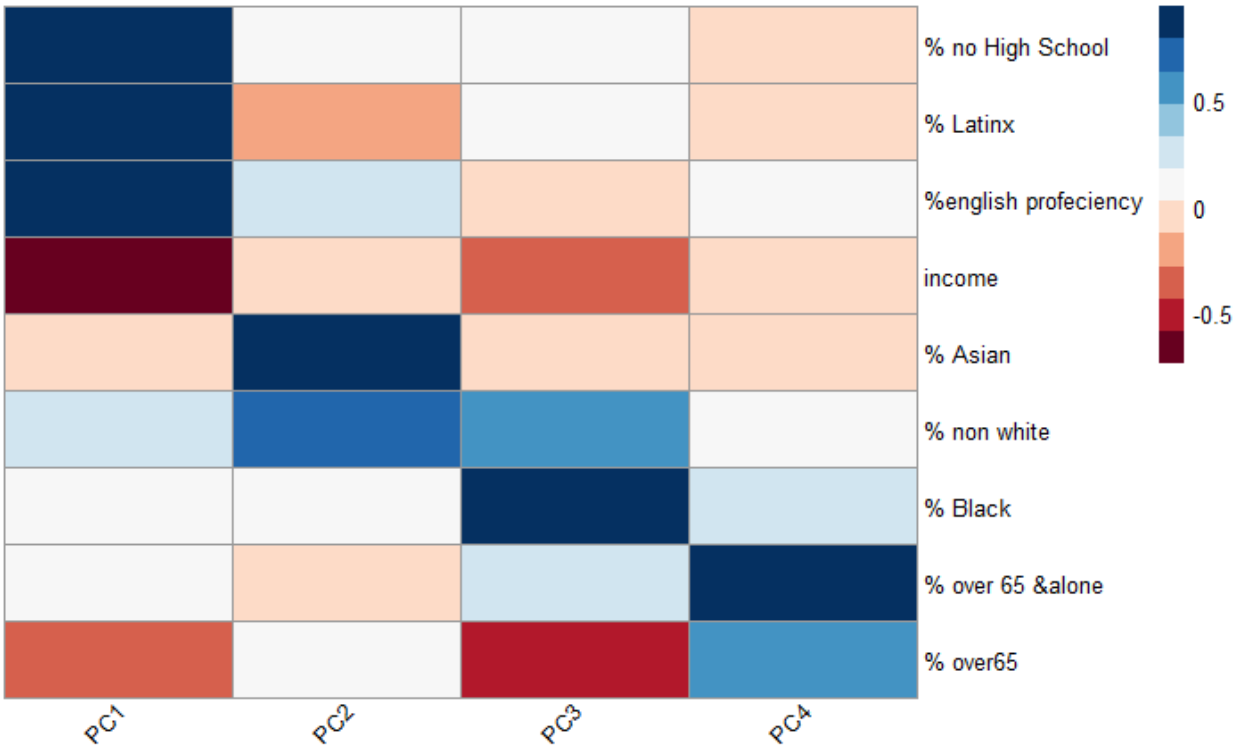

Figure 3.7: Heat Vulnerability Score (HVS) Principal Component Analysis (PCA) Correlation Map of Sociodemographic Variables: Fresno

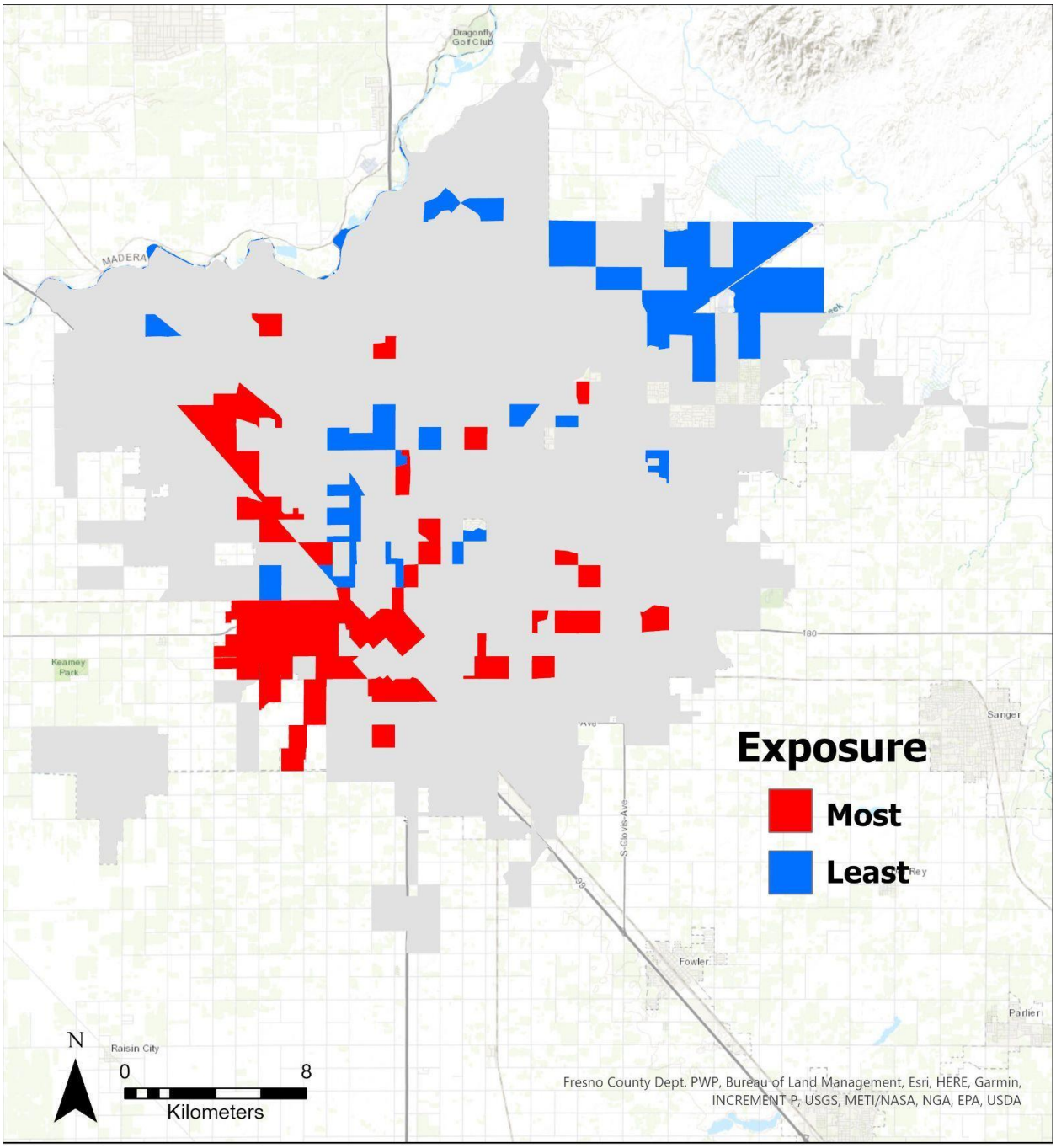

Figure 3.8: Vulnerability Indices by Block Group throughout Fresno

Census Block groups with the highest heat exposure were located in the southwestern portion of the city west of Highway 99. The neighborhoods west of downtown also had high scores of heat exposure. High heat exposure scores were consistent with the neighborhoods that had the highest temperature readings from the remotely sensed imagery with the exception of

neighborhoods next to the Yosemite Fresno Airport which had slightly lower exposure scores. The areas of lowest exposure were in wealthier neighborhoods including Fig Gardens in west central Fresno and wealthy neighborhoods in northwestern Fresno and adjacent to Clovis, California. Overall using the thermal imagery from 2015-2020 the block groups with the highest exposure metrics were 2.5° C (4° F) warmer during the day than the city wide mean and 1.2° C (2° F warmer at night).

Vulnerability indices (Figure 3.9) for Fresno reveal that the most vulnerable block groups are located in areas along both the California 41 and California 99 corridors. These neighborhoods include Fresno high and Edison neighborhoods. The least vulnerable neighborhoods include Fig Gardens in the north central part of the City neighborhoods in the southeastern portion of the city. Most neighborhoods with high exposure indices also had high vulnerability values with the exception of the neighborhoods in the southeast. Low vulnerability neighborhoods showed consistently low exposure throughout Fresno.

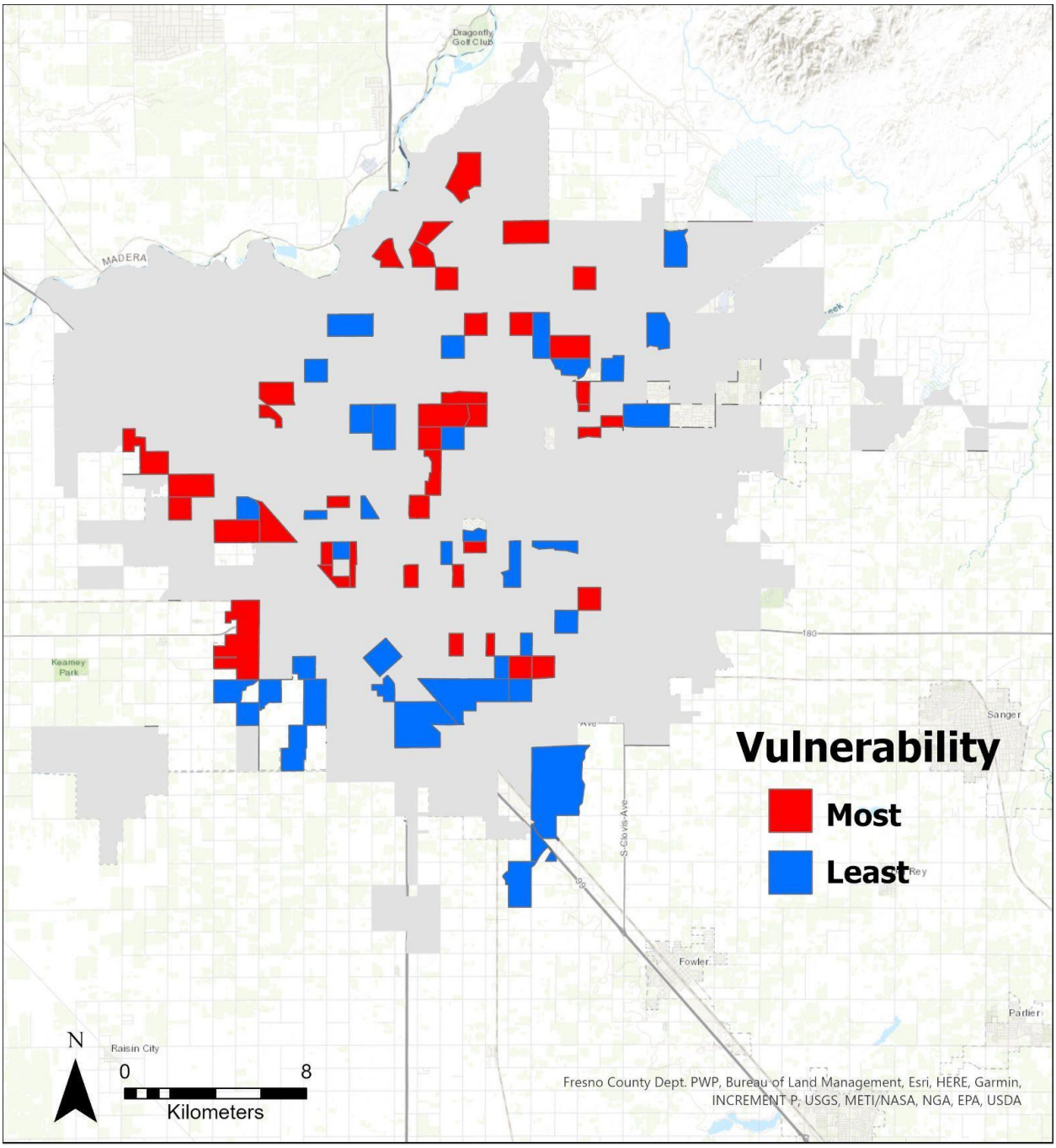

Figure 3.9: Vulnerability Indices by Block Group throughout Fresno

The PCA run on the block group level for Bakersfield had four principal components explaining over 80% of the variance. The first three principal components alone explained a combined variance of 74% and consisted of English Language Proficiency, percent of population over 25 without high school education and LatinX population having positive

loadings with the first principal component, and Income having a negative loading on the first principal component. Black and percent nonwhite had strong positive loadings on the second principal component. The last principal components (PC4) each explained the remaining variance, respectively. These results indicate that the social variables of percent of the population with no high school education and percent of LatinX population are also important when measuring heat vulnerability at the block group level. The vulnerability PCA for Bakersfield had a root mean square of the residuals of 0.04 and a fit of 0.98.

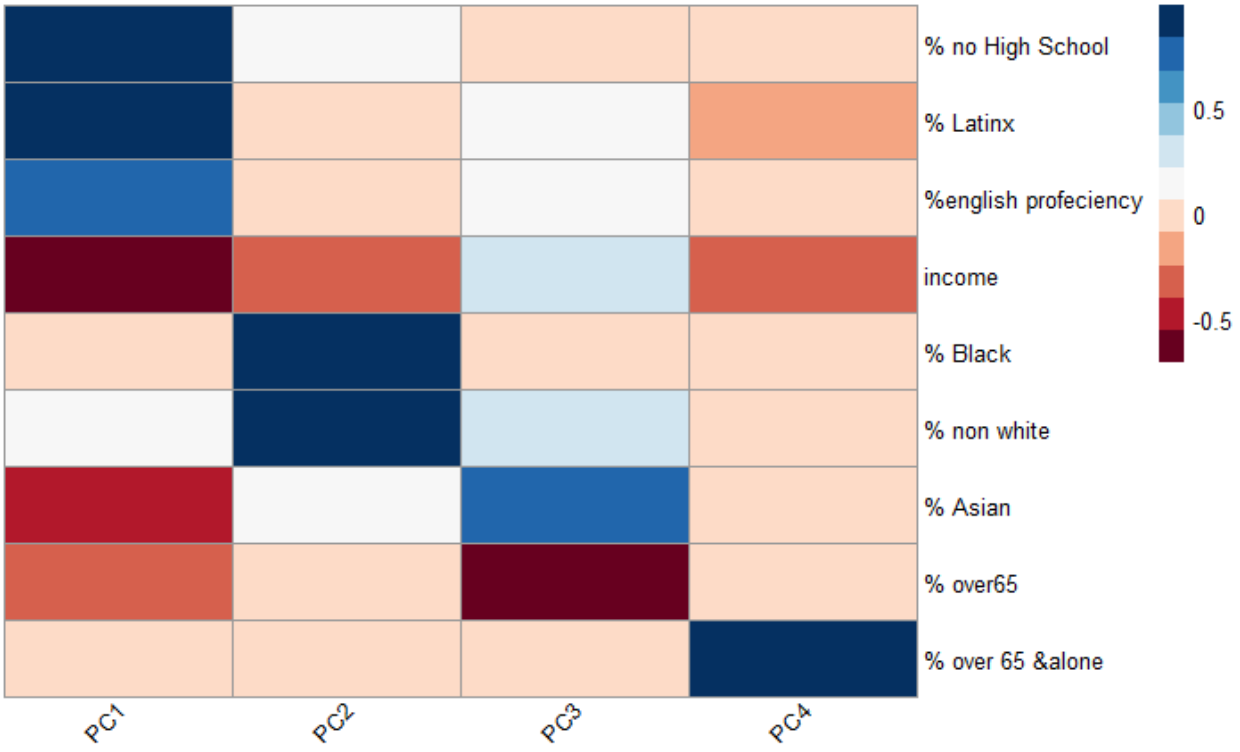

Figure 3.10: Heat Vulnerability from Principal Component Analysis (PCA) Correlation Map of Sociodemographic Variables: Bakersfield

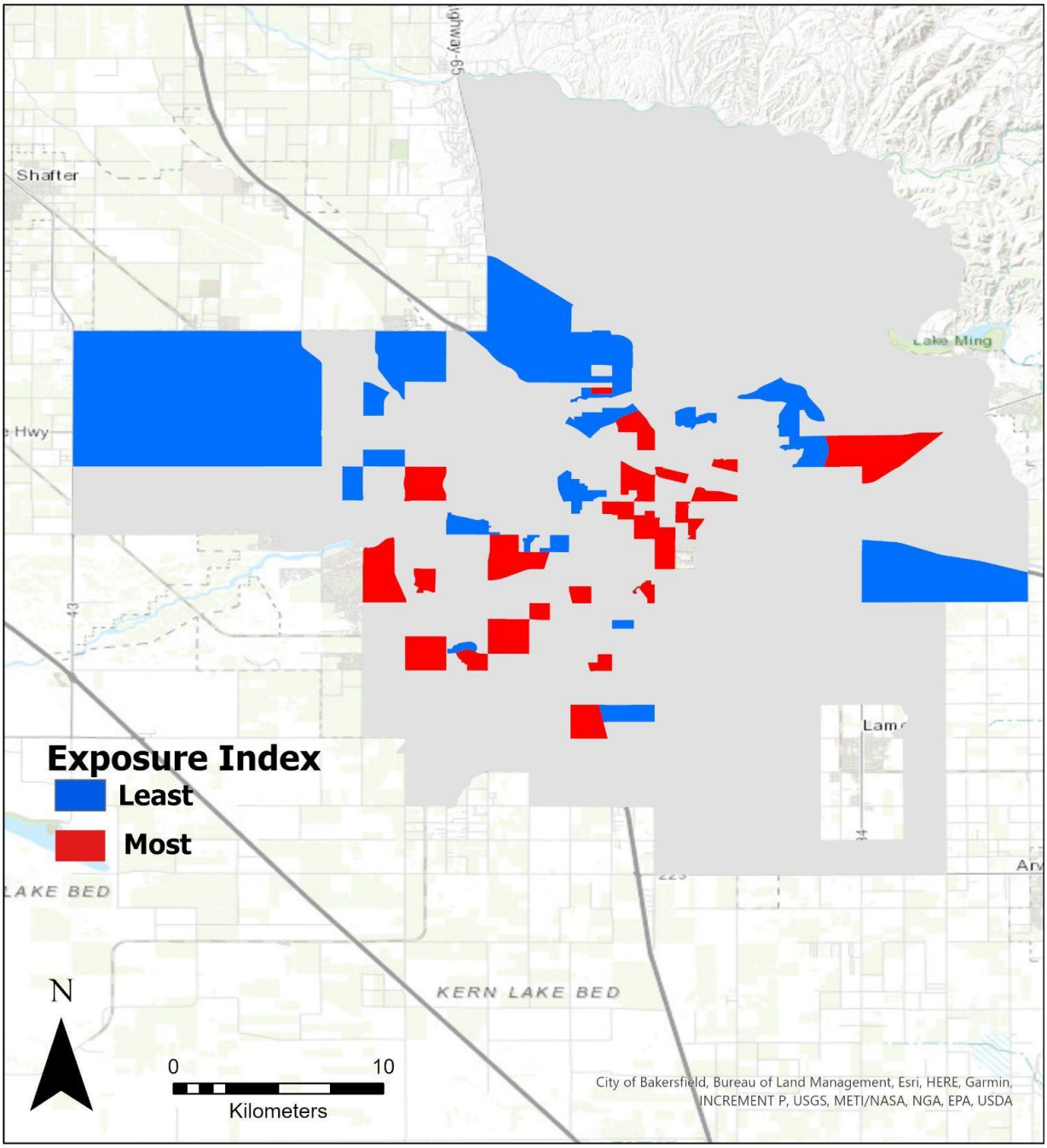

Figure 3.11: Exposure Indices by Block Group throughout Bakersfield

The block groups with the highest exposure included the Stone Creek, Silver Creek, and Ridgeview Estates neighborhoods in East Central Bakersfield. The neighborhoods of East Bakersfield, directly east or south of downtown, also scored high for exposure. Lower exposure

values were found in neighborhoods in the western part of the city, and the Tuscany neighborhood in the eastern portion of the city. The temperatures in the block groups with the highest exposure were 2.7°C (4.3°F) warmer than the rest of the city during the day and 1.2° C (1.9° F) warmer at night.

Bakersfield has 273 census block groups. The most vulnerable neighborhood block groups (figure 3.12) are located in eastern Bakersfield. This area also has a reported crime rate of 270% of California's average (Bakersfield.gov). Neighborhoods that also scored high on the vulnerability indices were the Sagepointe and Spice Tract neighborhoods west of Highway 99 and north of Stockdale Highway. Ridgeview Estates (known locally), a low income neighborhood in southern Bakersfield also had high vulnerability ratings.

Census Block groups with the highest heat vulnerability indexes were similar in most cases to those that had high exposure scores. The few exceptions were in neighborhoods along the banks of the Kern River where the high vulnerability was found based on the PCA but low exposure from higher than average tree canopy, and lower than average temperatures were observed. However, no areas had high vulnerability but low exposure.

Our results indicate that within both cities, populations that share the demographics of low percent English language proficiency, high LatinX population, and high percent of over 25 year olds without high school diploma consistently scored the highest in our vulnerability scores. In some cases such as within the Bakersfield area, over 65 year olds and living alone groups were highly correlated to our vulnerability scores, however, similar trends were less pronounced in the Fresno region.

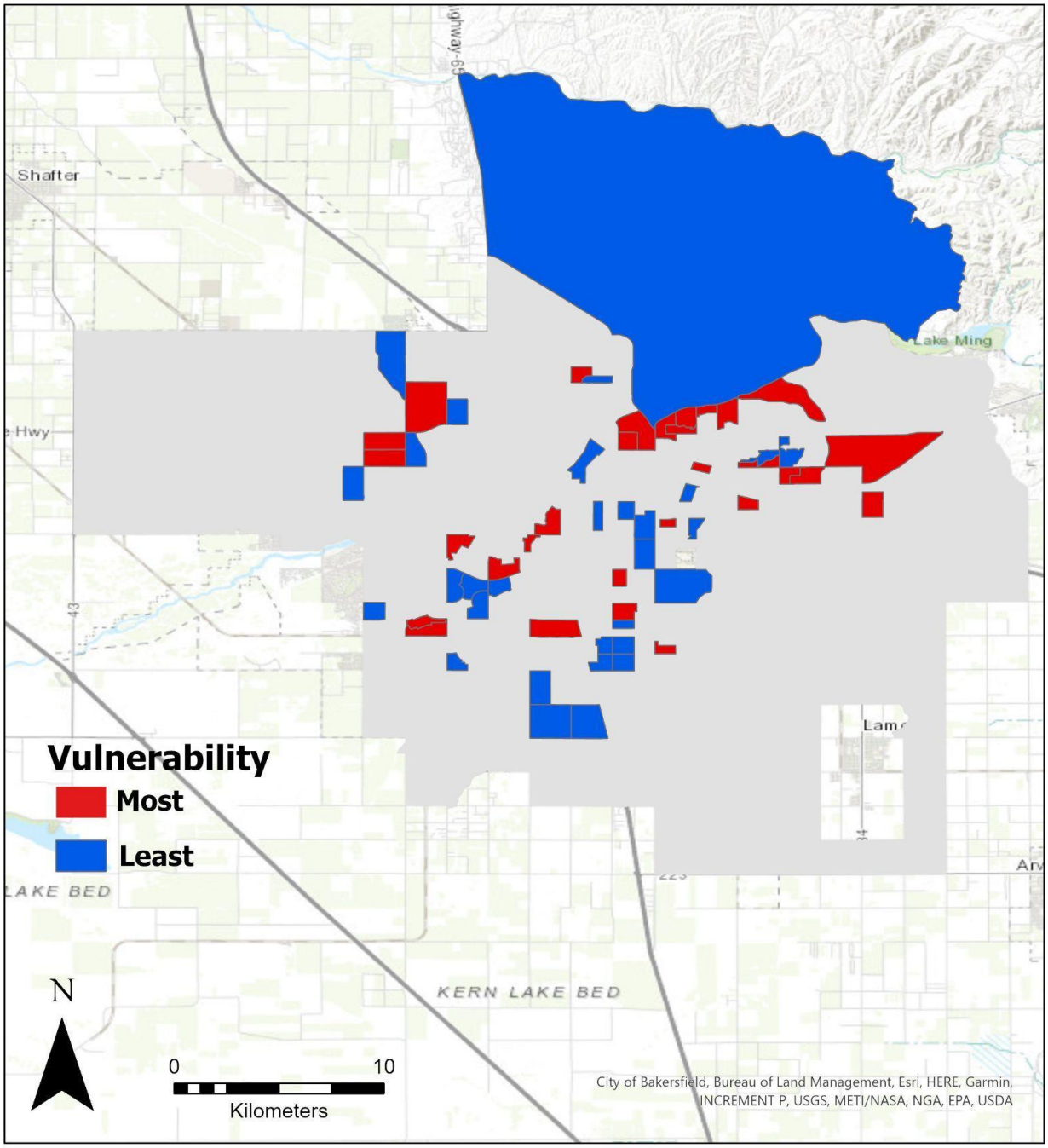

Figure 3.12: Vulnerability Indices by Block Group throughout Bakersfield

While the contributors to vulnerability may vary between regions to some degree, consistent patterns of socio demographics such as English language proficiency and high percent of over 25

year olds without high school diploma are common attributes of high vulnerability census block groups.

Biophysical and socio demographic attributes of most vulnerable and least vulnerable block groups

Amongst the two regions in the study, the block groups with the highest social vulnerability also had higher rates of LatinX population, greater populations without high school diploma, greater populations with limited English language proficiency, and lower income. The least vulnerable census block groups had a greater percent of tree canopy and lower amounts of impervious surfaces. In comparison, the highest vulnerable census block groups had 50% less tree canopy and 10-30% greater impervious surface areas. Amongst block groups with high vulnerability scores, impervious surface albedo was not substantially higher or lower than block groups with low vulnerability scores.

There was a strong inverse relationship between areas of high tree canopy and high LST. Conversely there was a comparably strong relationship between impervious surface and LST (Figure 3.15). The R value for LST and tree canopy for Fresno was -0.63 indicating that 63% of the variation in daytime temperature was explained by the amount of tree canopy. The R value for impervious surfaces and LST was moderately high (0.40). Nighttime LST had a moderately strong relationship with impervious surfaces (0.32). The percent of population without a high school diploma (0.45), percent of LatinX population (0.4), and percent of limited English proficiency (0.45) all had strong inverse relationships with higher temperatures for both day and night. Nighttime temperatures had lower correlations with the social variables of income (-0.05) and percent of over 65 year olds living alone (-0.27).

The 40 block groups that had the highest vulnerability score were located in central and eastern Fresno. These neighborhoods had differing characteristics from both the region-wide

mean as well as compared to neighborhoods that were least vulnerable. For example, the median income in these 40 block groups was only $30,186 compared to $52,000 for the region-wide mean and $82,000 for neighborhoods modeled as least vulnerable (Figure 3.13). In addition, the 40 neighborhoods that ranked as most vulnerable also had a high percent of population over 25 years without a high school diploma (29%) vs 21% for the city-wide average. One neighborhood ranked as high as 65% of residents not having a high school diploma. The most vulnerable neighborhood also had more than double the percent of population with limited English language proficiency (19.3% vs. 9.8%). The percentage of Black populations was also substantially higher in the most vulnerable neighborhoods compared to the rest of Fresno (12% vs. 5%) Finally, the percent of LatinX population was also significantly higher in the neighborhoods with the highest vulnerability scores at 54% vs 27% in the least vulnerable neighborhoods and 45.6% for Fresno as a whole.

The most vulnerable neighborhoods also varied in biophysical characteristics. For example, not only were day and nighttime temperatures warmer for the most vulnerable block groups 41° vs 36° C daytime and 17° vs. 13.4° C night (105.5° F vs 97.2° F, and 64.1° F vs. 55.7° F), but impervious surfaces were a much higher percentage (58% vs 31%) of overall land cover. Percent tree canopy was also much lower in vulnerable neighborhoods (0.9% vs 4.1%).

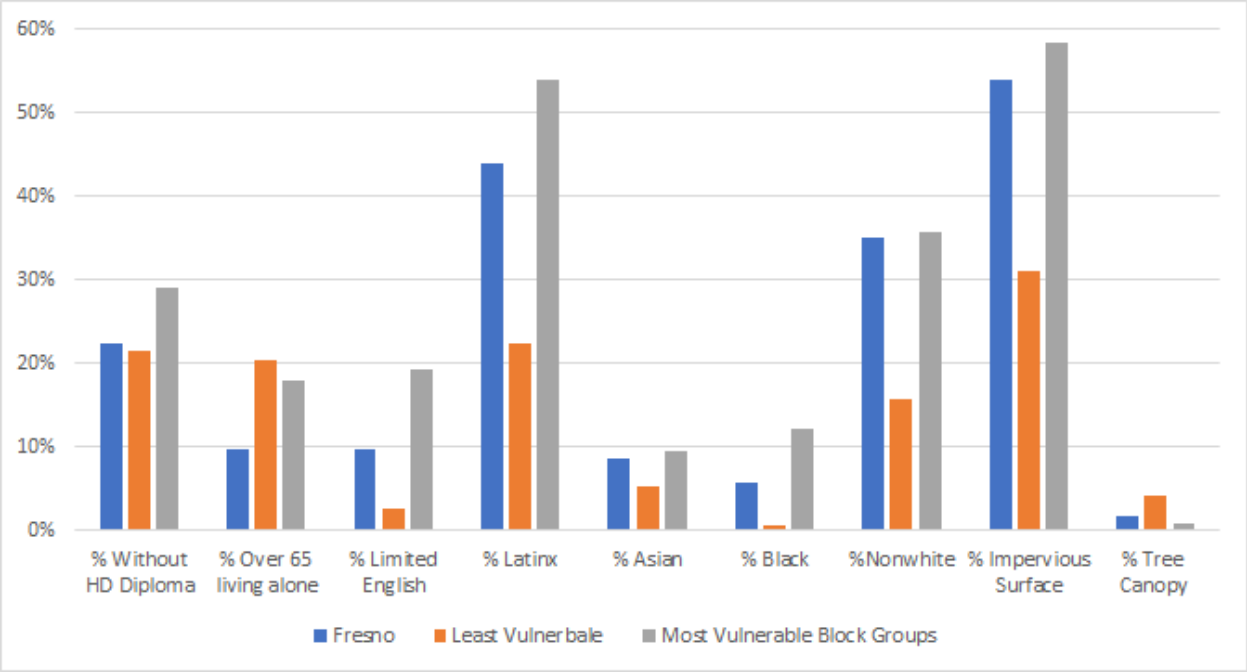

Figure 3.13: Social and biophysical characteristics of Fresno's Most Vulnerable block Groups

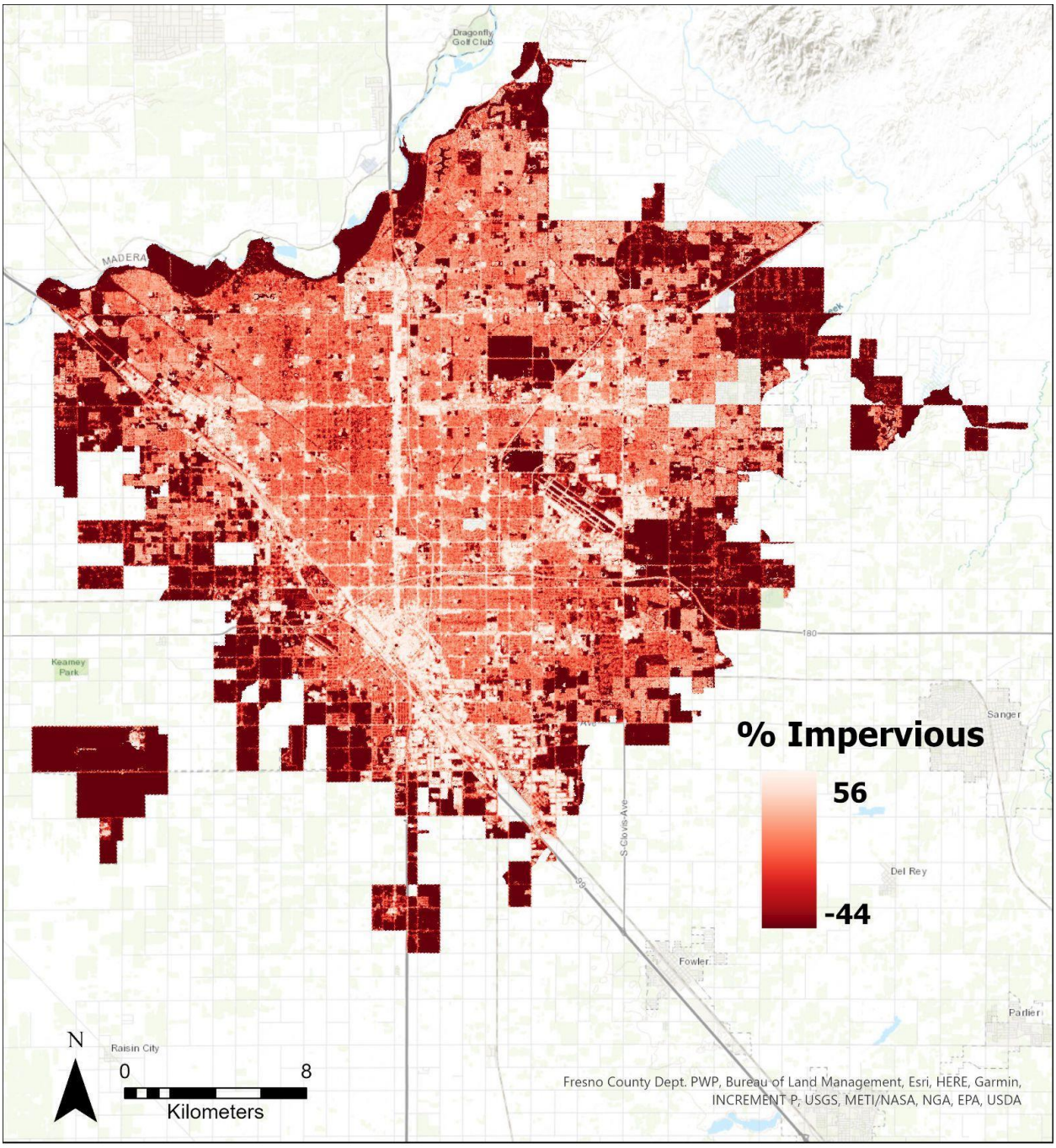

Figure 3.14: Map of Impervious Surface throughout Fresno compared to the city wide average. Source: NLCD

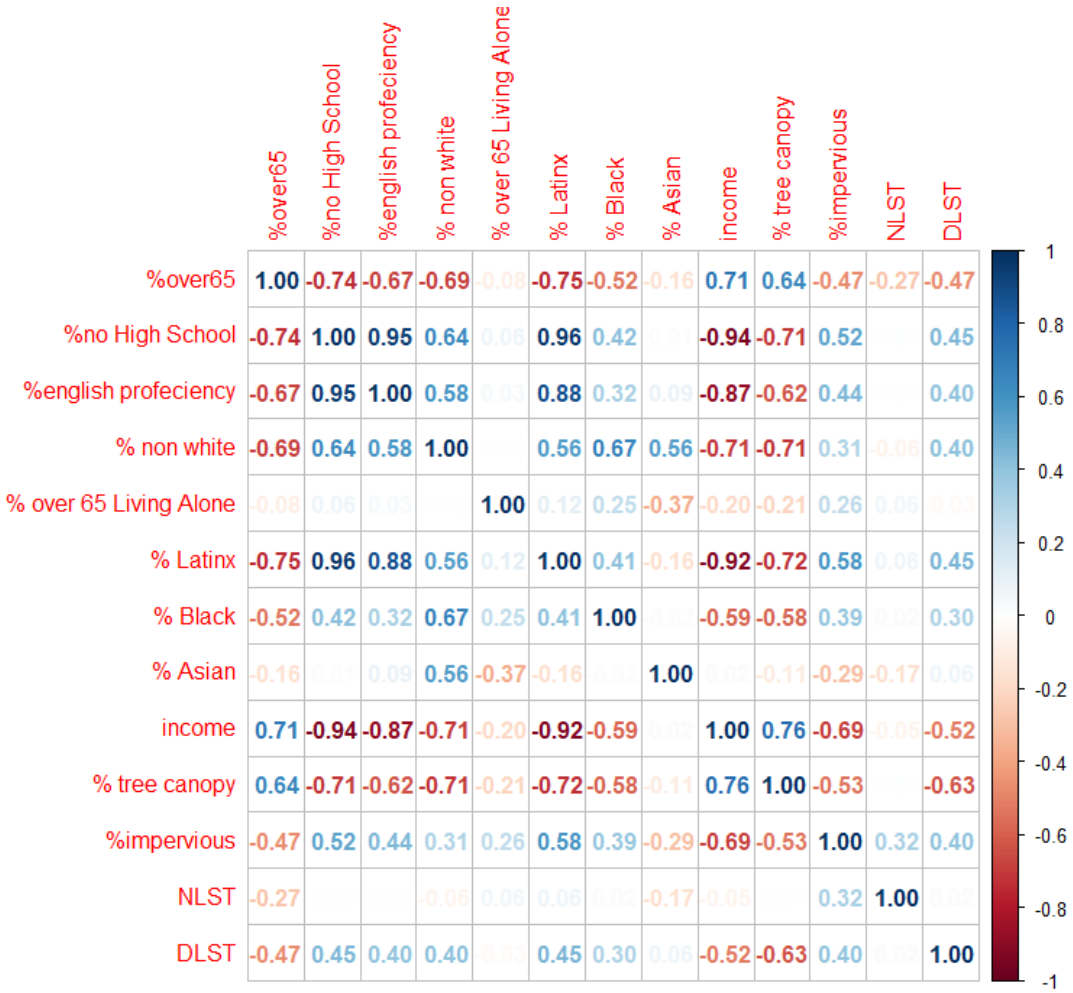

Figure 3.15: Correlation matrix between both socioeconomic and biophysical variables for Fresno, California

Similar to Fresno, within Bakersfield there was a strong inverse relationship between areas of high tree canopy and high LST (-0.74). Those neighborhoods with a high percentage of people without a high school education, limited English language proficiency, and percent LatinX population had a strong correlation with higher daytime temperatures. All three of these variables were also strongly correlated with one another (Figure 3.17). Income was also strongly correlated to lower day time LST (-0.86), with a weaker association between income and nighttime LST (-0.48). The relationship between impervious surface and land surface temperature were also moderately strong (0.33).These results show a strong correlation between

high LST and impervious surface and low tree canopy. This correlation is supported in previous literature such as Yuan and Bauer 2007, Dialesandro et al. 2021, and Morabito et al. 2021.

The most vulnerable neighborhoods had differing characteristics from both the region-wide mean as well as compared to neighborhoods that were least vulnerable. For example, the median income was only $29,000 in the most vulnerable neighborhoods compared to $52,871 for the region-wide mean and $68,371 for neighborhoods modeled as least vulnerable (Figure 3.16). In addition, the 40 neighborhoods that ranked most vulnerable also had a high percent of population over 25 years without a high school diploma at 42% vs 26% for the city-wide average. In three neighborhoods more than 70% of the population did not have a high school diploma. The most vulnerable neighborhood also had substantially higher LatinX and black populations. The percent of population with limited English language proficiency was similar to Fresno in that the most vulnerable block groups had double the percent of residents (17.6% vs. 8.5%).

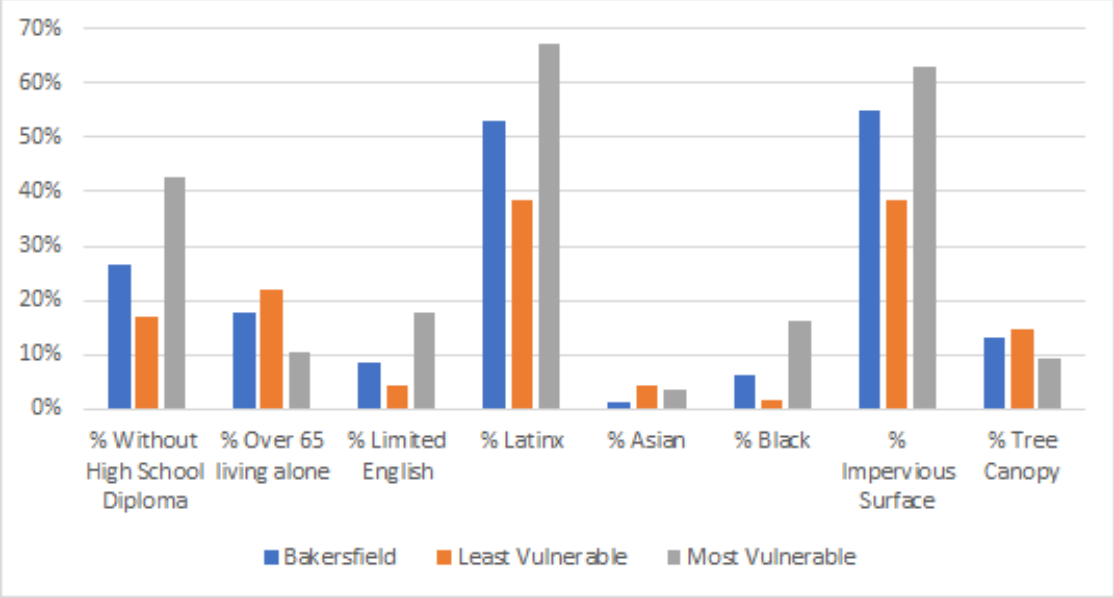

Figure 3.16: Social and Biophysical Characteristics of Bakersfield's Most Vulnerable Block Groups

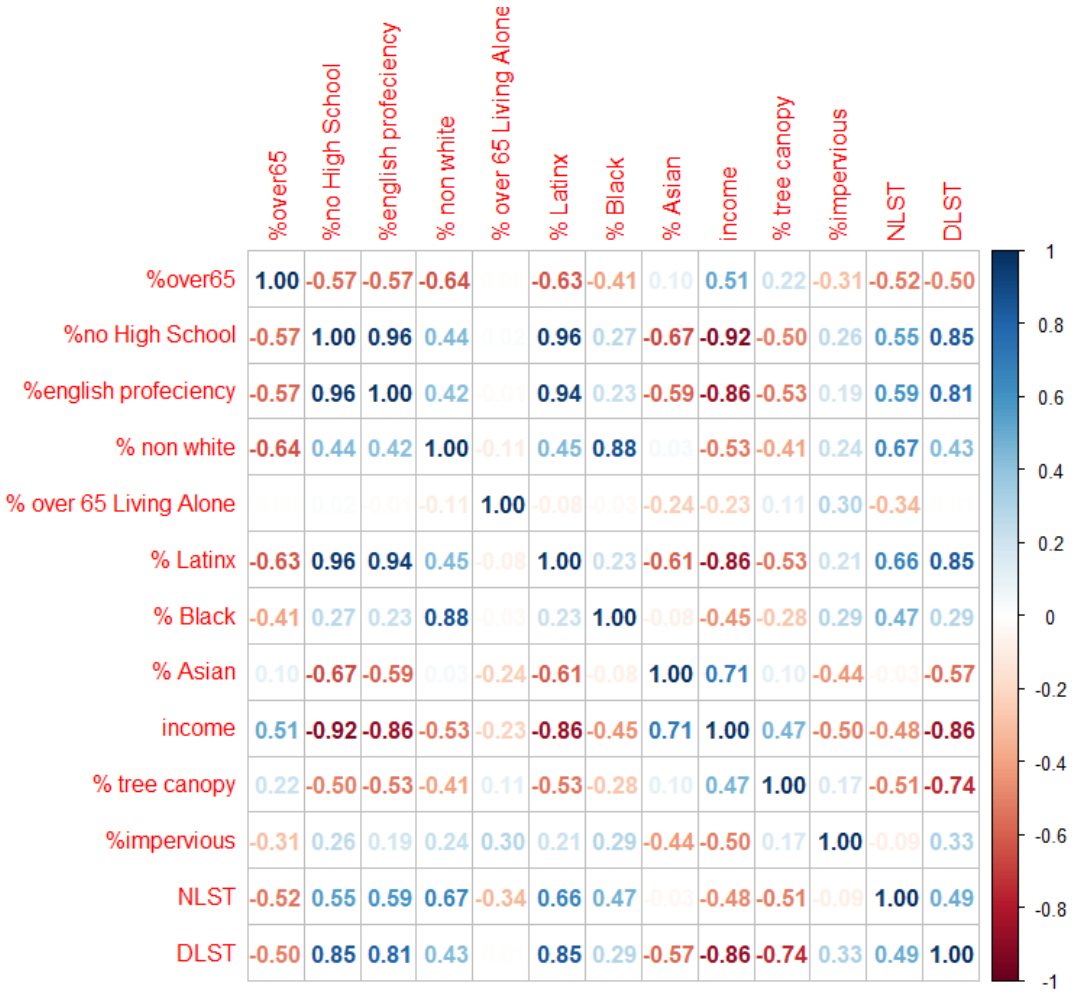

Figure 3.17: Correlation matrix between both socioeconomic and biophysical variables for Bakersfield, California

InVEST Model Results

Cooling capacity is an intermediary output of the InVEST urban cooling model and is a product of shade, albedo, and evapotranspiration by land use type. It represents an area's ability to counteract extreme heat. The darker red areas (Figure 3.18) represent areas that have low capacity to cool, and in general experience higher temperatures both during the day and at night. These areas are not only opportunities for improvement but also areas within the region that can be prioritized for urban planning and policy initiatives directed at heat mitigation. In addition, some agricultural areas can at times produce low cooling potential due to having both low albedo and low shade.

The Heat Mitigation Index (HMI) is quantified on a unitless scale. High HMI scores indicate areas that have the greatest ability to mitigate the effects of urban heat while areas with low heat mitigation scores are the most vulnerable to impacts of urban heat such as areas of high impervious surface, low albedo, and low tree canopy coverage. While contextually similar, cooling capacity is a component of HMI. Cooling capacity is a measurement of an urban ecosystem's ability to remove heat, and HMI is an index modeling the cooling capacity of each pixel and the effect of green spaces on the pixel's ability to mitigate heat. If a pixel falls far enough away from a green space to be unaffected by it, then cooling capacity will equal HMI.

The heat mitigation index output for the existing daytime conditions generally shows what is expected given our knowledge of the model. Natural areas (areas outside of anthropogenic influences such as preserves and rangeland) show up in blue and green while more developed areas are shown red-orange to yellow. While open water was classified as a "green area" in this study there is not an extensive cooling effect in both cities due to open water being only a small portion of our two study regions (<0.2%). The rural periphery with a lot of agricultural land that already has reached maximum green space potential especially during the peak of the growing season also shows up as red-orange areas indicating that heat mitigation has already been maximized from evaporation, shade and albedo.

The highest heat mitigation index was located around the agriculture fields adjacent to the California State University campus in Fresno in the northeastern portion of our study area. High heat mitigation indices were also found on the southeastern side of the Fresno Yosemite Airport. There were also substantially higher HMI scores west of the California 41 Highway corridor where values were 30-50% higher than in the eastern part of the region. Our model was validated using a comparison between the current air temperature raster generated from the

model and measured LST data from Landsat 8 with the use of the ordinary least squares (OLS) linear regression for the area examined. Our R2 value was 0.68 which was consistent with the literature (Zawadzka, Harris and Corstanje 2021).

The urban cooling model yielded substantial cooling in Fresno with only a modest 10% increase in tree canopy. Within the built area, cooling effects of up to 5° C (7.6° F) could be achieved (Figure 19). In neighborhoods where tree canopy exceeded 30%, the cooling gain was much lower. For example, for Fig Gardens, a wealthier neighborhood located west of Highway 41, only a decrease of 2.5-4° C (4-6° F) was predicted, compared to the decreases of 4-5.2° C (6-8° F) in poorer neighborhood areas east of Highway 41. With an additional 15% increase in tree canopy to 25%, the cooling gain simulated was minimal with only an additional cooling gain of 0.6 °C(<1° F)(Figures 19).

The third cooling scenario investigated in this study solely increased the albedo of built forms throughout Fresno by 10%. The model parameters were only adjusted for buildings within the four developed LULC categories. Cooling in general was restricted to less than 1° F and only within the developed land covers with little to no cooling gain to adjacent land covers (Figure 19). This demonstrates that while increasing roof or ground albedo may provide cooling and energy cost benefits to the building whose albedo is altered, the adjacent cooling is non-substantial.

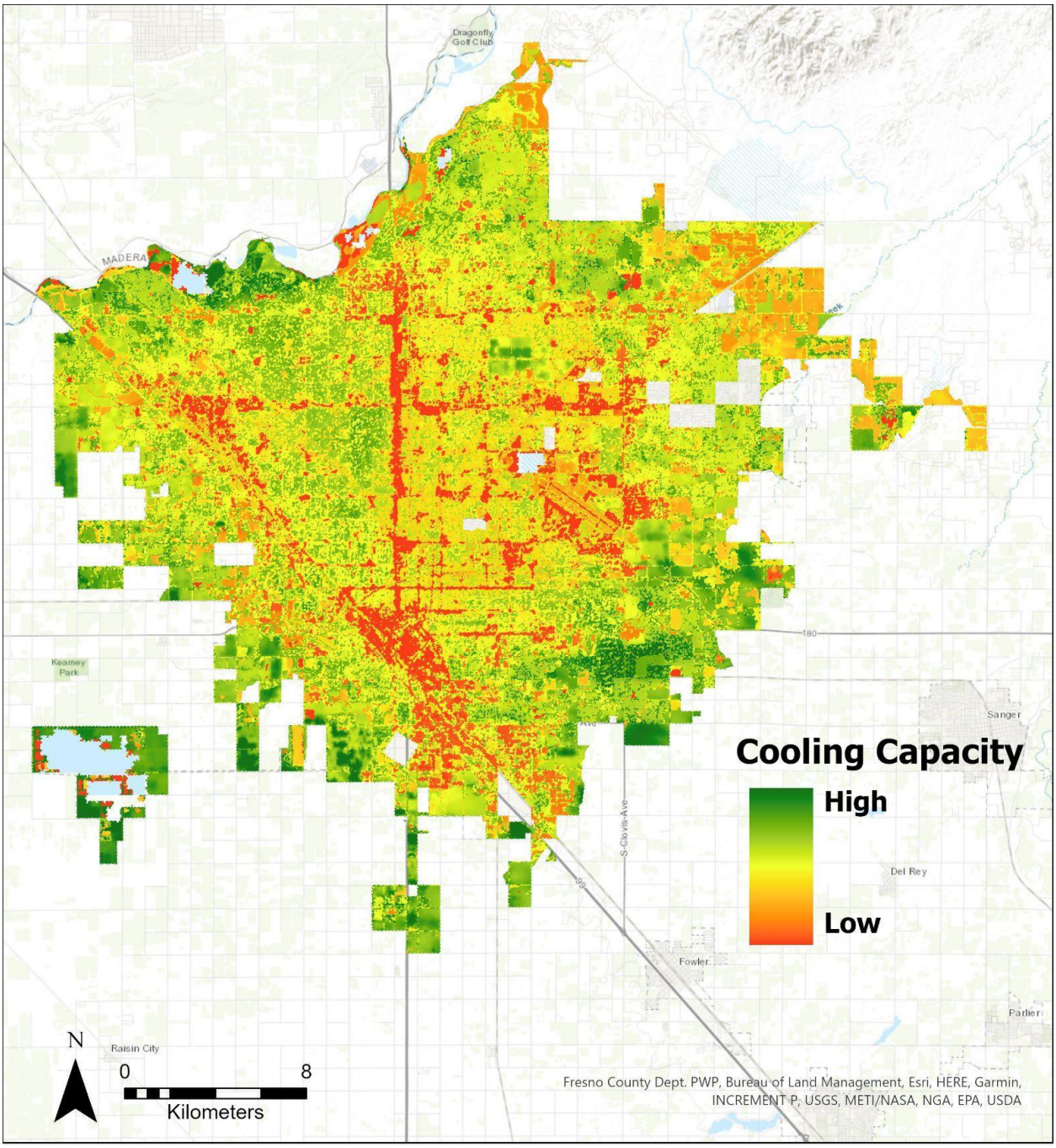

Figure 3.18: Cooling capacity of Fresno based on the InVEST urban cooling model

The last planning intervention scenario evaluated in this study was the combined increase in tree canopy by 25% and a 10% increase in albedo for all developed land cover classes. This combined scenario resulted in the highest urban cooling effect of any of the four scenarios evaluated for Fresno. While this scenario did produce the most cooling (Figure 19), the cooling

gain was less than 0.25° F compared to the 25% tree canopy increase alone. All four developed land covers were modeled to cool between3.5 -4.2° C 5 (and 7° F) on average.

Modeling the 10% and 25% tree canopy increase was completed by increasing the shade parameter for developed areas. This subsequently resulted in an overall temperature decrease of 2.5-4.5°C (4-7°F) throughout the entire city. Albedo had a much lower impact when increasing by 10%, but still decreased temperature by up to 0.5° C (0.8°F) for developed land covers. Overall, tree canopy increases also cooled all land cover types collectively (Table 3.4) indicating that there is significant spillover from increasing tree canopy in the developed land cover into surrounding areas.

Neighborhoods that had high vulnerability indices registered substantially more cooling from the planning interventions. For example, for tree canopy increases of both 10% and 25%, vulnerable neighborhoods cooled an additional 1°F compared to the least vulnerable neighborhoods (Table 3.4). Vulnerable neighborhoods were also found to see an extra 0.5°F of cooling for a 25% increase in surface albedo. The increased cooling impact could potentially be from high vulnerability neighborhoods having less tree canopy and more impervious surface (Figure 3.13).

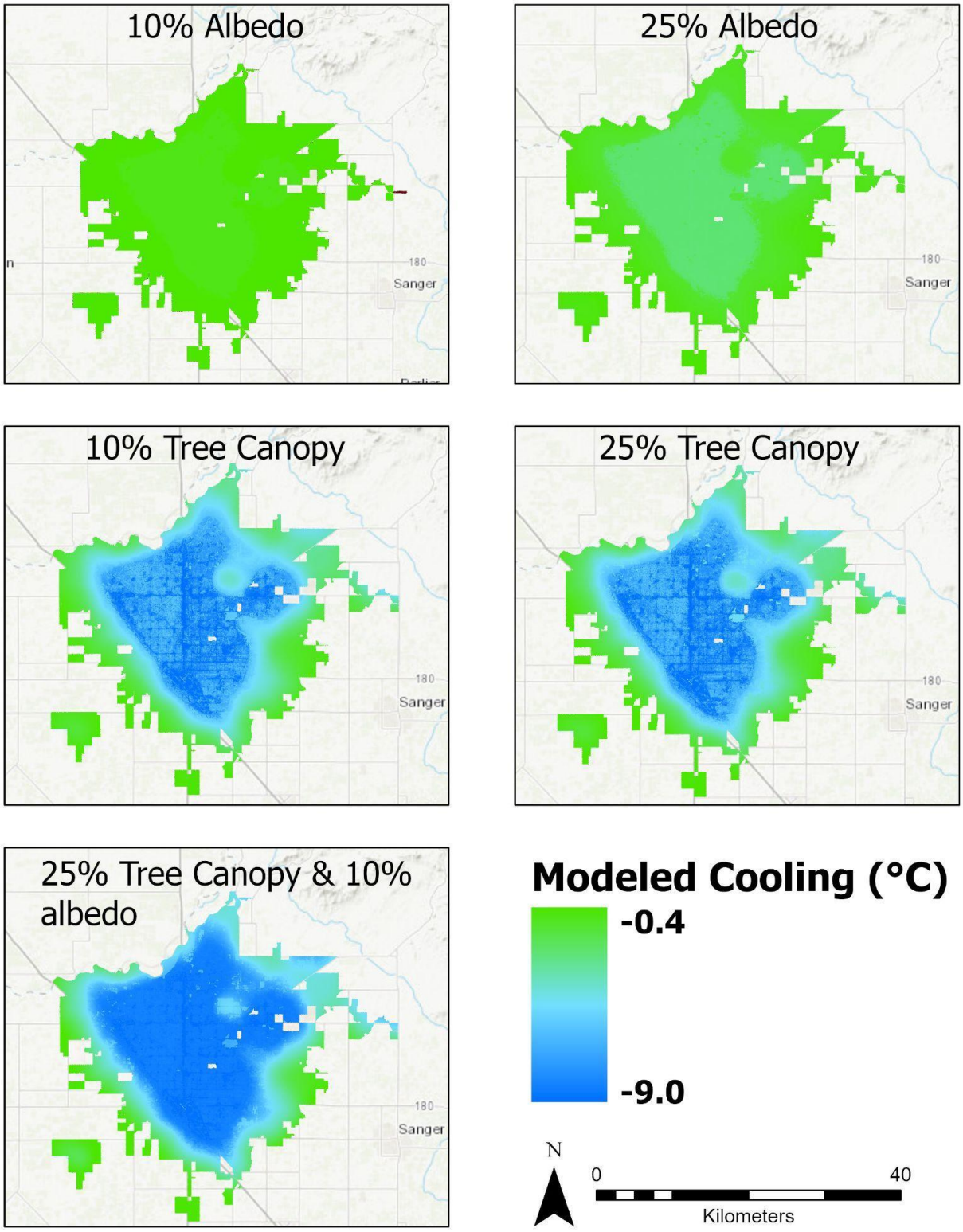

Figure 3.19: Modeled daytime temperature decrease (°C) for a planning scenarios in Fresno, California

Neighborhood Type	Temp °C	Tree Canopy 10% Increase, °C	Tree Canopy 25% Increase, °C	Albedo 10% Increase, °C	Albedo 25% Increase, °C	Tree Canopy 25% Increase & albedo 10% Increase, °C	Cooling Capacity
Developed Open Space	41.2	-3.23	-3.51	-0.29	-0.68	-3.59	0.20
Developed Low Intensity	42.7	-3.71	-4.17	-0.46	-0.88	-4.56	0.21
Developed Medium Intensity	43.5	-3.94	-4.44	-0.51	-0.94	-4.56	0.20
Developed High Intensity	44.3	-4.13	-4.64	-0.51	-0.96	-4.76	0.16
Most Vulnerable	43.0	-4.44	-5.13	-0.49	-1.21	-5.25	0.22
Least Vulnerable	36.5	-3.81	-4.31	-0.23	-0.94	-4.44	0.19

Table 3.4: Cooling by land cover for each planning scenario in Fresno, California

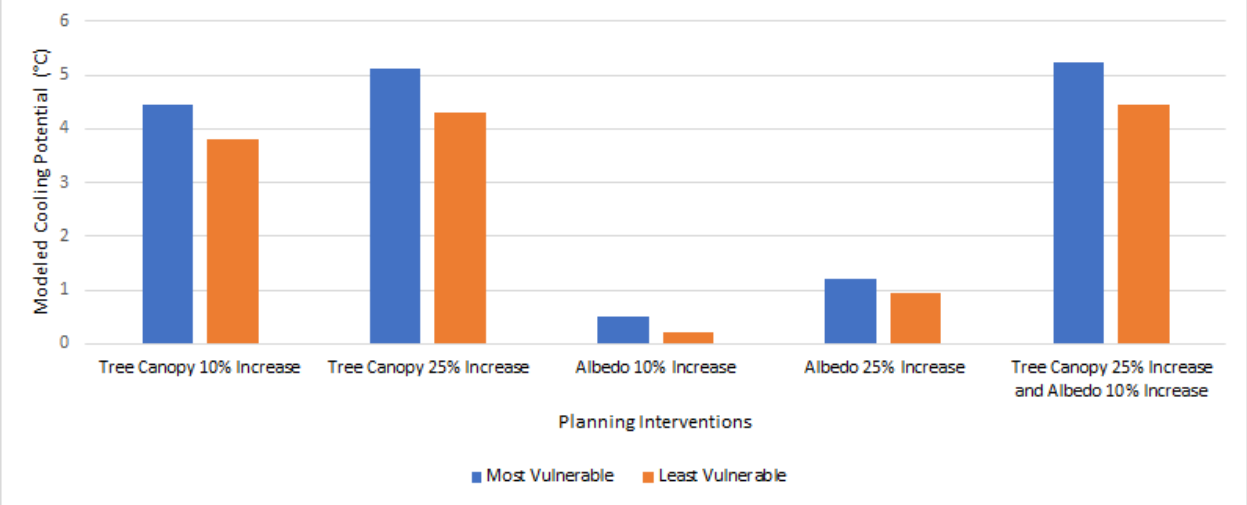

Figure 3.20: Modeled daytime cooling potential (°C) for most and least vulnerable neighborhoods in Fresno

The nighttime InVEST urban cooling model option considers only building intensity because buildings retain heat from the day and re-emit it at night. Residential areas are particularly red in the nighttime map (Figure 3A1), illustrating low capacity for cooling. This is apparent as areas with one-story homes in the northern and eastern area of the city have a much higher heat mitigation index than areas closer to downtown where there are more high story

buildings This is likely a function of the high number of housing units packed very tightly together on small parcels of land, more so than a function of their height.

Cooling capacity varied across the region of Bakersfield. The lowest areas were areas represented in orange and red in figure 3.21 are areas that have low capacity to cool, typically experiencing higher temperatures in the rangeland and oil fields in the northeast, as well as areas in downtown which had very low tree canopy (>1%) and very high impervious surface (>75%). Bakersfield Meadows field airport also had low cooling capacity values. These values were represented by darker reds and oranges in figure 3.21. Areas with high cooling capacity represented by green and light yellow (figure 3.21) were areas of higher green space, tree canopy and lower values of impervious surface and higher albedo. CSU Bakersfield campus, parks along the Kern River, and the Stockdale and Sundale Country clubs located in western Bakersfield were areas of high cooling capacity, and thus have a high functionality to cool. Agriculture areas along the urban periphery such as orchards with high evapotranspiration, and high shade had the highest cooling capacity.

The main InVEST urban cooling model output is a heat mitigation index raster. Heat mitigation is equal to cooling capacity unless pixels are given the green space designation in the biophysical table or are within the 'Green Area Maximum Cooling Distance,' as defined in the model GUI. Within Bakersfield areas of low heat mitigation were found in the central core of the city and southeast of the Kern River. Areas on the urban periphery adjacent to the oil fields in northeastern Bakersfield also had low heat mitigation and thus represent opportunistic areas for the City to improve or prioritize. As for Fresno, our model was validated using ordinary least squares (OLS) linear regression between the current air temperature raster generated from the

model and measured LST data from Landsat 8. Our R^2 value was 0.71 which was consistent with the literature (Zawadzka, Harris and Corstanje 2021).

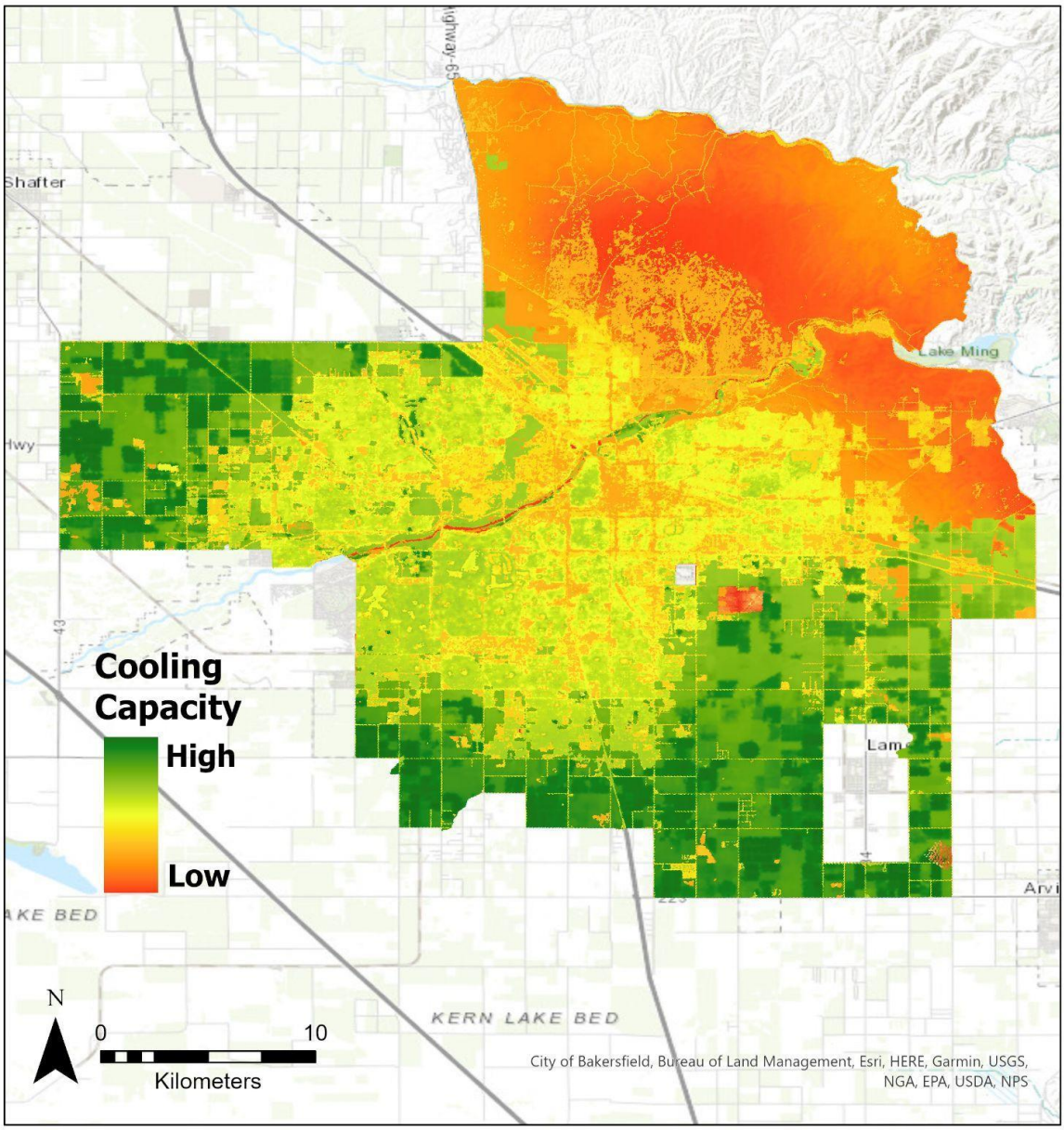

Figure 3.21: Cooling Capacity (0-1) of current building intensity, evapotranspiration, tree canopy and albedo in Bakersfield

The urban planning scenarios examined using the InVEST Urban Cooling Model were the same for Bakersfield as it was for Fresno. With much of the planning scenarios focusing on the urban core, the urban periphery especially the agriculture sectors were unaffected and had

similar thermal outcomes to the current baseline with no planning intervention for cooling capacity (Figure 3.22). A 10% increase in tree canopy yielded cooling between 1 and 2.6° F throughout the city of Bakersfield. The greatest cooling was observed in the residential areas in western and southeastern Bakersfield. The cooling impact fairly quickly deteriorated when approaching the urban periphery and agricultural regions surrounding the city. These areas either had little capacity to change albedo or shade, or they already reached their cooling potential through evapotranspiration (e.g. from field crops and orchards). Unlike Fresno, the increase in tree canopy from 10 to 25% throughout the urban core led to more substantial cooling adding 1.3° C(2° F) to the overall cooling gain (Figure 3.22). Bakersfield overall had less cooling 2,5-4.5° C (4° vs 7.2°F) compared to Fresno.

Increasing albedo by 10% throughout the developed areas in Bakersfield provided a much lower thermal decrease compared to tree canopy. The lower cooling from albedo could be from cooling only stemming from reflectivity and not from the combination of shade and evaporative cooling that tree canopy provides. Based on the InVEST model the increase of albedo only yielded a 0.4° F degree temperature decrease. For most of the areas throughout the built environment the decrease in temperature varied between 0.3 and 0.5. On a more hyper local data level the spatial resolution of 30 meters does not allow for simulating and assessing the micro cooling that could happen at the building scale which would lower energy costs for cooling but would have a lesser cooling effect on surrounding areas compared to greenspace (Morini et al. 2018).

The last model scenario run was a combined increase in tree canopy by 25% and a 10% increase in albedo in built form. Compared to the previous three models run, the cooling impacts extended into the rangelands of the urban periphery (Figure 3.22). The cooling was also the most

substantial of the four models run in that it cooled parts of the city by up to 3.2° C (5° F). Within the urban core, the cooling was the most significant with the peri urban areas cooling less than 0.6°C (1°F).

Similar to Fresno, neighborhoods that had high vulnerability indices registered substantially more cooling from the planning interventions. For example, for tree canopy increases of both 10% and 25%, vulnerable neighborhoods cooled an additional 0.4-0.7° C (0.5-1°F) compared to the least vulnerable neighborhoods (Table 3.5). Vulnerable neighborhoods also were modeled to benefit an extra 0.5°F for a 25% increase in surface albedo. The increased cooling impact could potentially be from high vulnerability neighborhoods having less tree canopy and more impervious surface (Figure 3.16).

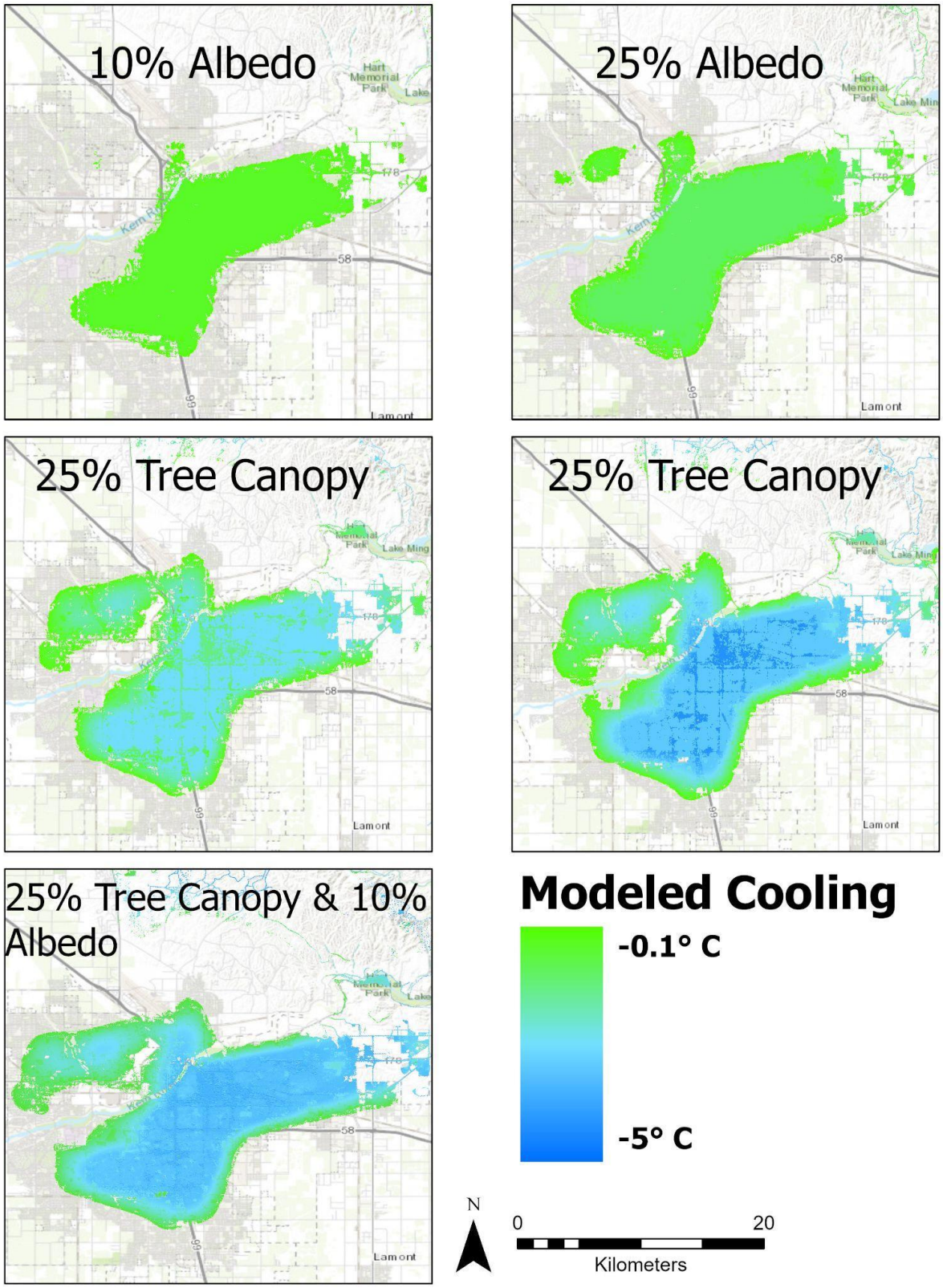

Figure 3.22: Modeled daytime temperature decrease (°C) for a planning scenarios in Bakersfield, California

Neighborhood Type	Temp. °C	Tree Canopy 10% Increase, °C	Tree Canopy 25% Increase, °F	Albedo 10% Increase, °C	Albedo 25% Increase, °C	Tree Canopy 25% Increase & albedo 10% Increase, °C	Cooling Capacity
Developed Open Space	38.3	-0.84	-1.41	0.00	0.00	-2.42	0.12
Developed Low Intensity	40.6	-1.11	-1.71	0.00	-0.07	-2.34	0.14
Developed Medium Intensity	43.0	-1.36	-2.08	-0.23	-0.39	-2.75	0.14
Developed High Intensity	43.8	-1.14	-2.68	-0.27	-0.44	-2.69	0.11
Most Vulnerable	45.0	-1.31	-2.69	-0.24	-0.54	-2.88	0.16
Least Vulnerable	42.8	-1.15	-2.25	-0.19	-0.43	-2.44	0.14

Table 3.5: Cooling by land cover for each planning scenario in Bakersfield, California

The cooling benefit for developed high intensity areas increased more than any other land cover when increasing tree canopy from 10 to 25%. This was despite developed high intensity being the least cooled of all developed land covers from a modest 10% tree canopy increase. Developed high intensity areas cooled nearly 1°F more than medium and low intensity areas with a 25% increase in tree canopy. High intensity development areas had much lower tree canopy compared to low and medium density development zones (9% vs 15-18%), yet benefited far more from the 25% tree canopy increase simulation. The additional cooling that the high intensity development land cover experiences indicates perhaps a certain threshold of canopy may need to be met for cooling to increase. As was the case with Fresno, neighborhoods with high heat vulnerability scores had slightly higher cooling benefits from the modeled scenarios (Figure 3.23).

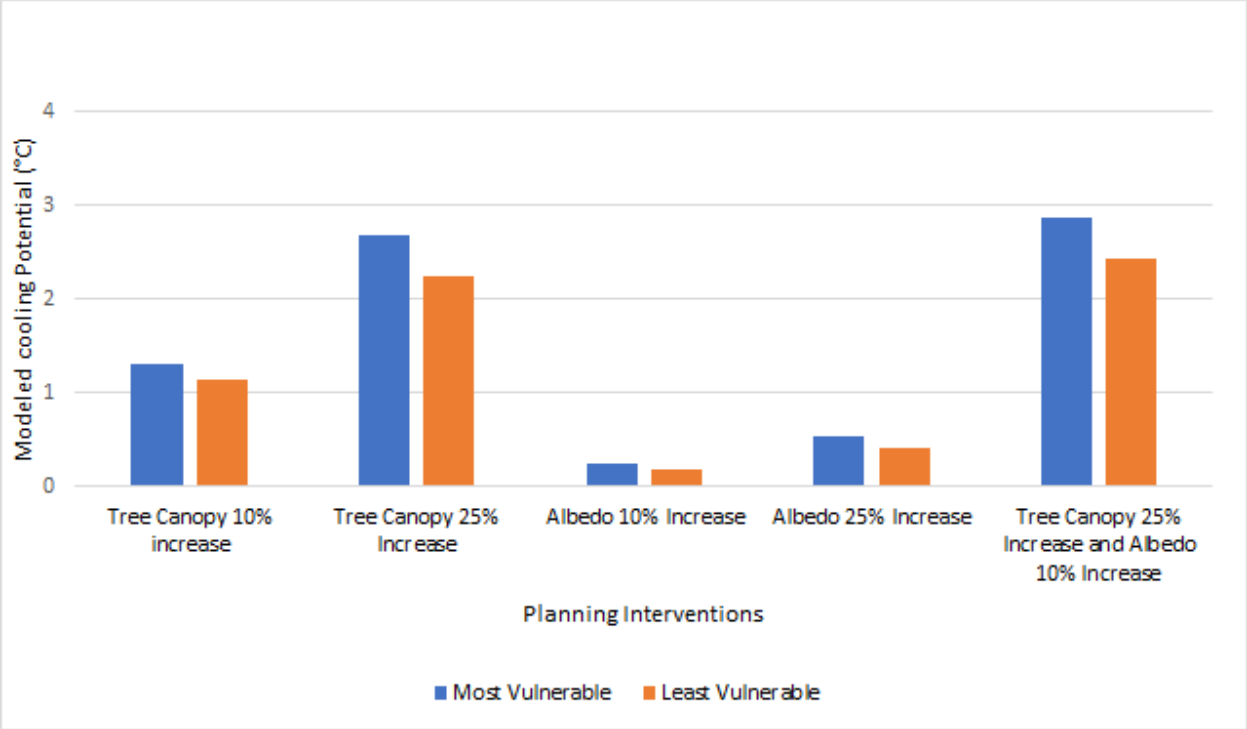

Figure 3.23: Modeled daytime cooling potential (°C) for most and least vulnerable neighborhoods in Bakersfield, California

The nighttime InVEST urban cooling model option considers only building intensity because buildings retain heat from the day and re-emit it at night. Residential areas in Bakersfield have particularly low capacity for cooling (Figure A2). Similar to Fresno, Bakersfield has a large number of neighborhoods with high density development of housing units. Due to the density on these small parcels, the cooling capacity at night is very low. This is not necessarily a function of building height that is driving the low cooling capacity.

Discussion

The Urban Cooling Model relies entirely on the LULC use and drives the model depending on how the attributes of shade, albedo or evapotranspiration are altered. The NLCD LULC dataset also has more generalized categories when describing development and accuracy of model predictions could be improved by using local land cover data created by a county or city GIS group. For example a city created LULC classification would differentiate between

airport, industry, and commercial, but with the NLCD these categories would all be aggregated to one category. Additionally, when it comes to more specific land covers, intervention such as tree planting and surface albedo increases can more seamlessly be modeled. Finally, more precise land cover data would allow better accuracy to where tree canopy can be added in the model (i.e. not within recreation fields, or other areas where it is not feasible). It should also be noted that NLCD has 30m resolution so in an urban environment it can mis-classify many areas since it is not designed for that use. NLCD categories are focused on ecosystem types and are geared toward natural resource and land management, and not urban environments. Additionally, when implementing an increase in tree canopy for the planning intervention scenarios, the model does not allow the user to allocate where specifically to add trees within each land cover type. As such, the model applied the 10% and 25% increase in tree canopy uniformly across the developed open space, developed low intensity, developed medium intensity and developed high intensity areas.

Additionally, the InVEST Urban cooling models air temperature data as input values, not remotely-sensed surface temperature. Therefore, the intermediate air temperature outputs are not true air temperatures. Using surface temperatures introduces more potential error into the model, as surface temperature does not perfectly correlate with air temperature (Shiflett et al. 2017; Hadria et al. 2018). Our model also used a default value of 2000 meters for green space cooling distance (Zardo et al. 2017), which could also introduce bias into the model. We also used default values for several parameters in the model. For example, the Green Area Maximum Cooling Distance (GAMCD) was kept at the default value of 400 m and Air Temperature Maximum Blending Distance (ATMBD) was kept at 500 m (McDonald et al., 2016; Zardo et al., 2017). The GAMCD determines the extent of the cooling effect of land uses labeled as green

areas. This GAMCD extent and influence may change with climate, vegetation type, and air mixing dynamics as outlined by Zardo et al. 2017 if applying the urban cooling model to a different urban region. .

The inputs to the model relied on some assumptions due to lack of high-resolution input data. These included using generalized building heights from, estimated numbers of floors each building has, default values for the green area cooling distance, and the calculation of shade based only on tree canopy cover, which ignores building shade. Tree canopy cover was calculated using the lower resolution NLCD, which did not always correspond well with City-owned tree data.

The combination of identifying the most vulnerable and exposed census block groups as well as the block groups with lowest day and nighttime cooling capacity provides an opportunity for city planners to develop heat mitigation initiatives. For example, a block group that scores high on vulnerability and has low cooling capacity could be prioritized for mitigation measures. In most dryland cities in California, the lack of resources such as ample water supply for irrigation often makes it difficult to plant trees at a city- or region-wide scale, however, knowing which neighborhoods to prioritize could be vital. Allocation of resources to appropriate locations will also help to make sure resources are not wasted on areas that have already reached their cooling potential (i.e. wealthy neighborhoods with high amounts of tree canopy and green space).

Conclusion

In this study we demonstrated that a substantial amount of excess urban heat exists during both day and night in two large cities, Fresno and Bakersfield, in California's Central Valley. The aggregation of excess heat was centered around high impervious surface and low tree

canopy areas such as near airports, industrial areas, and shopping centers in both Fresno and Bakersfield. The warmest areas were up to 12.8° C (20°F) warmer than the city wide averages during the day and up to 7.3° C (12°F) degrees warmer at night. The coolest areas in both regions were areas near parks, golf courses, and along the San Joaquin River in Fresno, and the Kern River in Bakersfield. Interestingly, both the CSU Fresno and CSU Bakersfield campuses were cooler both day and night than the surrounding areas. Garden suburbs (neighborhoods with high tree canopy) (Wheeler 2015) and neighborhoods such as Fig Gardens in Fresno and Stockdale Estates in Bakersfield were also cooler 4°C (>6°F) than the city wide mean.

This study also utilized a PCA analysis of social and biophysical characteristics to derive exposure and vulnerability metrics for both Bakersfield and Fresno. There were differences between areas of heat vulnerability and heat exposure, meaning that higher heat areas do not necessarily correlate to higher vulnerability, although in many cases the two metrics overlapped. Certain demographic groups including LatinX populations, income, populations with limited English proficiency, and those without a high school diploma had higher exposure to both day and nighttime temperature. Our PCA allowed us to more closely examine the factors that put residents at risk.

We also provided insight into the distribution of heat mitigation throughout the urban landscape. By introducing these metrics of heat exposure and heat vulnerability, we were better able to quantify the impacts of major bodies of water and urban green areas (> 2 ha in size) and increasing tree canopy and albedo on surface temperature throughout the two study regions. This is important because it demonstrates not only how increasing tree canopy will reduce city temperatures, but also explores the role of water and open green spaces. Much of the work

conducted with InVEST highlights the limitations of the model and the need to develop and refine the model and its data inputs to better tailor the model to research questions or objectives. Overall we were able to show that increasing tree canopy by 10% in the developed area of Bakersfield and Fresno can lead to a 1.3-2.5° C (2-4°F) cooling effect throughout the city. An additional increase in tree canopy to 25% could result in even more cooling 1.2-2° C (2-3°F), especially in high intensity development areas where the 10% increase in tree canopy had smaller or negligible cooling effects. The cooling impacts extended for up to 2 km from green spaces into surrounding neighborhoods. Increasing albedo of built form by 10% can result in a 0.5°F decrease in temperature in developed areas. The cooling impacts of increasing albedo was regulated to just the built form where the increase was established with no spillover to adjacent areas.

The planning intervention scenarios tested in this study suggest that abundant urban cooling is possible. The scenarios display both combined water intensive initiatives as well as ones that would require less environmental resources (i.e. increasing albedo). Albedo had a far lower impact on cooling. While increasing albedo has been shown to cool individual buildings, and lower cooling load, high albedo, LST mitigating surfaces can re-radiate heat, driving increased thermal burden for pedestrians during midday hours (Erell et al., 2014; Middel et al., 2020). The cost effectiveness of increasing albedo at a city wide scale may be inferior to other mitigation and adaptation measures.

A tree canopy increase program would require significant water, but would provide benefits slowly over time as trees mature. By utilizing the heat vulnerability index cities can target and prioritize neighborhoods with the highest heat vulnerability and lower amounts of

capital to combat urban heat impacts. Maintenance of these trees and green spaces can be costly however, and funding these initiatives and the maintenance of these initiatives are challenging (Voekel et al. 2018; Sanchez and Reamas 2019). This method would be less costly as well as providing relief where it is needed most. Additionally, on the other hand more immediate results could be reached by applying cool pavements or high albedo pavements. This research presents a way to develop an urban heat island risk metric in the form of vulnerability and exposure metrics. Additionally we demonstrated that planning interventions of tree canopy increase and increase in surface albedo yield cooler surface temperatures, and can be implemented at the neighborhood or city wide scale.

References:

Allen, Richard & Pereira, L. & Raes, D. & Smith, M. (1998). *FAO Irrigation and drainage paper* No. 56. Rome: Food and Agriculture Organization of the United Nations. 56. 26-40.

Araujo, R.V., Albertini, M.R., Costa-da-Silva, A.L., Suesdek, L., Franceschi, N.C.S., Bastos, N.M., Katz, G., Cardoso, V.A., Castro, B.C., Capurro, M.L. and Allegro, V.L.A.C.(2015). São Paulo urban heat islands have a higher incidence of dengue than other urban areas. *The Brazilian Journal of Infectious Diseases*, 19(2), 146-155.

Chander, G., Markham, B. L., & Helder, D. L. (2009). Summary of current radiometric calibration coeffecients for Landsat MSS, TM, ETM+, and EO-1 ALI sensors. *Remote Sensing of Environment* 113(5), 893-903.

Cheela, V. R., John, M., Biswas, W., & Sarker, P. (2021). Combating Urban Heat Island Effect—A Review of Reflective Pavements and Tree Shading Strategies. *Buildings*, 11(3), 93.

Chow, W.T.L., Chuang, W.-C., Gober, P., 2012. Vulnerability to extreme heat in metropolitan phoenix: spatial, temporal, and demographic dimensions. *Professional Geographer*, 64(2), 286–302.

Conlon, K. C., Mallen, E., Gronlund, C. J., Berrocal, V. J., Larsen, L., & O'neill, M. S. (2020). Mapping human vulnerability to extreme heat: a critical assessment of heat vulnerability indices created using principal components analysis. *Environmental health perspectives*, 128(9), 097001.

Cutter, S. L., Boruff, B. J., & Shirley, W. L. (2003). Social vulnerability to environmental hazards. *Social Science Quarterly*, 84(2), 242-261. https://doi.org/10.1111/1540-6237.8402002.

Declet-Barreto, J., Brazel, A. J., Martin, C. A., Chow, W. T., & Harlan, S. L. (2013). Creating the park cool island in an inner-city neighborhood: heat mitigation strategy for Phoenix, AZ. *Urban Ecosystems*, 16(3), 617-635.

Dialesandro, J., Brazil, N., Wheeler, S., & Abunnasr, Y. (2021). Dimensions of Thermal Inequity: Neighborhood Social Demographics and Urban Heat in the Southwestern US. *International journal of environmental research and public health*, 18(3), 941.

Erell, E., Pearlmutter, D., Boneh, D., & Kutiel, P. B. (2014). Effect of high-albedo materials on pedestrian heat stress in urban street canyons. Urban Climate, 10, 367–386. https://doi.org/10.1016/j.uclim.2013.10.005

Fresno Police department. (n.d.). https://www.fresno.gov/police/community-and-neighborhood-resources/crime-watch-map/. . Accessed 7 August 2021.

Flocks, J., Escobedo, F., Wade, J., Varela, S., & Wald, C. (2011). Environmental justice implications of urban tree cover in Miami-Dade County, Florida. *Environmental Justice*, 4(2), 125-134.

Ferreira, L. S., & Duarte, D. H. S. (2019). Exploring the relationship between urban form, land surface temperature and vegetation indices in a subtropical megacity. *Urban Climate*, 27, 105-123. https://doi.org/10.1016/j.uclim.2018.11.002

Giridharan, R., & Emmanuel, R. (2018). The impact of urban compactness, comfort strategies and energy consumption on tropical urban heat island intensity: a review. *Sustainable cities and society*, 40, 677-687.

Glorfeld, L. W. (1995). An improvement on Horn's parallel analysis methodology for selecting the correct number of factors to retain. *Educational and Psychological Measurement*, 55(3), 377–393. https://doi.org/10.1177/0013164495055003002.

Hadria, R., Benabdelouahab, T., Mahyou, H., Balaghi, R., Bydekerke, L., El Hairech, T., & Ceccato, P. (2018). Relationships between the three components of air temperature and remotely sensed land surface temperature of agricultural areas in Morocco. *International Journal of Remote Sensing*, 39(2), 356-373.

Hajat, S., Kovats, R., Atkinson, R., & Haines, A. (2002). Impact of hot temperatures on death in London: A time series approach. *Journal of Epidemiology and Community Health*, 56(5), 367–372. https://doi.org/10.1136/jech.56.5.367

Harlan, S. L., Brazel, A. J., Darrel Jenerette, G., Jones, N. S., Larsen, L., Prashad, L., & Stefanov, W. L. (2007). In the shade of affluence: the inequitable distribution of the urban heat island. In Equity and the Environment (pp. 173-202). Emerald Group Publishing Limited.

Harlan, S. L., Declet-Barreto, J. H., Stefanov, W. L., & Petitti, D. B. (2013). Neighborhood effects on heat deaths: social and environmental predictors of vulnerability in Maricopa County, Arizona. *Environmental health perspectives*, 121(2), 197-204.

Hsieh, C.M, Aramaki, T., Hanaki, K. (2007). The feedback of heat rejection to air conditioning load during the nighttime in subtropical climate. *Energy and Buildings*, 39, 1175–1182.

Hondula, D.M., Barnett, A.G., 2014. Heat-related morbidity in Brisbane, Australia: spatial variation and area-level predictors. *Environmental. Health Perspectives* 122 (8), 831–836. https://doi.org/10.1289/ehp.1307496.

Kadaverugu, R., Gurav, C., Rai, A., Sharma, A., Matli, C., & Biniwale, R. (2021). Quantification of heat mitigation by urban green spaces using InVEST model—a scenario analysis of Nagpur City, India. *Arabian Journal of Geosciences*, 14(2), 1-13.

Kaiser, H. F. (1960). The application of electronic computers to factor analysis. *Educational and Psychological Measurement*, 20(1), 141-151. https://doi.org/10.1177/001316446002000116.

Kolosna, C., & Spurlock, D. (2019). Uniting geospatial assessment of neighborhood urban tree canopy with plan and ordinance evaluation for environmental justice. *Urban Forestry & Urban Greening*, 40, 215-223.

Kuo, F. E. (2001). Coping with poverty: Impacts of environment and attention in the inner city. *Environment and behavior*, 33(1), 5-34.

Leal Filho, W., Icaza, L. E., Neht, A., Klavins, M., & Morgan, E. A. (2018). Coping with the impacts of urban heat islands. A literature based study on understanding urban heat vulnerability and the need for resilience in cities in a global climate change context. *Journal of cleaner production*, 171, 1140-1149.

Livingston, Ian (13, August 2021). 'Punishing heat waves peaking in Northwest and Northeast to ease this weekend: The heat domes responsible for record-breaking temperatures are set to sink south. *The Washington Post.* https://www.washingtonpost.com/weather/2021/08/13/heat-wave-northeast-northeast/.

Locke, D. H., Hall, B., Grove, J. M., Pickett, S. T., Ogden, L. A., Aoki, Christopher G. Boone. & O'Neil-Dunne, J. P. (2021). Residential housing segregation and urban tree canopy in 37 US Cities. *npj Urban Sustainability*, 1(1), 1-9.

Mallen, E., Stone, B., & Lanza, K. (2019). A methodological assessment of extreme heat mortality modeling and heat vulnerability mapping in Dallas, Texas. *Urban Climate*, 30, 100528.

Morini, E., Touchaei, A. G., Rossi, F., Cotana, F., & Akbari, H. (2018). Evaluation of albedo enhancement to mitigate impacts of urban heat island in Rome (Italy) using WRF meteorological model. *Urban climate*, 24, 551-566.

Jiménez-Muñoz, J. C., Sobrino, J. A., Skoković, D., Mattar, C., & Cristóbal, J. (2014). Land surface temperature retrieval methods from Landsat-8 thermal infrared sensor data. *IEEE Geoscience and remote sensing letters*, 11(10), 1840-1843.

Konisky, D. M. (2016). Environmental justice delayed: Failed promises, hope for the future. *Environment: Science and Policy for Sustainable Development*, 58(2), 4–15.

Macintyre, H. L., Heaviside, C., Taylor, J., Picetti, R., Symonds, P., Cai, X. M., & Vardoulakis, S. (2018). Assessing urban population vulnerability and environmental risks across an urban area during heatwaves–Implications for health protection. *Science of the total environment*, 610, 678-690.

Middel, A., Turner, V. K., Schneider, F. A., Zhang, Y., & Stiller, M. (2020). Solar reflective pavements—A policy panacea to heat mitigation? Environmental Research Letters, 15(6), 064016. https://doi.org/10.1088/1748-9326/ab87d4

Mihalakakou, G., Santamouris, M., Papanikolaou, N., Cartalis, C., & T. Sangrassoulis, A. (2004). Simulation of the urban heat island phenomenon in Mediterranean climates. *Pure and Applied Geophysics*, 161(2), 429–451.

Miner, M. J., Taylor, R. A., Jones, C., & Phelan, P. E. (2017). Efficiency, economics, and the urban heat island. *Environment and Urbanization*, 29(1), 183-194.

Mitchell, B. C., & Chakraborty, J. (2018). Exploring the relationship between residential segregation and thermal inequity in 20 US cities. *Local Environment*, 23(8), 796-813.

Morabito, M., Crisci, A., Guerri, G., Messeri, A., Congedo, L., & Munafò, M. (2021). Surface urban heat islands in Italian metropolitan cities: Tree cover and impervious surface influences. *Science of The Total Environment*, 751, 142334.

Nayak SG, Shrestha S, Kinney PL, Ross Z, Sheridan SC, Pantea CI, et al. 2018. Development of a heat vulnerability index for New York State. Public Health 161:127–137, PMID: 29195682, https://doi.org/10.1016/j.puhe.2017.09.006.

Ramírez-Aguilar, E. A., & Souza, L. C. L. (2019). Urban form and population density: Influences on Urban Heat Island intensities in Bogotá, Colombia. *Urban Climate*, 29, 100497.

Reid, C. E., O'neill, M. S., Gronlund, C. J., Brines, S. J., Brown, D. G., Diez-Roux, A. V., & Schwartz, J. (2009). Mapping community determinants of heat vulnerability. *Environmental health perspectives*, 117(11), 1730-1736.

Ronchi, S., Salata, S., & Arcidiacono, A. (2020). Which urban design parameters provide climate-proof cities? An application of the Urban Cooling InVEST Model in the city of Milan comparing historical planning morphologies. *Sustainable Cities and Society*, 63, 102459.

Sanchez, L., & Reames, T. G. (2019). Cooling Detroit: A socio-spatial analysis of equity in green roofs as an urban heat island mitigation strategy. *Urban Forestry & Urban Greening*, 44, 126331.

Sass, C. K., Lodder, R. A., & Lee, B. D. (2019). Combining biophysical and socioeconomic suitability models for urban forest planning. *Urban forestry & urban greening*, *38*, 371-382.

Shiflett, S. A., Liang, L. L., Crum, S. M., Feyisa, G. L., Wang, J., & Jenerette, G. D. (2017). Variation in the urban vegetation, surface temperature, air temperature nexus. *Science of the Total Environment*, 579, 495-505.

Schwartz, J. (2005). Who Is Sensitive to Extremes of Temperature? A Case-Only Analysis. Epidemiology, 16(1), 67–72. JSTOR. http://www.jstor.org/stable/20486001.

Sera, F., Armstrong, B., Tobias, A., Vicedo-Cabrera, A. M., Åström, C., Bell, M. L., ... & Dang, T. N. (2019). How urban characteristics affect vulnerability to heat and cold: A multi-country analysis. *Int. J. Epidemiol.*, 1-12.

Seroka C, Kaiser P, Heany J. 2011. Mapping Heat Vulnerability in Michigan. https:// www.michigan.gov/documents/mdch/Heat_Mapping_FY11_Final_Report_9.30.11_ 433139_7.pdf [accessed 13 May 2021].

Shen, H., Huang, L., Zhang, L., Wu, P., & Zeng, C. (2016). Long-term and fine-scale satellite monitoring of the urban heat island effect by the fusion of multi-temporal and multi-sensor remote sensed data: A 26-year case study of the city of Wuhan in China. *Remote Sensing of Environment*, 172, 109-125. https://doi.org/10.3390/rs9060536.

Tang, Z., Zheng, H., Ren, Z., Zhang, D., Wang, P., Zhai, C., ... & He, X. (2018). Evaluating environmental equities of urban forest in terms of cooling services using ETM+ and Google data. Journal of the Indian Society of Remote Sensing, 46(2), 287-296.

Taylor, J., Wilkinson, P., Davies, M., Armstrong, B., Chalabi, Z., Mavrogianni, A., Symonds, P., Oikonomou, E. and Bohnenstengel, S.I., (2015). Mapping the effects of urban heat island, housing, and age on excess heat-related mortality in London. *Urban Climate*, (14).517-528.

U.S. Census Bureau (2019). Selected demogrpahics characteristics, 2015-2019 American Community Survey 5-year estimates. Retrieved from http://factfinder2.census.gov/faces/tableservices/jsf/pages/productview.xhtml?pid=ACS_19_5YR_DP04.

USGS EROS (2017) Landsat Collection 1 Level 1 Product Definition. Retrieved from https://landsat.usgs.gov/sites/default/files/documents/LSDS-1656_Landsat_Level-1_Product_Co

Voelkel, J., Hellman, D., Sakuma, R., & Shandas, V. (2018). Assessing vulnerability to urban heat: A study of disproportionate heat exposure and access to refuge by socio-demographic status in Portland, Oregon. *International journal of environmental research and public health*, 15(4), 640.

Watkins, L. E., Wright, M. K., Kurtz, L. C., Chakalian, P. M., Mallen, E. S., Harlan, S. L., & Hondula, D. M. (2021). Extreme heat vulnerability in Phoenix, Arizona: A comparison of all-hazard and hazard-specific indices with household experiences. *Applied Geography*, 102430.

Weinberger, K. R., Haykin, L., Eliot, M. N., Schwartz, J. D., Gasparrini, A., & Wellenius, G. A. (2017). Projected temperature-related deaths in ten large US metropolitan areas under different climate change scenarios. *Environment international*, 107, 196-204. doi: 10.1016/j.envint.2017.07.006

Wilson, S. M., Richard, R., Joseph, L., & Williams, E. (2010). Climate change, environmental justice, and vulnerability: an exploratory spatial analysis. Environmental Justice, 3(1), 13-19.

Wheeler, S. M. (2015). Built landscapes of metropolitan regions: An international typology. *Journal of the American Planning Association*, 81(3), 167-190.

Flocks, J., Escobedo, F., Wade, J., Varela, S., & Wald, C. (2011). Environmental justice implications of urban tree cover in Miami-Dade County, Florida. *Environmental Justice*, 4(2), 125-134.

Yang, L., Jin, S., Danielson, P., Homer, C., Gass, L., Bender, S. M., Case, A., Costello, C., DeWitz, J., Fry, J., & Funk, M. (2018). A new generation of the United States National Land Cover Database: Requirements, research priorities, design, and implementation strategies. *ISPRS journal of photogrammetry and remote sensing*, 146, 108-123.

Yuan, F., & Bauer, M. E. (2007). Comparison of impervious surface area and normalized difference vegetation index as indicators of surface urban heat island effects in Landsat imagery. *Remote Sensing of environment*, 106(3), 375-386.

Zawadzka, J. E., Harris, J. A., & Corstanje, R. (2021). Assessment of heat mitigation capacity of urban greenspaces with the use of InVEST urban cooling model, verified with day-time land surface temperature data. *Landscape and Urban Planning*, 214, 104163.

Zhang, K., Rood, R., Michailidis, G., Oswald, E., Schwartz, J., Zanobetti, A., Ebi, K., & O'Neill, M. (2012). Comparing exposure metrics for classifying 'dangerous heat' in heat wave and health warning systems. *Environment international*, 46(23–29). https://doi.org/10.1016/j.envint.2012.05.001

Appendix:

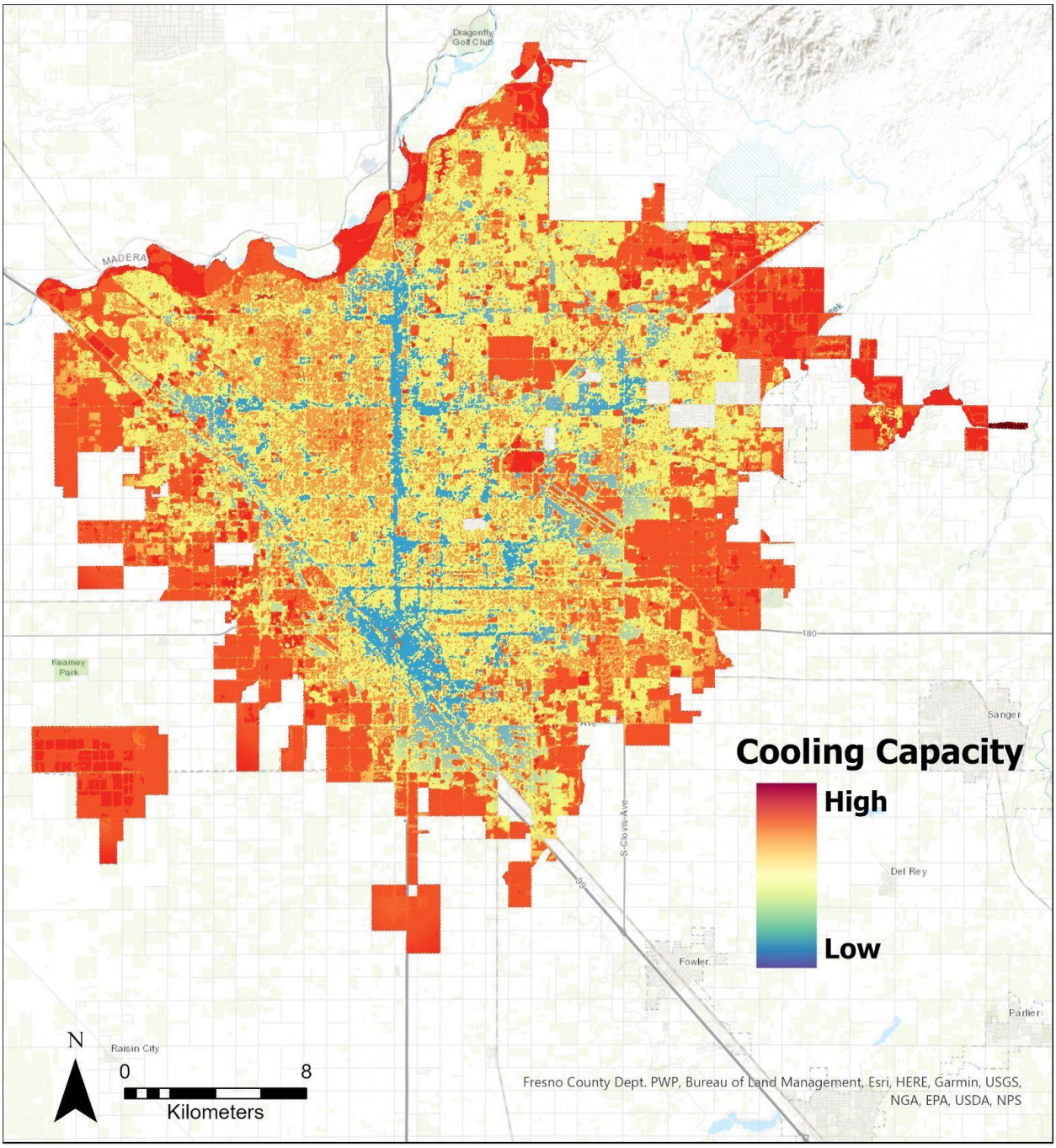

Figure A1: Nighttime cooling capacity (0-1) for the City of Fresno, California

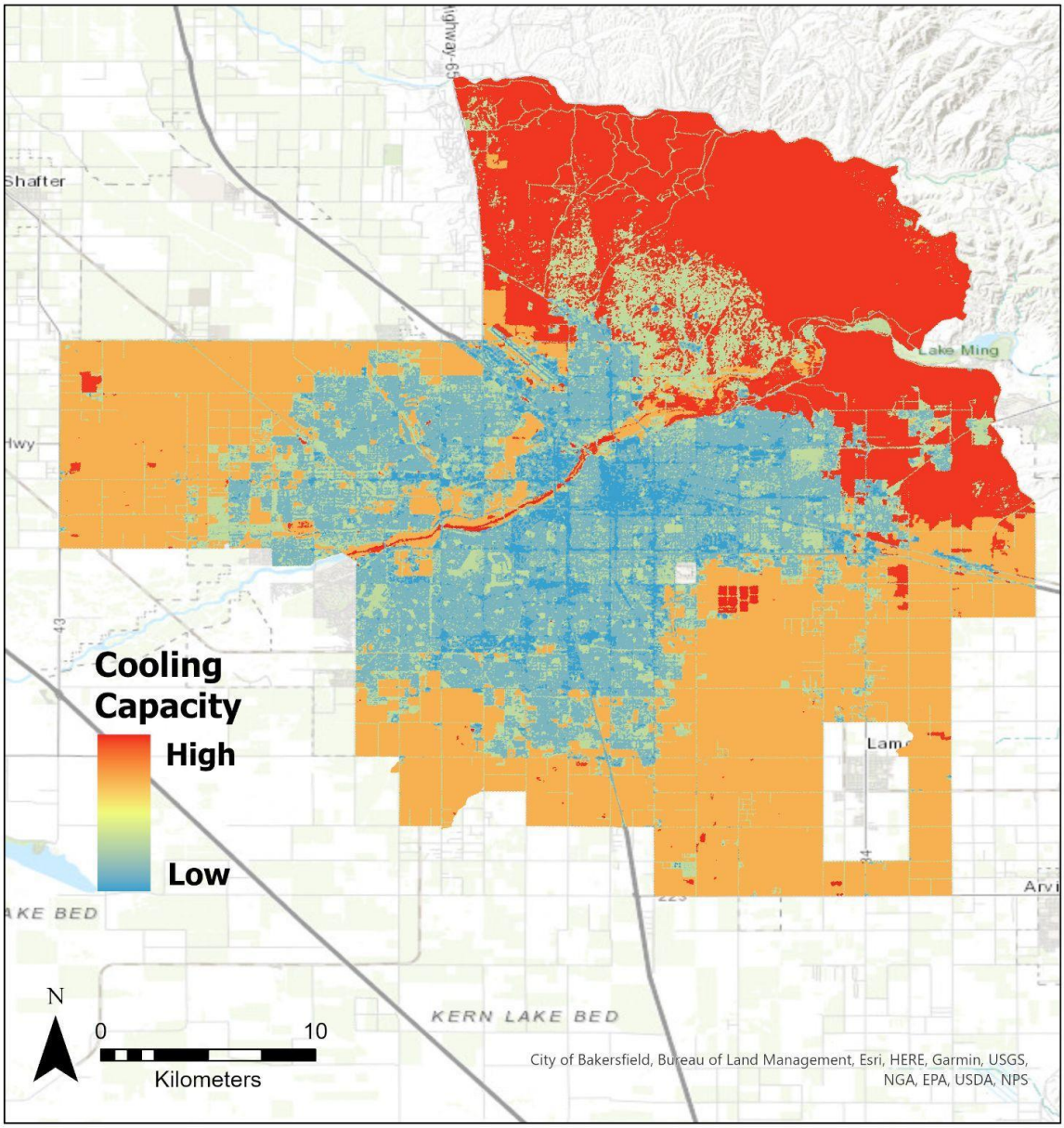

Figure A2: Nighttime cooling capacity (0-1) for the City of Bakersfield, California

IV. THREE PAPER CONCLUSION

The three papers described above provide an in-depth and multidisciplinary view of the urban heat island phenomenon focusing on dryland regions. These studies build onto one another through the exploration of the biophysical and social data that drive and are manipulated by the temperature patterns within a city. GIS, remote sensing, and statistical exploration are used as methods to determine what type of relationships exist between the dependent variable of land surface temperature and the suit of independent variables. Aspects of urban climatology, urban land use planning, and landscape, and urban ecology are also applied to these studies, and varying research aspects coalesce to provide insight on all aspects of urban heat islands in dryland regions.

Starting with a macro level approach, paper one provides a benchmark for the different behaviors of surface temperature variation through a variety of major metropolitan areas. Neighborhood dynamics on land surface temperature are also explored. Both the regional area as whole and specific land cover practice/temperature relationships are examined. The neighborhood examination also provides a glimpse into not only examining the dense urban areas but also the flow of energy between high density and more sparsely developed areas thus encapsulating the true impact of urban areas on the surrounding landscape. This supports Pickett et al. 2001 which stressed the importance of "comparisons along gradients of urbanization [which] can capture the full range of urban effects as well as the existence of thresholds." for understanding of urbanization impacts on the urban and rural ecosystems (Pickett et al 2001).

This portion of the research project is also especially important for informing city planners, stakeholders, and policy makers on the data necessary to make decisions on the planning process of mitigating increasing heat, and cooling load. The aspect of developing mitigation plans to offset the existing unequal burden population groups in these cities face will

be of particular importance. Communities similar in climate characteristics will also benefit from the results since they can use the same data to make decisions.

This research demonstrated a number of important findings. First is that urban heat islands behave differently not only between temperate and dryland climates but also within dryland climates depending on latitude, elevation, and cultural urban development practices. The patterns of urban heat differ from a traditional “heat island”, and represent more of an urban heat archipelago. The matrix of land covers throughout urban regions create patches of cool land surface temperature intermixed with warmer temperatures. Depending on aridity and irrigation these patches of heat and cool islands can extend beyond their boundaries and up to 2-3 km. Size and orientation of the patches of land cover also play a role in the thermal surface environment. While there are challenges extrapolating the patterns of mega cities to smaller regional and metropolitan areas, the land use/land cover and temperature dynamics are consistent across the literature including our published study.

This research also established that in major cities throughout the southwestern US there is a strong unequal burden of urban heat. In Particular, low income and predominantly LatinX neighborhoods were subject to 2.5-5° C higher temperatures compared to wealthy neighborhoods, and neighborhoods with low LatinX populations. The thermal inequity demonstrated by the data was even greater in California cities compared to the rest of the southwestern US. This was consistent for nighttime temperatures, daytime temperatures, and extreme heat events. Additionally, while accounting for spatial autocorrelation we found that income is a significant predictor of temperature, as is LatinX population for block group neighborhoods.

Finally this research built on the first two publications, and combined the biophysical and socio demographic characteristics to identify what block groups are the most vulnerable based on race, income, age, education level, english proficiency, impervious surface, and tree canopy. Then we used a micro climate modeling system to model the effects of planning interventions such as increasing surface albedo, and tree canopy. We found that increasing tree canopy by 10% in the developed area of Bakersfield and Fresno can lead to a 1.3-2.5° C (2-4°F) cooling effect throughout the city. An additional increase in tree canopy to 25% could result in even more cooling 1.2-2° C (2-3°F), especially in high intensity development areas where the 10% increase in tree canopy had smaller or negligible cooling effects. The cooling impacts extended for up to 2 km from green spaces into surrounding neighborhoods. Increasing albedo of built form by 10% can result in a 0.5°F decrease in temperature in developed areas. The cooling impacts of increasing albedo was regulated to just the built form where the increase was established with no spillover to adjacent areas. We also found that neighborhoods that scored high for heat vulnerability benefited slightly more from the cooling scenarios possibly from existing lack of tree canopy and excess impervious surface.